

AD-A124 290

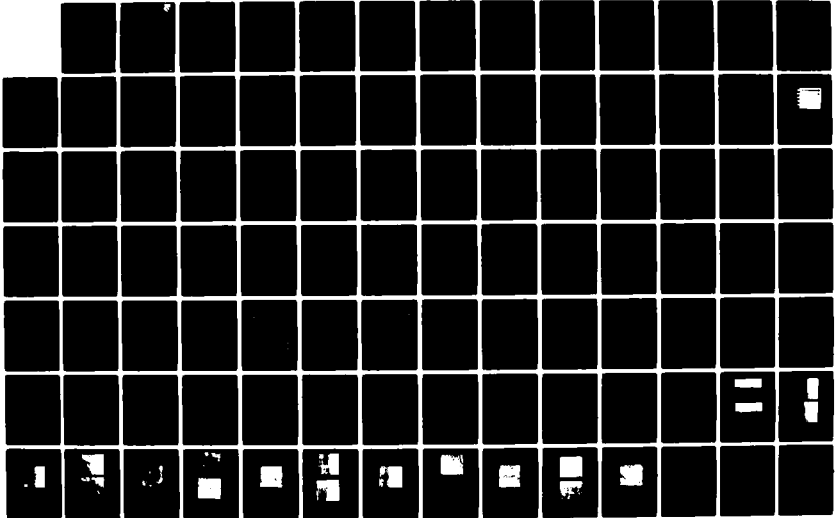
VITREOUS ENAMEL DAMPING MATERIAL DEVELOPMENT(U) DAYTON
UNIV OH RESEARCH INST B KUMAR NOV 82 UDR-TR-82-105
AFWAL-TR-82-4162 F33615-79-C-5108

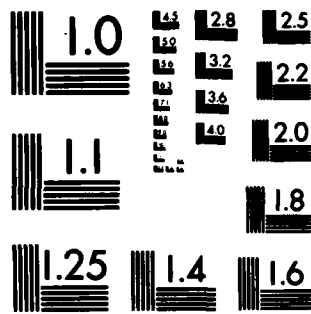
1/2

UNCLASSIFIED

F/G 11/3

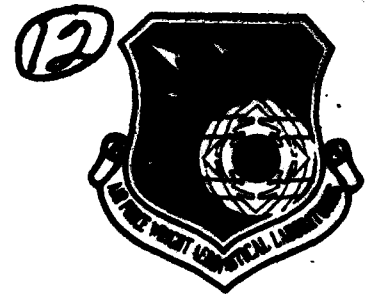
NL





MICROCOPY RESOLUTION TEST CHART
NATIONAL BUREAU OF STANDARDS-1963-A

AFWAL-TR-82-4162



VITREOUS ENAMEL DAMPING MATERIAL DEVELOPMENT

Binod Kumar
University of Dayton Research Institute
300 College Park
Dayton, Ohio 45469

November 1982

Final Report For Period October 1979 - July 1982

APPROVED FOR PUBLIC RELEASE; DISTRIBUTION UNLIMITED

DTIC
ELECTE
FEB 10 1983
S E D

MATERIALS LABORATORY
AIR FORCE WRIGHT AERONAUTICAL LABORATORIES
AIR FORCE SYSTEMS COMMAND
WRIGHT-PATTERSON AIR FORCE BASE, OHIO 45433

83 02 010 055

ADA 124290

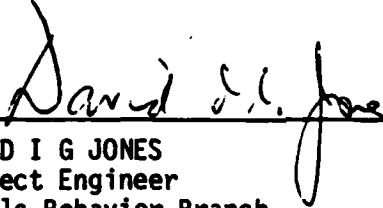
DTIC FILE COPY

NOTICE

When Government drawings, specifications, or other data are used for any purpose other than in connection with a definitely related Government procurement operation, the United States Government thereby incurs no responsibility nor an obligation whatsoever; and the fact that the government may have formulated, furnished, or in any way supplied the said drawings, specifications, or other data, is not to be regarded by implication or otherwise as in any manner licensing the holder or any other person or corporation, or conveying any rights or permission to manufacture use, or sell any patented invention that may in any way be related thereto.

This report has been reviewed by the Office of Public Affairs (ASD/PA) and is releasable to the National Technical Information Service (NTIS). At NTIS, it will be available to the general public, including foreign nations.

This technical report has been reviewed and is approved for publication.

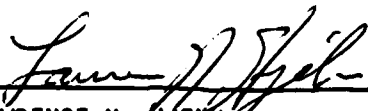


DAVID I G JONES
Project Engineer
Metals Behavior Branch



JOHN P. HENDERSON
Chief
Metals Behavior Branch

FOR THE COMMANDER



LAWRENCE N. HJELM
Assistant Chief
Metals and Ceramics Division

"If you address has changed, if you wish to be removed from our mailing list, or if the addressee is no longer employed by your organization please notify AFWAL/MLLN, W-PAFB, OH 45433 to help us maintain a current mailing list.

Copies of this report should not be returned unless return is required by security considerations, contractual obligations, or notice on a specific document.

Unclassified

SECURITY CLASSIFICATION OF THIS PAGE (When Data Entered)

REPORT DOCUMENTATION PAGE		READ INSTRUCTIONS BEFORE COMPLETING FORM
1. REPORT NUMBER AFWAL-TR-82-4162	2. GOVT ACCESSION NO. AD-4124 290	3. RECIPIENT'S CATALOG NUMBER
4. TITLE (and Subtitle) VITREOUS ENAMEL DAMPING MATERIAL DEVELOPMENT	5. TYPE OF REPORT & PERIOD COVERED Final Technical Report October 1979 - July 1982	
	6. PERFORMING ORG. REPORT NUMBER UDR-TR-82-105	
7. AUTHOR(s) Binod Kumar	8. CONTRACT OR GRANT NUMBER(s) F33615-79-C-5108	
9. PERFORMING ORGANIZATION NAME AND ADDRESS University of Dayton Research Institute Dayton, Ohio 45469	10. PROGRAM ELEMENT, PROJECT, TASK AREA & WORK UNIT NUMBERS 62102F 24180312	
11. CONTROLLING OFFICE NAME AND ADDRESS Materials Laboratory (AFWAL/MLLN) Air Force Wright Laboratories (AFSC) Wright-Patterson AFB, Ohio 45433	12. REPORT DATE November 1982	
	13. NUMBER OF PAGES 100	
14. MONITORING AGENCY NAME & ADDRESS (if different from Controlling Office)	15. SECURITY CLASS. (of this report) Unclassified	
	15a. DECLASSIFICATION/DOWNGRADING SCHEDULE	
16. DISTRIBUTION STATEMENT (of this Report) Approved for public release; distribution unlimited		
17. DISTRIBUTION STATEMENT (of the abstract entered in Block 20, if different from Report)		
18. SUPPLEMENTARY NOTES		
19. KEY WORDS (Continue on reverse side if necessary and identify by block number) Damping Glass Enamel Measurements Vitreous		
20. ABSTRACT (Continue on reverse side if necessary and identify by block number) This report describes the results of several experimental investigations pertaining to the effects of composition, viscosity, microstructure, and constraining layer on the damping properties of vitreous enamels. New vitreous enamels such as mixed alkali silicate, lead silicate, and two phase fluoride composition have been characterized. The mixed alkali and lead silicate compositions exhibits the characteristic, viscoelastic damping peak. The damping temperatures and the peak intensities are compositions dependent. The		

DD FORM 1473 1 JAN 73 EDITION OF 1 NOV 65 IS OBSOLETE

Unclassified
SECURITY CLASSIFICATION OF THIS PAGE (When Data Entered)

Unclassified

SECURITY CLASSIFICATION OF THIS PAGE(When Data Entered)

Continuation of block 20

Fluoride composition initially shows a typical vitreous enamel damping peak; however, after a heat treatment significant broadening of the damping peak is noted. It is believed that the broadening occurs due to a second phase which develops after the heat treatment. A relationship between the glass transition temperature and damping temperature have been developed. It has been determined that the viscosity in the damping range corresponds to approximately $10^6 - 10^7$ poise. The viscosity range is favorable for processes like nucleation and crystallization. Effects of nucleation and crystallization on the damping properties have been studied and analyzed for two compositions. The nucleation and crystallization have an adverse effect on the loss factor. Damping properties of three constrained layer systems have been evaluated and analyzed. The general effect of the constraining layer is to broaden the damping peak.

1000000 - 10000000

Unclassified

SECURITY CLASSIFICATION OF THIS PAGE(When Data Entered)

FOREWORD

The work described in this report was performed at the University of Dayton Research Institute for the Metals Behavior Branch, Metals and Ceramics Division, Materials Laboratory, Air Force Wright Aeronautical Laboratories (AFWAL/MLLN), under Contract number F33615-79-C-5108, "High Frequency Fatigue of Turbine Blade Material." The contract was administered under the direction of AFWAL by Dr. D. I. G. Jones (MLLN). The program was conducted by the Aerospace Mechanics Group, University of Dayton Research Institute, Dayton, Ohio with Mr. Michael L. Drake as the principal investigator.

The investigations of the effects of composition, viscosity, microstructure and constraining layers on the damping properties of vitreous enamels were conducted by Dr. Binod Kumar. Experimental evaluation and data reduction was accomplished by Mr. S. Hilton, Mr. W. Goddard, Mr. D. Hopkins, and Mr. P. Graf. This work was performed during the period October 1979 to July 1982.

Accession For	
NTIS GRA&I	<input checked="" type="checkbox"/>
DTIC TAB	<input type="checkbox"/>
Unannounced	<input type="checkbox"/>
Justification	
By _____	
Distribution/	
Availability Codes	
_____ for	
Dist _____	
A	



TABLE OF CONTENTS

<u>SECTION</u>		<u>PAGE</u>
1	INTRODUCTION	1
2	TECHNICAL PROCEDURES	3
	2.1. EXPERIMENTAL	3
	2.1.1. GLASS PREPARATION	3
	2.1.2. METHOD OF COATING APPLICATION	3
	2.1.3. VIBRATION DAMPING MEASUREMENTS	3
	2.2. CALCULATION OF DAMPING PROPERTIES	4
3	RESULTS AND DISCUSSION	12
	3.1. DAMPING PROPERTIES OF NEW COMPOSITIONS	12
	3.1.1. MIXED ALKALI GLASSES	12
	3.1.2. FLUORIDE GLASS	24
	3.1.3. LEAD SILICATE COMPOSITIONS	24
	3.1.4. LOW TEMPERATURE GLASSES	44
	3.2. RELATIONSHIP BETWEEN THE DAMPING TEMPERATURE AND GLASS TRANSITION TEMPERATURE	60
	3.3 EFFECT OF NUCLEATION AND CRYSTALLIZATION ON THE VISCOELASTIC DAMPING	64
	3.4. CONSTRAINED LAYER DAMPING WITH VITREOUS ENAMEL	86
	CONCLUSIONS	98
	REFERENCES	99

LIST OF ILLUSTRATIONS

<u>Figure</u>		<u>Page</u>
1	Typical Cantilever Beam Specimen for High Temperature Damping Material Evaluation.	5
2	High Temperature Damping Test Apparatus.	6
3	Block Diagram of High-Temperature Test Apparatus.	7
4	Schematic of High Temperature Damping Test Apparatus Cooling System.	8
5	Coated Oberst Test Beam.	9
6	Effect of K_2O Substitution for Li_2O on the Thermal Expansion Coefficient.	15
7	Appearance of the Glass Coatings After Damping Measurements. Numbers on the Left Indicate Glass Composition.	16
8	Reduced Frequency Nomogram Showing Loss Factor and Young's Modulus for Composition 2.	17
9	Reduced Frequency Nomogram Showing Loss Factor and Young's Modulus for Composition 3.	19
10	Reduced Temperature Nomogram Showing Loss Factor and Young's Modulus for Composition 4.	21
11	Loss Factor at 100 Hz Versus Temperature for 2, 3, and 4, Mixed Alkali Glasses.	23
12	Modal Damping from Fluoride Material Number Superimposed on the Curves Indicate Mode Number.	25
13	Modal Damping from Fluoride Material After Heat Treatment at 800°C for 20 hours.	26
14	Reduced Nomogram for Composition III.	27
15	Reduced Nomogram for Composition IV.	29
16	Reduced Nomogram for Composition VII.	31
17	Reduced Nomogram for Composition VIII.	33
18	Reduced Nomogram for Composition IX.	35
19	Reduced Nomogram for Composition X.	38
20	Reduced Nomogram for Composition XI.	41
21	Reduced Nomogram Displaying Loss Factor for LT-1.	45
22	Reduced Nomogram Displaying Loss Modulus for LT-1.	46
23	Reduced Nomogram Displaying Loss Factor for LT-3.	48
24	Reduced Nomogram Displaying Loss Modulus for LT-3.	49

LIST OF ILLUSTRATIONS
(continued)

<u>Figure</u>		<u>Page</u>
25	Nomogram for LT-4 with Modulus and Loss Factor.	51
26	Nomogram for LT-4 with Loss Modulus and Modulus.	52
27	Reduced Nomogram Displaying Loss Factor for LT-5.	54
28	Reduced Nomogram Displaying Loss Modulus for LT-5.	55
29	Nomogram for LT-6 with Modulus and Loss Factor.	57
30	Nomogram for LT-6 with Loss Modulus and Modulus.	58
31	Maximum Loss Factor (η_D) Temperature Versus the Glass Transition Temperature (T_g).	61
32	Log Viscosity Versus $1/T$ for Corning 0010 Glass (viscosity in poise).	63
33	Typical Viscosity Curve for Glass Showing Common Reference Points.	66
34	Loss Factor as a Function of Temperature and Heat Treatment Time at 760°C for Composition A.	67
35	Loss Factor as a Function of Temperature and Heat Treatment Time at 815°C for Composition B.	68
36	Optical Micrographs: (a) As Fired Specimen (150X); (b) Heat Treated for 112 hours at 1,500°F (150X).	71
37	Glass-Metal Interface for Composition "A" After Various Heat Treatments.	72
38	Morphology of Vitreous Enamel Coating "A" After Heat Treatment of 100 hours.	75
39	Microstructure of Vitreous Enamel "A" After 314 Hours of Heat Treatment.	76
40	Metal-Glass Interface for Composition "B" as a Function of Heat Treatment Time.	78
41	Enamel Coating at Various Magnifications After Heat Treatment for 112 Hours.	80
42	Enamel Coating at Various Magnifications After Heat Treatment for 309 Hours.	82
43	Test Beams for Corning Composition 1990.	90
44	(A) Vitreous Enamel Coated Iron Foil. (P) Spot Welded Iron Foil on Beam.	91
45	Loss Factor Versus Temperature for Free and Constrained Layer Damping Treatments [Mode-2].	92

LIST OF ILLUSTRATIONS
(concluded)

<u>Figure</u>		<u>PAGE</u>
46	Typical Temperature Dependence of Polymer Viscoelasticity.	93
47	Static Viscosity of Corning 1990 Glass.	94
48	Shape of the Function $\text{Log } \frac{\eta}{\phi}$ Versus Temperature.	97
49	Structural Damping Versus Temperature for Free Layer, Iron-Constrained, and Steel-Constrained Damping [Mode 4]	98

LIST OF TABLES

<u>Table</u>		<u>Page</u>
1	GLASS COMPOSITIONS AND THEIR PROPERTIES	14
2	EXPERIMENTAL AND REDUCED DATA OF COMPOSITION 2 (AM2)	18
3	EXPERIMENTAL AND REDUCED DATA OF COMPOSITION 3 (AM3)	20
4	EXPERIMENTAL AND REDUCED DATA OF COMPOSITION 4 (AM4)	22
5	COMPOSITIONS (PERCENT WEIGHT) OF LEAD SILICATE GLASSES	24
6	EXPERIMENTAL AND REDUCED DATA OF COMPOSITION III (AMB3)	28
7	EXPERIMENTAL AND REDUCED DATA OF COMPOSITION V (AMB5)	30
8	EXPERIMENTAL AND REDUCED DATA OF COMPOSITION VII (AMB7)	32
9	EXPERIMENTAL AND REDUCED DATA OF COMPOSITION VIII (AMB8)	34
10	EXPERIMENTAL AND REDUCED DATA OF COMPOSITION IX (AMB9)	36
11	EXPERIMENTAL AND REDUCED DATA OF COMPOSITION X (AMB10)	39
12	EXPERIMENTAL AND REDUCED DATA OF COMPOSITION XI (AMB11)	42
13	COMPOSITIONS OF LOW TEMPERATURE GLASSES	44
14	EXPERIMENTAL AND REDUCED DATA OF COMPOSITION LT-1	47
15	EXPERIMENTAL AND REDUCED DATA OF COMPOSITION LT-3	50
16	EXPERIMENTAL AND REDUCED DATA OF COMPOSITION LT-4	53
17	EXPERIMENTAL AND REDUCED DATA OF COMPOSITION LT-5	56
18	EXPERIMENTAL AND REDUCED DATA OF COMPOSTTION LT-6	59
19	GLASS TRANSITION TEMPERATURES (T_g) OF TEST MATRIX GLASS COMPOSITIONS	62
20	COMPOSITIONS IN WEIGHT PERCENT	65
21	CRYSTALLINE PHASES AFTER VARIOUS HEAT TREATMENTS	84
22	EXPERIMENTAL TEST MATRIX	88
23	$\frac{\eta}{\phi}$ AT VARIOUS TEMPERATURES	96

SECTION I INTRODUCTION

In order to control high cycle fatigue in vibrating structures at elevated temperatures, vitreous enamel coatings have been suggested and used [1,2,3]. The coatings dissipate vibratory energy due to their characteristic high mechanical loss in the viscoelastic range. The dissipation of vibratory energy by such treatment improves the performance, reliability, and reduces maintenance costs of the structure. At lower temperatures ($<400^{\circ}\text{C}$), polymeric coatings are commonly used. Preliminary feasibility experiments and viscoelastic damping data for vitreous enamel coatings have been reported by Nashif [4] and Sridharan [5].

The University of Dayton has been engaged, in developing viscoelastic damping measurement techniques and vitreous enamel compositions for damping applications in aircraft engines for approximately 10 years, under contracts funded by the Air Force Materials Laboratory, Wright-Patterson Air Force Base. Significant developments have been made in the measurement and application techniques. A better understanding has developed in regard to the effects of composition (6) on the damping properties.

The primary objectives of the studies reported here were to further evaluate damping properties of new compositions, analyze previous data and develop a relationship between the structure and the damping properties, evaluate the constrained layer damping concept with the vitreous enamel, and analyze the difficulties associated with the utilization such as nucleation and crystallization of vitreous enamels as a vibration damping material.

Vitreous enamel or inorganic silicate glasses exhibit damping peaks at various temperatures. For a frequency of 1 Hz a peak occurs at about -30°C , which is related to the alkali ion diffusion. A second peak at the same frequency occurs at about 200°C . The damping (η) of the first peak is approximately 0.001, whereas the damping of the second peak varies from 0.001 to 0.02, depending on the glass composition. For a single alkali glass, the

damping intensity (η) of the second peak is approximately 0.001. The addition of a second alkali causes a large increase in the intensity of this peak to as high as 0.02. The damping peaks are also frequency dependent. Increasing frequency increases the peak temperature. For example, a decade increase in frequency shifts the peak toward a higher temperature by approximately 15°C. These two peaks are the results of anelastic damping. Readers can refer to a recently published review paper (7) for the mechanisms and the related information concerning the two peaks.

A third peak of significantly higher damping intensity ($Q^{-1} \approx 1$) than the first two occurs at a higher temperature. Associated with this damping peak is a large change in the complex modulus. A change of about 40 percent in the modulus can be expected. This peak is frequently referred to as the viscoelastic peak. This is the peak of primary interest in dissipating the vibratory energy at elevated temperature and will be the main topic of discussion in this report.

SECTION II
TECHNICAL PROCEDURES

2.1 EXPERIMENTAL

2.1.1 Glass Preparation

All of the compositions, except the standard commercial compositions, were formulated and synthesized from the analytical grade raw materials. Required amounts of oxide and carbonate raw materials were weighed and mixed in a V-blender for approximately one hour. The weighed material was then melted in a platinum crucible at appropriate melting temperatures. The molten glass was quenched by pouring into a container of cold water. The quenched glass was then dry ball milled, using Al_2O_3 grinding media, for 24 hours. The milled powder was then screened to obtain various particle size splits. The test beams were coated with vitreous enamels of particle sizes passing through a 100-mesh screen but not through a 150-mesh screen.

2.1.2 Method of Coating Application

Prior to spraying, the metal substrate was sandblasted using 36-mesh silicon carbide grit and an air pressure of 75 psi. The powder material was applied to the metal substrate by plasma spraying. A Meteo 3MB plasma spray apparatus was operated at 400 amps DC, 75 volts DC at 30,000 watts setting with a gas flow of 15 scfh H_2 and 80 scfh Ar. A gas mixture of 84.2 percent Ar and 15.7 percent H_2 was used. The coated beam was then fired in a resistance-heated furnace for approximately three minutes or until the surface appeared to be smooth.

2.1.3 Vibration Damping Measurements

An apparatus and technique was developed to accurately and reliably excite, and measure the response of a beam specimen at temperatures exceeding $1,000^\circ\text{C}$.

The specimen used was a cantilever beam coated on one side with an enamel or glass. A typical specimen is illustrated in

Figure 1. The specimen was clamped in the fixture as illustrated in Figure 2. The air cylinder insured that a constant clamping pressure was maintained on the root section of the specimen over the entire temperature range. This fixture also allowed for thermal expansion of the fixture and high temperature creep of the clamping bolts.

The force gage, mounted in series with the clamping bolt and the air cylinder, was used to measure the response of the specimen. The force gage was well removed from the high temperature environment.

An electromagnetic transducer was used to excite the specimen. This transducer was specially designed to operate from room temperature to at least 1,000°C. The design used a closed loop cooling system incorporating a modified room air conditioner. A block diagram of the apparatus and complete measuring system is shown in Figure 3, and Figure 4 is a schematic of the transducer cooling system.

The specimen and fixture were placed in the furnace and heated to the desired temperature, usually above the annealing temperature of the enamel. The cantilever beam specimen was excited at its free end by a sinusoidally varying magnetic force induced by the electromagnetic transducer. A high Curie temperature cobalt disc was attached to the end of the beam to allow for excitation of the nonmagnetic specimens. The frequency of oscillation was varied until a resonance was detected. At resonance the shear force in the beam reached a maximum and was measured by the dynamic force gage. The force gage measured the variation of the shear force at the root of the cantilever beam specimen.

2.2 CALCULATION OF DAMPING PROPERTIES

The damping characteristics of the coatings were determined by measuring the vibration response of a composite cantilever beam at varying temperatures over the viscoelastic range. It is assumed that the enamel is a viscoelastic material; that is, the modulus of the enamel can be treated as a complex quantity

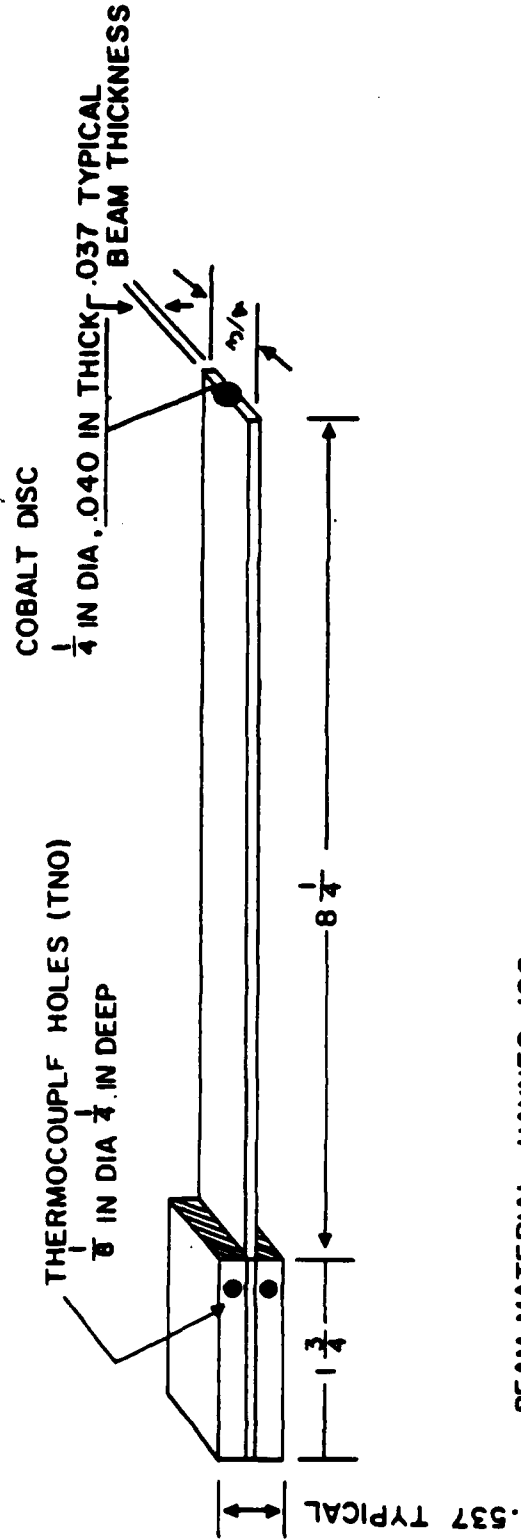
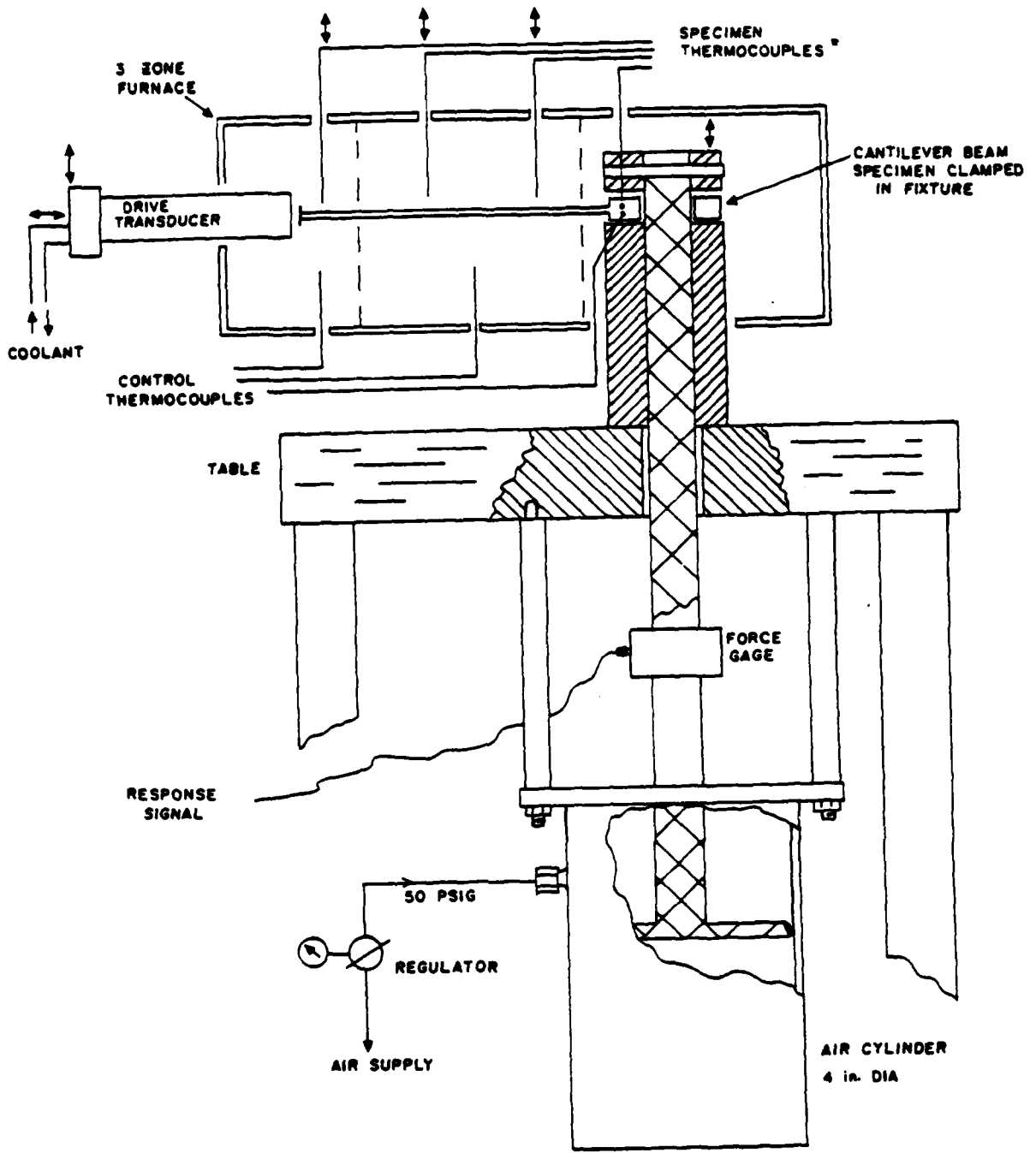
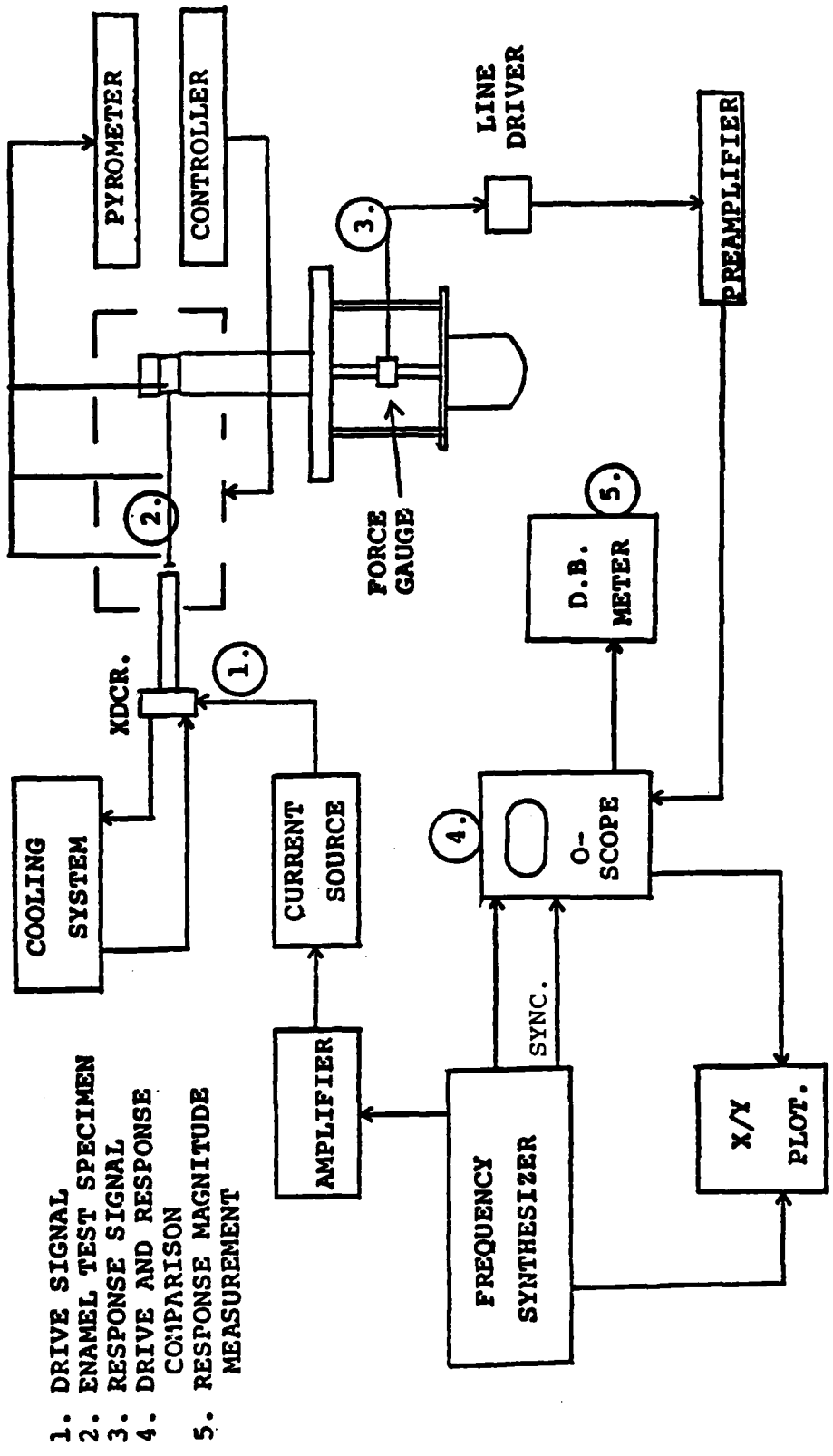


Figure 1. Typical Cantilever Beam Specimen for High Temperature Damping Material Evaluation.



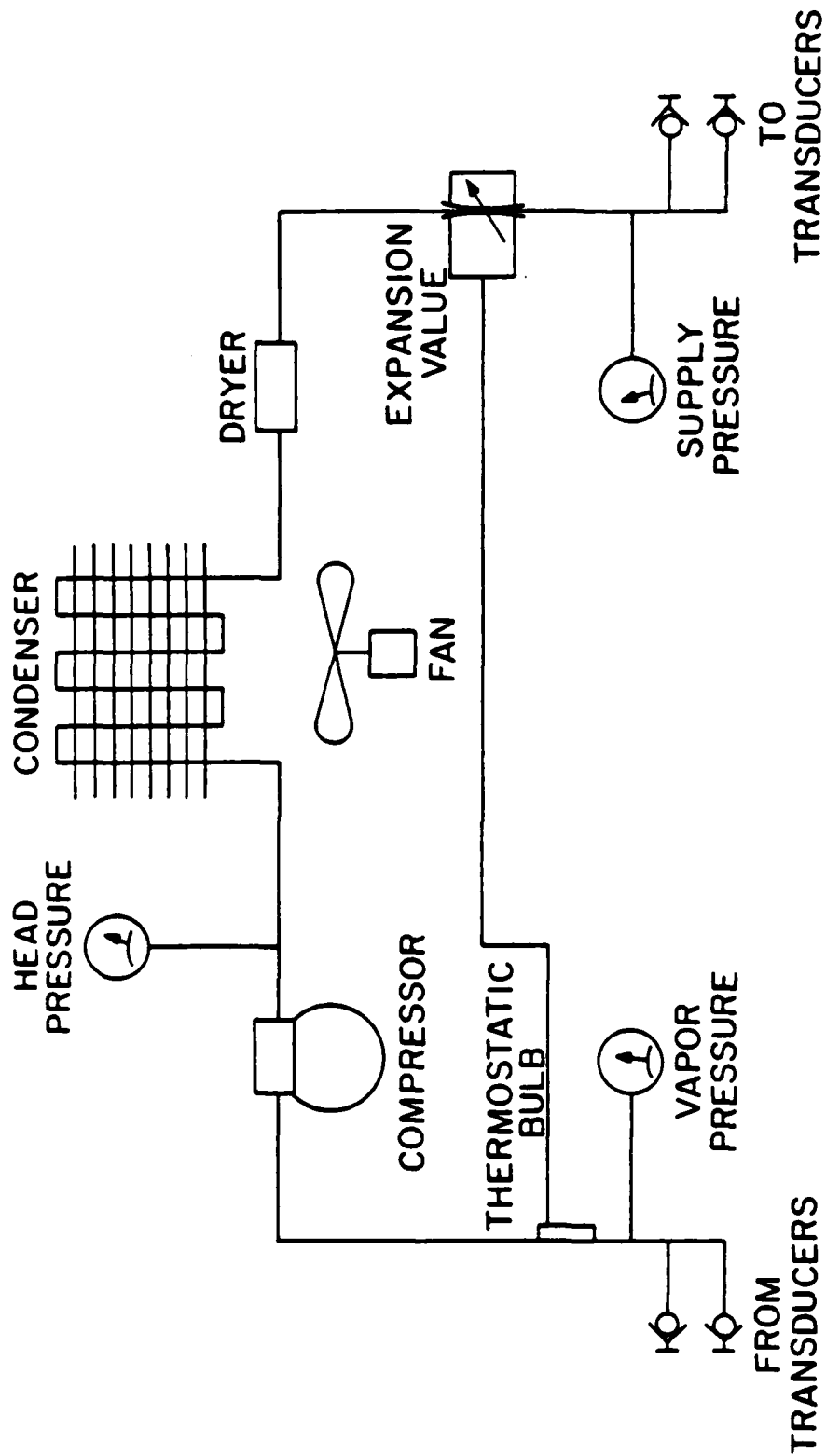
* LIFTED OFF BEAM WHEN MEASUREMENTS MADE; ONE FIXED IN ROOT

Figure 2. High Temperature Damping Test Apparatus.



1. DRIVE SIGNAL
2. ENAMEL TEST SPECIMEN
3. RESPONSE SIGNAL
4. DRIVE AND RESPONSE COMPARISON
5. RESPONSE MAGNITUDE MEASUREMENT

Figure 3. BLOCK DIAGRAM OF HIGH-TEMPERATURE TEST APPARATUS



(REFRIGERANT IS R-12)

Figure 4. Schematic of High Temperature Damping Test Apparatus Cooling System.

$$E_D^* = E_D' + iE_D'' = E_D' (1 + i \tan \delta)$$

$$\eta_2 = \tan \delta = E_D''/E_D'$$

where E_D' is the storage or Young's Modulus of the enamel and $\tan \delta$ is the ratio of the dissipative modulus, E_D'' , to the storage modulus.

Consider the metal beam with an enamel coating on one side as shown in Figure 5.

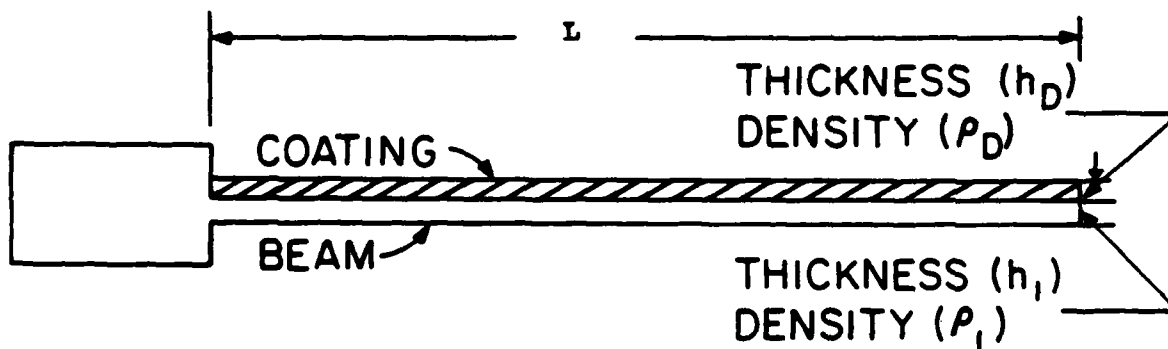


Figure 5. Coated Oberst Test Beam

The formulas developed by Oberst [8] and used by many other investigators were used to determine the damping properties of the enamel as a function of frequency and temperature. These formulas are:

$$(\omega_n/\omega_{1n})^2 (1+h_D \rho_D/h_1 \rho_1) = \frac{1 + 2(E_D/E_1)(h_D/h_1)A + (E_D/E_1)^2(h_D/h_1)^4}{1 + (E_D/E_1)(h_D/h_1)} \quad (1)$$

and

$$\frac{\eta}{\eta_2} = \frac{(E_D/E_1)(h_D/h_1)[2A+2(E_D/E_1)(h_D/h_1)^3 + (E_D/E_1)^2(h_D/h_1)^4 - 1]}{[1+(E_D/E_1)(h_D/h_1)][1+2A(E_D/E_1)(h_D/h_1) + (E_D/E_1)^2(h_D/h_1)^4]} \quad (2)$$

where:

$$A = 2 + 3(h_D/h_1) + 2(h_D/h_1)^2. \quad (3)$$

ω_n = natural frequency of the nth mode of the composite beam,
 $2\pi f_n$, rad/sec

ω_{1n} = natural frequency of the nth mode of the metal beam,
 $2\pi f_{1n}$, rad/sec

h_D = thickness of enamel coating applied to composite beam

h_1 = thickness of metal beam

ρ_D = density of enamel coating

ρ_1 = density of metal beam

E_D = real part of the modulus of enamel coating

E_1 = Young's modulus of metal beam

$\tan \delta_e$ = effective loss factor of composite beam (= η)

$\tan \delta$ = loss factor of enamel coating (= η_2)

The quantities of h_D , h_1 , ρ_D , and ρ_1 are known and are assumed to remain constant with temperature. The parameters, ω_n , ω_{1n} , and η are experimentally measured. The value of η is determined from

$$\eta = \tan \delta_e = \frac{\Delta \omega_n}{\omega_n} = \frac{\Delta f_n}{f_n} \quad (4)$$

where Δf_n is the bandwidth at the half-power points of the response peak for the nth mode. The value of E_1 can be determined from the measured response of the uncoated metal beam using

$$\xi_n^4 = \mu_1 \omega_{1n}^2 L^4 / E_1 I_1 \quad (5)$$

where:

ξ_n^4 = the eigen value corresponding to the nth mode and is a constant, determined by the boundary conditions

$\mu_1 = \rho_1 b h_1$ = the mass per unit length of the metal beam

L = the length of the beam

$I = \frac{1}{12} b h_1^3$ = the second moment of area of the metal beam about its centerline.

The values of ξ_n^4 for beam with classical boundary conditions are well known and can be found in reference [9]. Thus, from the measured resonant frequencies of the coated and bare beams and the measured composite loss factor, $\tan \delta_e$, the damping properties of the enamel can be determined as a function of temperature and frequency.

The resonant frequencies and modal damping of five to six modes of the coated beam, covering a frequency range of 100 Hz to 1,500 Hz, can usually be measured for each temperature. Thus, the damping properties of the vitreous coating over a decade of frequency at a given temperature can be easily and quickly determined.

SECTION III
RESULTS AND DISCUSSION

During the development of high temperature vibration damping enamels, one of the primary goals has been to develop a better understanding of the effects of structure, composition, and physical properties on the damping behavior of vitreous enamels. In view of this goal, several experimental and theoretical investigations were conducted. Those investigations can be broadly classified as follows:

- Damping properties of new compositions;
- Relationship between the glass transition temperature and the damping temperature;
- Effect of nucleation and crystallization on the viscoelastic damping;
- Constrained layer damping with vitreous enamels.

3.1 DAMPING PROPERTIES OF NEW COMPOSITIONS

3.1.1 Mixed Alkali Glasses

As indicated in Section I, mixed alkali glasses exhibit a characteristic damping peak at lower temperatures (100-200°C). It has also been noted that some commercial glasses containing mixed alkali exhibit intense and broad damping peaks. Therefore, it was hypothesized that there is a relationship between the viscoelastic damping and presence of mixed alkali in the composition. In order to verify the hypothesis, an experiment was designed in which alkali oxides were systematically varied. Properties of the glasses, i.e., the thermal expansion, damping behavior, and their thermal stability in the damping range were determined. This subsection describes the results of the experimental design on the mixed alkali glasses and also recommends the future course of the investigation.

Molar composition of the glasses and their properties are summarized in Table 1. Compositions numbered 1 through 6 have been obtained from the $\text{Li}_2\text{O}-\text{K}_2\text{O}-\text{SiO}_2$ system. The coefficient of

thermal expansion shows a linear increase as Li_2O is replaced by the K_2O , which is also graphically shown in Figure 6. The coefficients of thermal expansion of $\text{Li}_2\text{O}\cdot 3\text{SiO}_2$ and $\text{K}_2\cdot 3\text{SiO}_2$ glasses are $53 \times 10^{-7}/^\circ\text{C}$ and $140 \times 10^{-7}/^\circ\text{C}$ respectively. There is a slight variation in T_g ; however, the diatomic softening point exhibits a general decrease as the Li_2O is replaced by K_2O . These glasses also exhibited varying degrees of thermal stability. For example, the composition 1 becomes opaque after the powdered frit was applied and vitrified on the metallic substrate. Compositions 2 and 2A became opaque during the damping measurements. Compositions 3, 3A, and 4 remained unchanged after the damping measurements. General appearance of the glass compositions 2, 2A, 3, 3A, and 4 after damping measurements are shown in Figure 7. Compositions 5 and 6 could not be successfully applied on to the metallic substrate, possibly because of the extreme hygroscopic nature of these compositions.

All compositions from the system $\text{Li}_2\text{O}\text{-Na}_2\text{O}\text{-SiO}_2$ (7 through 11) exhibited unstable behavior during application and damping measurements and therefore were dropped . experimental investigation.

Reduced Temperature Nomograms for compositions 2, 3, and 4 are shown in Figures 8, 9, and 10 respectively, with experimental and reduced data given in Tables 2, 3, and 4. Composition 2 shows a broad and relatively high loss factor as compared to compositions 3 and 4. In order to make a direct comparison of loss factor of the three compositions, Figure 11 exhibits a plot of the loss factor at 100 Hz versus temperature.

It is obvious that only a narrow compositional range of the mixed alkali series exhibit stable glasses whose damping properties could be satisfactorily determined. It appears that the damping properties of these stable compositions are superior than other multicomponent commercial compositions. However, further investigations are needed to substantiate any relationship between the presence of mixed alkali and viscoelastic damping.

TABLE 1
GLASS COMPOSITIONS AND THEIR PROPERTIES

	Molar Composition	α ($\times 10^7$)	T _g	Dialtomic Soft. Point	Remarks
1	Li ₂ O · 3SiO ₂	52.3	475	630°C	Opaque during application
2	2K ₂ O · 8Li ₂ O · 3SiO ₂	70.9	481	537°C	} Opaque after damping measurement
2A					
3	0.4K ₂ O · 0.6Li ₂ O · 3SiO ₂	89.3	475	531°C	} Stable compositions
3A					
4	0.6K ₂ O · 0.4Li ₂ O · 3SiO ₂	104.6	469	518°C	} Powder could not be vitrified
5	0.8K ₂ O · 0.2Li ₂ O · 3SiO ₂	121.0	469	518°C	
6	K ₂ O · 3SiO ₂	140.0			} All of these glasses exhibited unstable behavior during application and damping measurements
7	0.2Na ₂ O · 0.8Li ₂ O · 3SiO ₂				
8	0.4Na ₂ O · 0.6Li ₂ O · 3SiO ₂				
9	0.6Na ₂ O · 0.4Li ₂ O · 3SiO ₂				
10	0.8Na ₂ O · 0.2Li ₂ O · 3SiO ₂				
11	Na ₂ O · 3SiO ₂				

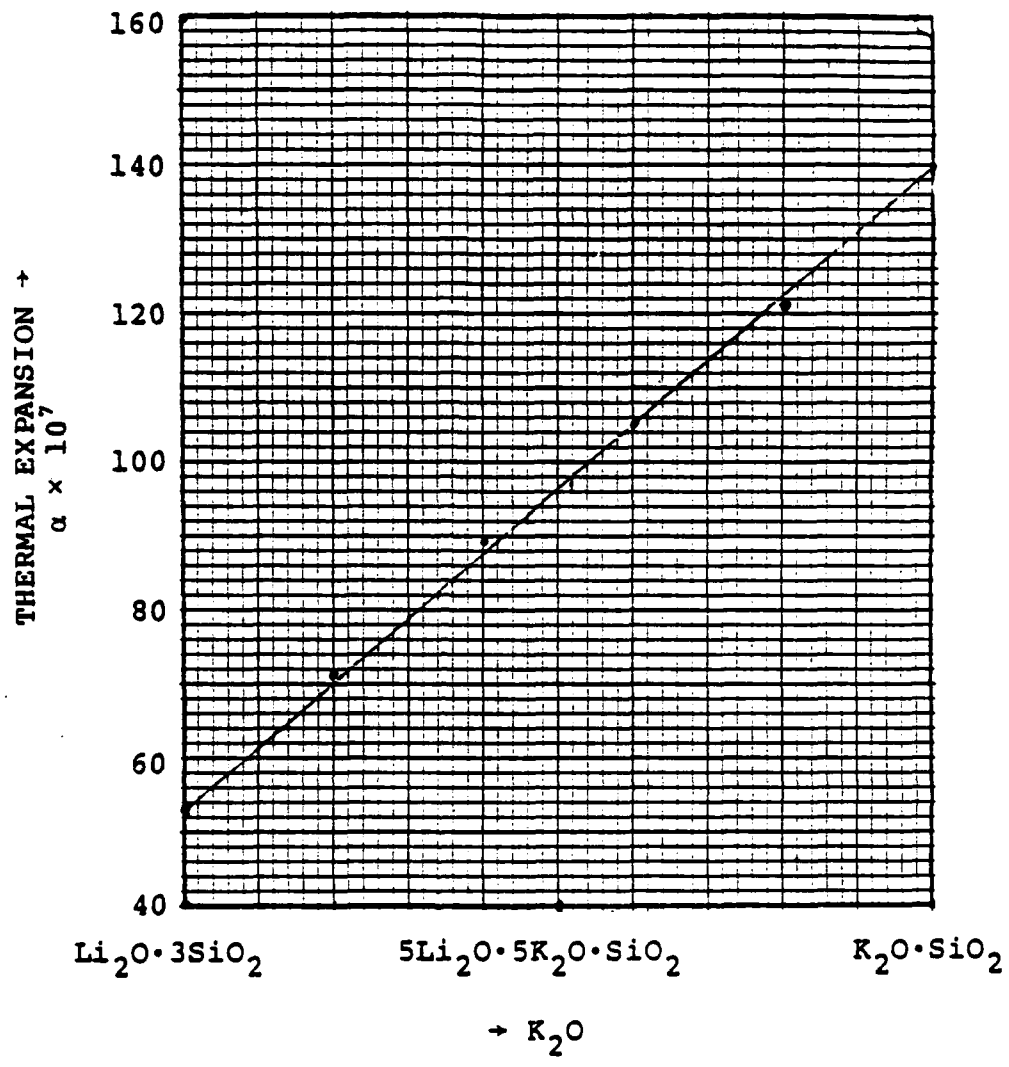


Figure 6. Effect of K_2O Substitution for Li_2O on the Thermal Expansion Coefficient.

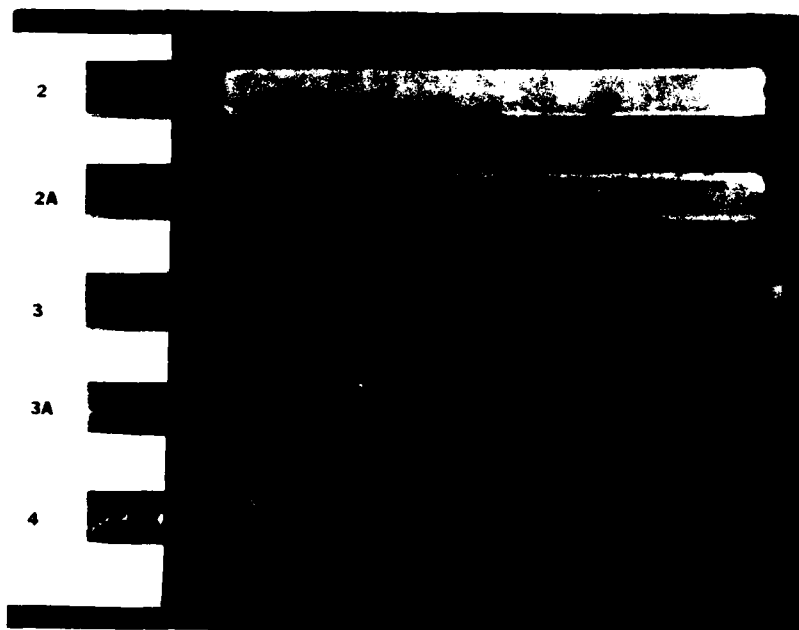


Figure 7. Appearance of the Glass Coatings After Damping Measurements. Numbers on the Left Indicate Glass Composition.

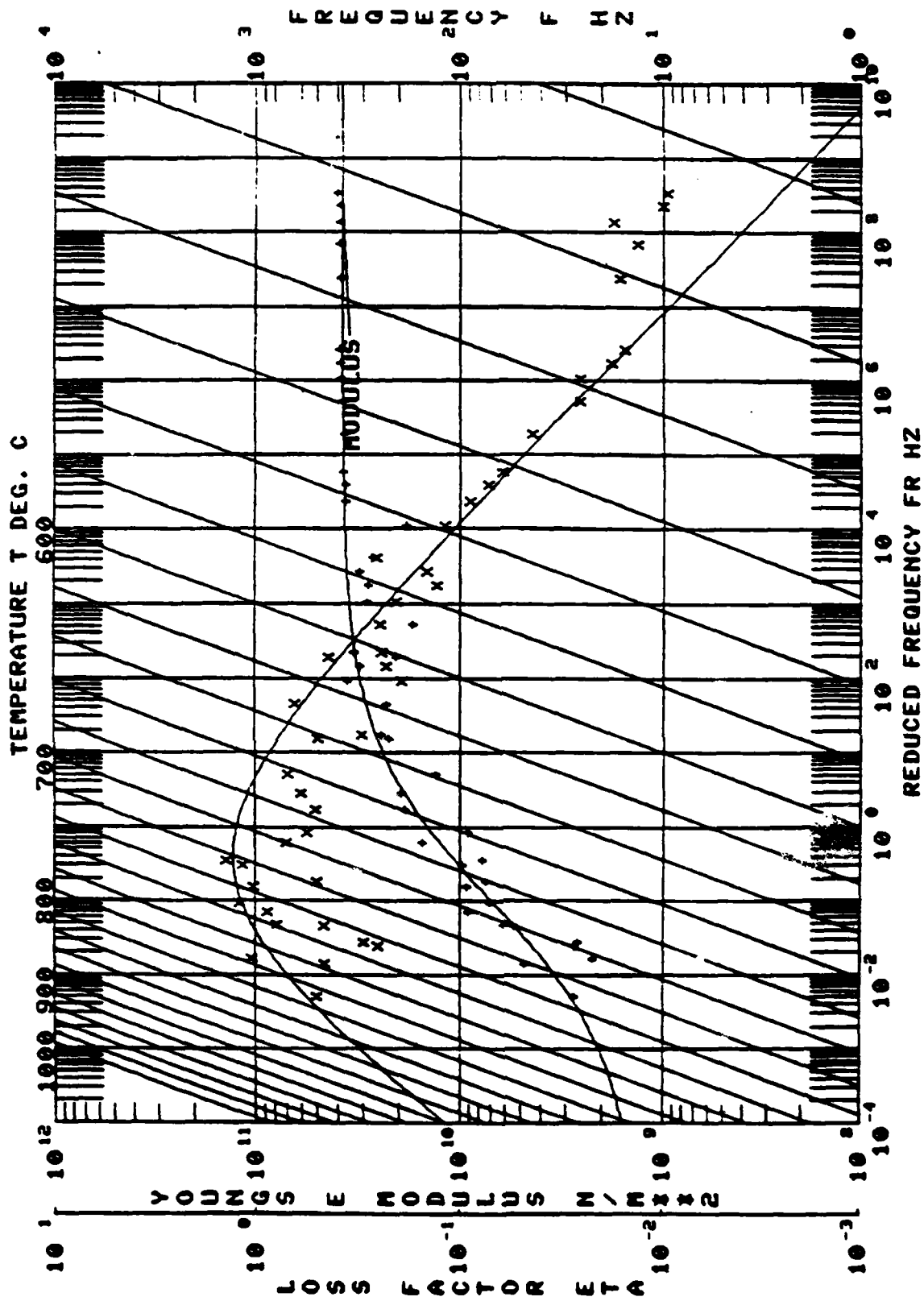


Figure 8. Reduced Frequency Nomogram Showing Loss Factor and Young's Modulus for Composition 2.

TABLE 2
EXPERIMENTAL AND REDUCED DATA OF COMPOSITION 2 (AM2)

EXPERIMENTAL CODE	LOSS FACTOR	TEMP. DEG. C	FREQ. MZ	MODE NO.	BEAM MOD. N/MR2	COMPOSITE LOSS FAK.	BEAM FREQ. MZ	LOSS MOD. N/MR2
1 2-09491E+10	.4184	593.3	105.3	3.	1.88517E+11	.0680	100.8	9.39423E+09
1 74589E+10	.2508	593.3	292.9	2.	1.89179E+11	.0328	282.8	4.37877E+09
3 92132E+10	.2119	593.3	597.4	4.	1.88515E+11	.0412	553.3	6.19037E+09
2 85451E+10	.1330	593.3	987.9	6.	1.89569E+11	.0254	917.2	3.81025E+09
5 15096E+10	.1481	593.3	1491.1	5.	1.90906E+11	.0301	1372.4	4.65599E+09
3 21717E+09	3.5973	648.9	98.0	3.	1.83577E+11	.1541	99.5	1.73289E+10
1 34654E+10	.7151	648.9	284.4	3.	1.84273E+11	.0774	278.4	9.62928E+09
2 47741E+10	.3076	648.9	964.0	5.	1.84437E+11	.0533	904.7	7.62111E+09
2 18148E+09	2.5310	704.4	95.5	3.	1.77759E+11	.0344	93.1	5.54661E+09
7 5803E+09	.5121	704.4	273.6	3.	1.77916E+11	.0997	274.2	3.88570E+09
1 56397E+10	1.4258	704.4	537.2	4.	1.79577E+11	.0981	537.5	1.13196E+10
8 41596E+08	2.4308	760.0	93.4	5.	1.72818E+11	.0203	96.6	2.04573E+09
4 92972E+09	.4766	760.0	266.6	3.	1.72636E+11	.0221	270.2	2.34932E+09
2 52725E+09	.3025	760.0	517.2	4.	1.72842E+11	.0079	529.8	8.16374E+08
6 20661E+09	.8055	760.0	873.2	5.	1.74504E+11	.0458	880.0	4.99022E+09
9 36896E+09	.3033	760.0	1323.0	6.	1.75165E+11	.0744	1314.6	8.48063E+09
2 79161E+09	.5142	787.8	261.9	3.	1.69963E+11	.0141	268.1	1.43549E+02
1 45397E+03	2.3752	787.8	851.9	6.	1.73715E+11	.0324	878.0	3.30899E+09
2 81542E+09	.2569	787.8	1244.7	6.	1.72616E+11	.0070	1305.0	7.23536E+08
2 27805E+02	1.4764	732.2	95.3	3.	1.75589E+11	.0245	97.9	2.42524E+09
5 09153E+02	1.2321	732.2	269.6	4.	1.75286E+11	.0812	272.5	2.65898E+09
7 32531E+09	1.0453	732.2	532.0	5.	1.77091E+11	.0858	533.5	9.02560E+09
9 44988E+02	1.1711	732.2	892.6	5.	1.82235E+11	.0585	886.5	9.82255E+09
9 38923E+02	.5749	676.7	99.6	3.	1.82099E+11	.0458	277.5	5.40332E+09
1 92233E+10	.5200	676.7	278.8	3.	1.80693E+11	.0762	541.7	9.99578E+09
2 28880E+10	.5363	621.1	941.6	5.	1.82046E+11	.0917	898.8	1.21805E+10
3 60479E+10	.6544	621.1	106.0	2.	1.86095E+11	.0833	100.2	1.16394E+10
1 87353E+10	1.369	621.1	297.0	3.	1.85426E+11	.1101	280.0	1.54385E+10
3 15975E+10	.2342	621.1	922.0	4.	1.86139E+11	.0446	910.8	7.40024E+09
3 40208E+10	.2487	621.1	1495.0	5.	1.88933E+11	.0844	1402.4	8.46241E+09
1 87353E+10	1.202	565.6	111.5	2.	2.03225E+11	.0458	104.7	7.12379E+09
3 71789E+10	.0911	565.6	294.7	3.	1.87781E+11	.0166	283.3	3.38637E+09
3 74444E+10	.0742	565.6	616.0	4.	1.91045E+11	.0697	557.0	3.38637E+09
3 84529E+10	.0633	565.6	1020.6	5.	1.91766E+11	.0169	922.5	2.77835E+09
3 75577E+10	.0262	565.6	1530.3	6.	1.93041E+11	.0146	1380.1	2.43895E+09
3 8027E+10	.0262	537.8	112.3	2.	1.93031E+11	.0103	102.0	1.74396E+02
3 9653E+10	.0262	537.8	316.3	3.	1.92879E+11	.0060	285.6	9.95200E+08
3 9672E+10	.0125	537.8	622.0	4.	1.93039E+11	.0061	559.9	1.02216E+09
3 90478E+10	.0158	537.8	1030.3	5.	1.94066E+11	.0043	928.0	7.23015E+08
3 93747E+10	.0168	537.8	1544.5	6.	1.95488E+11	.0037	1388.7	6.59973E+08
3 96626E+10	.0136	510.0	113.9	3.	1.95155E+11	.0032	102.0	6.59973E+08
3 94071E+10	.0180	510.0	318.9	4.	1.94093E+11	.0042	286.5	5.41045E+08
3 90710E+10	.0107	510.0	625.9	4.	1.95391E+11	.0024	553.3	7.12774E+08
4 00886E+10	.0098	510.0	1037.1	5.	1.96192E+11	.0024	933.1	4.09348E+08
4 00886E+10	.0098	510.0	1564.4	6.	1.97614E+11	.0023	1396.4	3.97007E+08

REDUC : PAUSE 0000

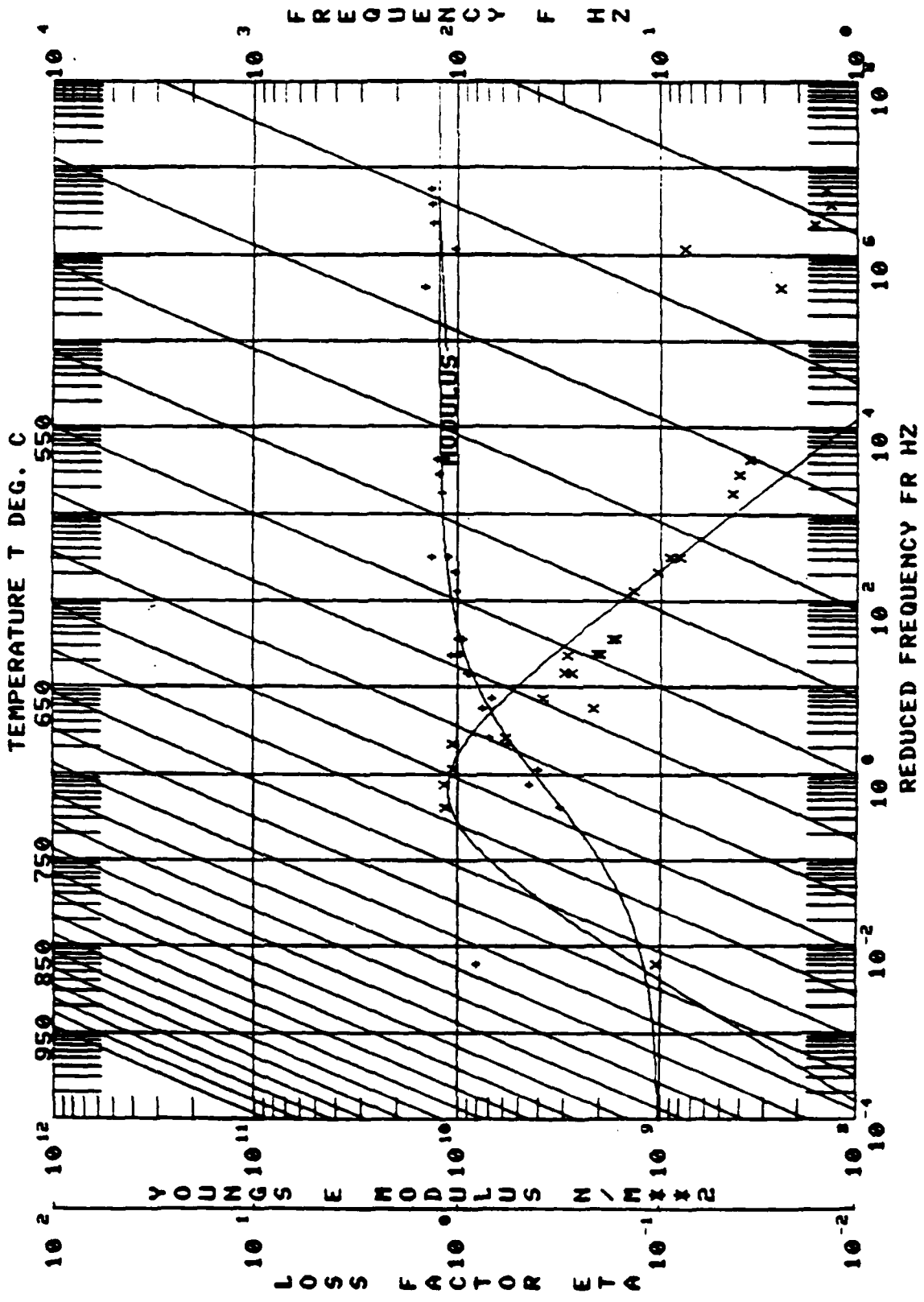


Figure 9. Reduced Frequency Nomogram Showing Loss Factor and Young's Modulus for Composition 3.

TABLE 3
EXPERIMENTAL AND REDUCED DATA OF COMPOSITION 3 (AM3)

NO.	MODULUS N/MHz	LOSS FACTOR	TEMP. DEG. C	FREQ. HZ	MODE NO.	BEAM MOD. N/MHz	COMPOSITE LOSS FAC.	BEAM FREQ. HZ	LOSS MOD. N/MHz
1	8.22310E+09	.1068	732.2	254.5	3	2.63037E+10	.0023	256.5	8.78419E+08
2	2.01079E+10	.2315	704.4	279.7	3	2.85302E+10	.0388	257.5	4.65563E+09
3	1.90555E+10	.2516	676.7	279.8	3	2.67382E+10	.0386	258.9	4.85214E+09
4	1.53587E+09	3.0993	676.7	1257.0	6	2.71725E+10	.0485	1259.2	4.76019E+09
5	2.70890E+10	.1978	648.9	291.0	3	2.73956E+10	.0378	261.3	5.35921E+09
6	1.59830E+09	3.3800	648.9	511.0	4	2.26670E+10	.0548	511.8	5.40219E+09
7	4.54881E+09	1.1947	648.9	359.0	5	2.73592E+10	.0524	847.9	5.13424E+09
8	4.09717E+09	1.0646	648.9	1282.0	6	2.75198E+10	.0421	1268.3	4.36172E+09
9	3.20703E+09	1.1302	621.1	94.3	2	2.75198E+10	.0371	93.7	3.78504E+09
10	5.78747E+09	1.0567	621.1	525.0	4	2.78456E+10	.0590	515.3	6.28941E+09
11	7.72716E+09	.2504	621.1	1312.0	6	2.79236E+10	.0154	1276.6	1.70553E+09
12	7.12644E+09	.5894	593.3	95.7	2	2.79020E+10	.0383	94.4	4.20036E+09
13	9.85019E+09	.3045	593.3	536.0	2	2.80008E+10	.0273	518.6	2.74855E+09
14	9.02722E+09	.2099	593.3	891.0	5	2.81195E+10	.0180	859.1	2.06774E+09
15	9.63473E+09	1.769	593.3	1331.0	2	2.82930E+10	.0148	1284.9	1.70392E+09
16	1.10151E+10	.2900	565.6	59.0	2	2.82387E+10	.0273	95.0	3.20452E+09
17	1.03252E+10	.1376	565.6	542.1	4	2.83474E+10	.0122	521.8	1.42075E+09
18	1.05955E+10	.1053	565.6	399.2	5	2.84873E+10	.0095	864.7	1.11520E+09
19	1.12991E+10	.0813	565.6	1347.6	6	2.86331E+10	.0077	1292.6	9.16385E+08
20	1.35679E+10	.0906	537.8	100.6	2	2.86352E+10	.0077	95.6	1.22830E+09
21	1.25390E+10	.0402	537.8	549.5	4	2.86754E+10	.0045	524.3	5.43936E+08
22	1.29436E+10	.0408	537.8	911.3	5	2.88217E+10	.0042	869.2	5.11382E+08
23	1.05577E+10	.0361	537.8	1364.5	6	2.89223E+10	.0038	1300.5	4.67422E+08
24	1.05577E+10	.0777	482.2	282.7	3	2.96658E+10	.0067	272.4	2.13803E+08
25	1.34922E+10	.0167	482.2	527.1	4	2.95608E+10	.0018	570.1	2.24747E+08
26	1.36243E+10	.0138	482.2	923.6	5	2.96038E+10	.0015	878.5	1.86425E+08
27	8.04158E+09	.6931	593.3	97.1	2	2.79029E+10	.0595	94.4	5.61343E+09
28	6.01981E+09	3.001	593.3	271.0	2	2.80123E+10	.0246	264.7	2.69911E+09
29	9.1353E+09	.2802	593.3	556.4	4	2.80008E+10	.0227	518.6	2.57336E+09
30	9.87001E+09	.2026	593.3	891.1	5	2.81195E+10	.0174	859.1	1.99936E+09
31	1.03252E+10	.1639	593.3	1335.0	6	2.82930E+10	.0150	1284.9	1.74396E+09
32	1.47876E+10	.0250	482.2	102.1	2	2.93102E+10	.0029	96.7	3.68963E+08
33	1.37888E+10	.0147	482.2	1382.6	6	2.96251E+10	.0016	1314.8	2.02661E+08

REDUC : PAUSE 0000
REDUC SUSP

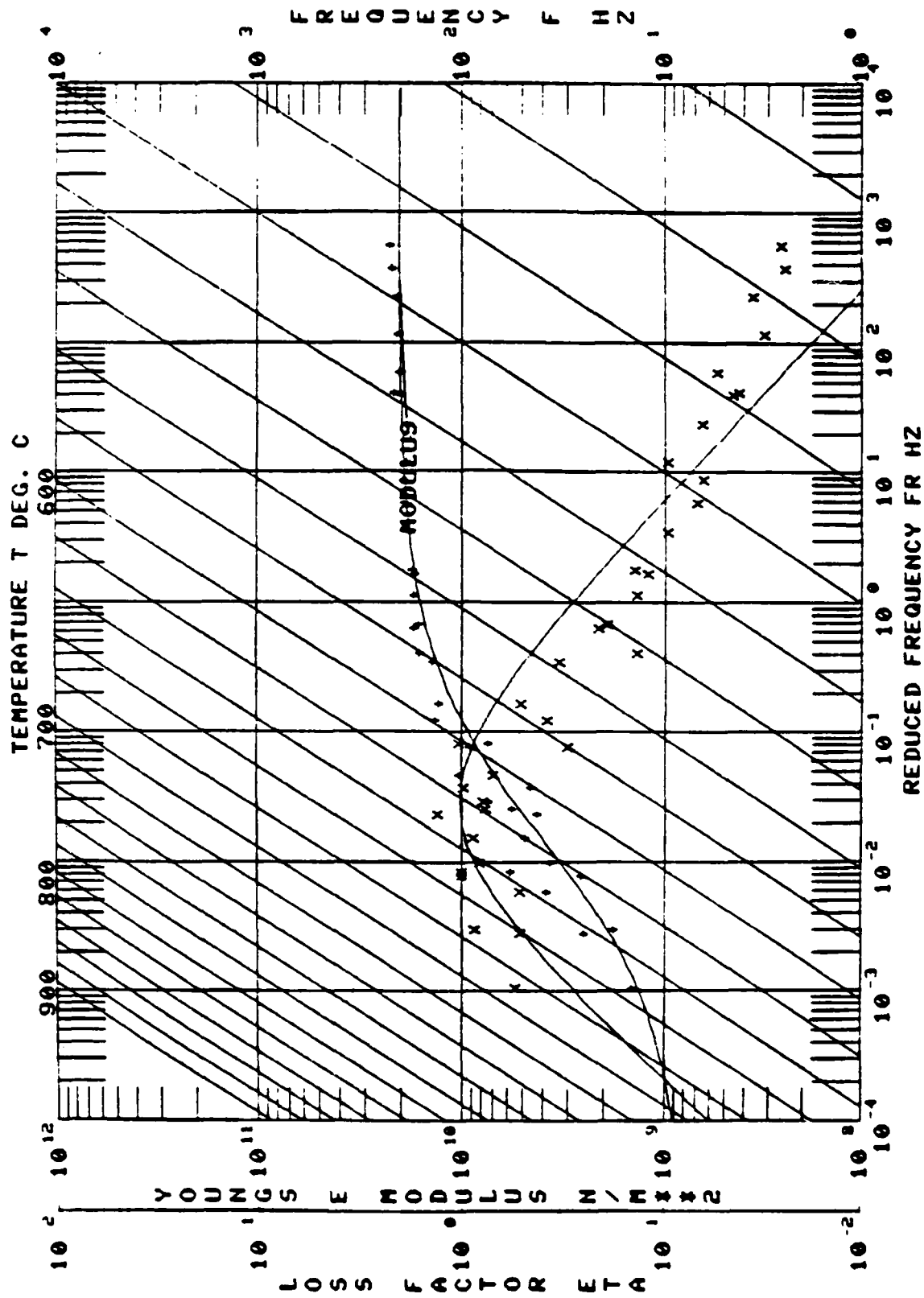


Figure 10. Reduced Temperature Nomogram Showing Loss Factor and Young's Modulus for Composition 4.

TABLE 4
EXPERIMENTAL AND REDUCED DATA OF COMPOSITION 4 (AM4)

EXPERIMENTAL CODE 1189
MATERIAL :01-40-3,4084,72.48NS102.22.72V.20.4.8VLI20

MANUFACTURER INONE
DATA SOURCES

UDRI :UDRI
OTHER INONE

NO.	MODULUS N/MIKZ	LOSS FACTOR	TEMP. DEG. C	FREQ. HZ	MODE NO.	BEAM MOD. H/MIKZ	COMPOSITE LOSS FAC.	BEAM FREQ. HZ	LOSS MOD. N/MIKZ
1	1.49922E+09	.5616	704.4	95.1	2	1.53366E+11	.0072	98.0	9.41892E+08
2	1.87826E+09	.8852	704.4	266.3	3	1.23128E+11	.0139	274.0	1.62715E+09
3	3.95185E+09	.5296	704.4	525.6	4	1.52493E+11	.0175	536.0	2.09296E+09
4	3.78597E+09	.3753	704.4	872.0	5	1.84125E+11	.0263	890.0	3.16618E+09
5	2.56848E+09	.5284	676.7	96.0	2	1.35545E+11	.0114	98.5	1.35729E+09
6	2.64235E+09	1.0296	676.7	269.1	3	1.35311E+11	.0227	276.0	2.75067E+09
7	5.09315E+09	1.9001	676.7	532.7	4	1.85914E+11	.0368	541.0	4.53568E+09
8	5.83131E+09	.7876	676.7	855.0	5	1.85228E+11	.0384	896.0	4.59255E+09
9	4.68835E+09	1.0020	676.7	1308.8	6	1.85228E+11	.0482	1331.0	4.69763E+09
10	5.89734E+09	1.0249	648.9	97.8	2	1.87434E+11	.0473	99.0	6.04434E+09
11	4.35183E+09	1.3459	648.9	272.9	3	1.88514E+11	.0573	278.0	5.86136E+09
12	1.06104E+10	.7172	648.9	548.2	4	1.88514E+11	.0573	545.0	7.60997E+09
13	9.40075E+09	.3095	642.9	904.9	5	1.89543E+11	.0221	903.0	2.90930E+09
14	7.59365E+09	.8075	621.1	99.3	2	1.90957E+11	.0472	279.9	6.13217E+09
15	7.67278E+09	1.0512	621.1	278.2	3	1.90957E+11	.0502	549.3	6.95473E+09
16	1.33304E+10	.5217	621.1	557.7	4	1.91662E+11	.0162	1354.5	2.31939E+09
17	1.64943E+10	1.1406	621.1	1390.7	5	1.91927E+11	.0381	100.6	5.35313E+09
18	1.38505E+10	.3855	593.3	286.7	2	1.93565E+11	.0341	281.7	4.80992E+09
19	1.41368E+10	.3398	593.3	566.8	3	1.93565E+11	.0227	552.1	3.27947E+09
20	1.66198E+10	.1973	593.3	940.3	4	1.93595E+11	.0170	912.6	2.48141E+09
21	1.76703E+10	1.1444	593.3	1403.5	5	1.94338E+11	.0149	1363.3	2.17783E+09
22	1.70005E+10	1.245	593.3	204.3	2	1.96283E+11	.0255	101.3	3.80924E+09
23	1.76745E+10	.2155	565.6	104.3	2	1.96283E+11	.0175	282.7	2.59267E+09
24	1.80093E+10	1.1440	565.6	292.4	3	1.96283E+11	.0122	555.9	1.81597E+09
25	1.85045E+10	.0981	565.6	573.9	4	1.96283E+11	.0122	913.0	1.38496E+09
26	1.98213E+10	.0784	565.6	952.4	5	1.96277E+11	.0092	1322.7	1.3321E+09
27	2.00399E+10	.0658	565.6	1424.1	6	1.97017E+11	.0087	285.4	1.88979E+09
28	1.90915E+10	.0990	537.2	295.0	3	1.98683E+11	.0125	550.3	1.27124E+09
29	1.91901E+10	.0562	537.2	578.3	4	1.98774E+11	.0034	924.5	9.32854E+08
30	2.05998E+10	.0460	537.2	959.9	5	1.98676E+11	.0061	1381.1	1.15475E+09
31	2.06925E+10	.055	537.2	1334.7	6	1.99435E+11	.0075	102.5	9.57130E+08
32	2.20304E+10	.0434	510.0	106.9	2	2.01039E+11	.0064	287.5	6.89552E+08
33	2.1954E+10	.0320	510.0	299.2	3	2.01618E+11	.0050	562.6	7.78911E+08
34	2.1731E+10	.0365	510.0	585.4	4	2.01656E+11	.0036	930.0	5.67084E+08
35	2.24580E+10	.0253	510.0	971.0	5	2.01030E+11	.0038	1389.2	6.03810E+08
36	2.30810E+10	.0262	510.0	1453.0	6	2.0171E+11	.0023	107.1	3.75550E+08
37	1.84680E+10	.0203	398.9	109.8	2	2.19360E+11	.0021	299.7	3.41444E+08
38	1.81913E+10	.0128	398.9	307.1	3	2.19092E+11	.0021	587.0	5.51211E+08
39	1.79782E+10	.0307	398.9	601.1	4	2.18974E+11	.0034	974.6	3.42273E+08
40	1.77278E+10	.0193	398.9	936.2	5	2.20793E+11	.0020	1409.6	3.38210E+08
41	2.75254E+10	.0123	398.9	1491.1	6	2.07771E+11	.0020		

REDUC 1 PAUSE 0000
REDUC SUSP

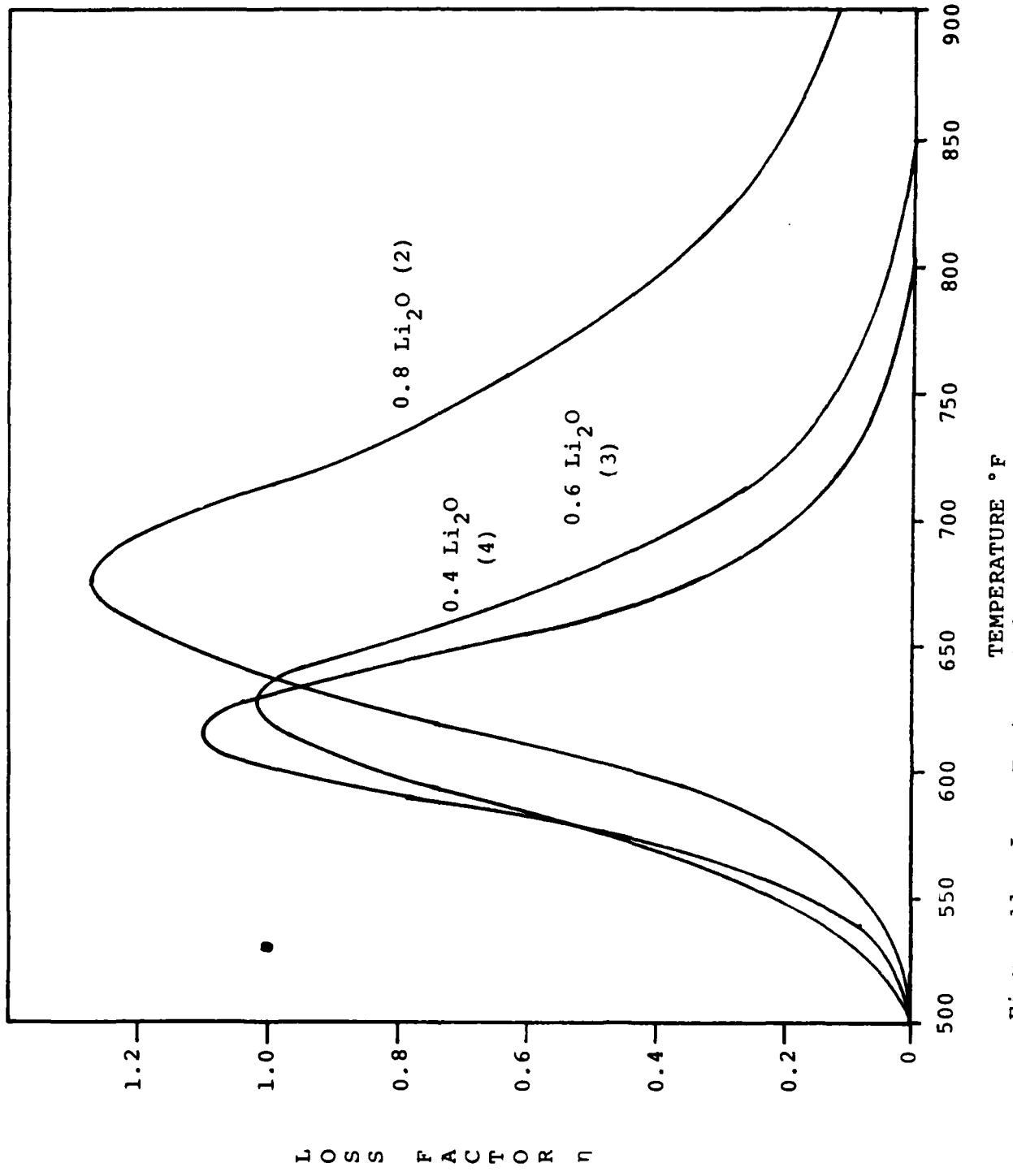


Figure 11. Loss Factor at 100 Hz Versus Temperature for 2, 3, and 4, Mixed Alkali Glasses.

3.1.2 Fluoride Glass

This material was formulated and synthesized in our laboratory and is different from other materials in the sense that it develops two phase structure upon heat treatment. The beams were coated using the standard plasma spray technique. Damping data for the material before and after heat treatment are shown in Figures 12 and 13 respectively. Before heat treatment, the material exhibits a damping peak typical of many vitreous enamel compositions (Figure 12). After heat treatment, the peak becomes broader and the peak intensity decreases. This interesting damping behavior of the material after heat treatment believed to have resulted from the two phase structure.

3.1.3. Lead Silicate Compositions

Damping properties of several compositions from the PbO-SiO₂-R₂O system were evaluated. Table 5 shows the compositions of the glasses as calculated from the batch ingredients. The table also shows general characteristics of the glasses. It is noted that the incorporation of alkali oxide (R₂O) in mixture rather than a single oxide helps in stabilizing the glass as evidenced by compositions III, V, VII, IX, X, and XI.

Loss factors as a function of temperature of the seven stable compositions from Table 5 are shown in Figures 14 through 20, with experimental and reduced data given in Tables 6, 7, 8, 9, 10, 11, and 12.

TABLE 5
COMPOSITIONS (PERCENT WEIGHT) OF LEAD SILICATE GLASSES

	I	II	III	IV	V	VI	VII	VIII	IX	X	XI
SiO ₂	49.02	45.9	44.3	49.02	44.3	44.3	43.9	43.9	44.3	44.3	44.3
PbO	40.02	45.9	44.3	49.02	44.3	44.3	43.9	43.9	44.3	44.3	44.3
K ₂ O	1.96	--	1.7	--	1.7	--	1.7	3.3	1.7	3.4	5.1
Na ₂ O	--	8.2	8.0	1.96	9.7	11.4	7.2	7.2	6.3	6.3	6.3
Li ₂ O	--	--	1.7	--	--	--	3.3	1.7	3.4	1.7	--
Remarks	Devitrified (Opacified)	Devitrified	Stable Glass	Devitrified	Stable Glass	Devitrified	Stable Glass	Stable Glass	Stable Glass	Stable Glass	Stable Glass

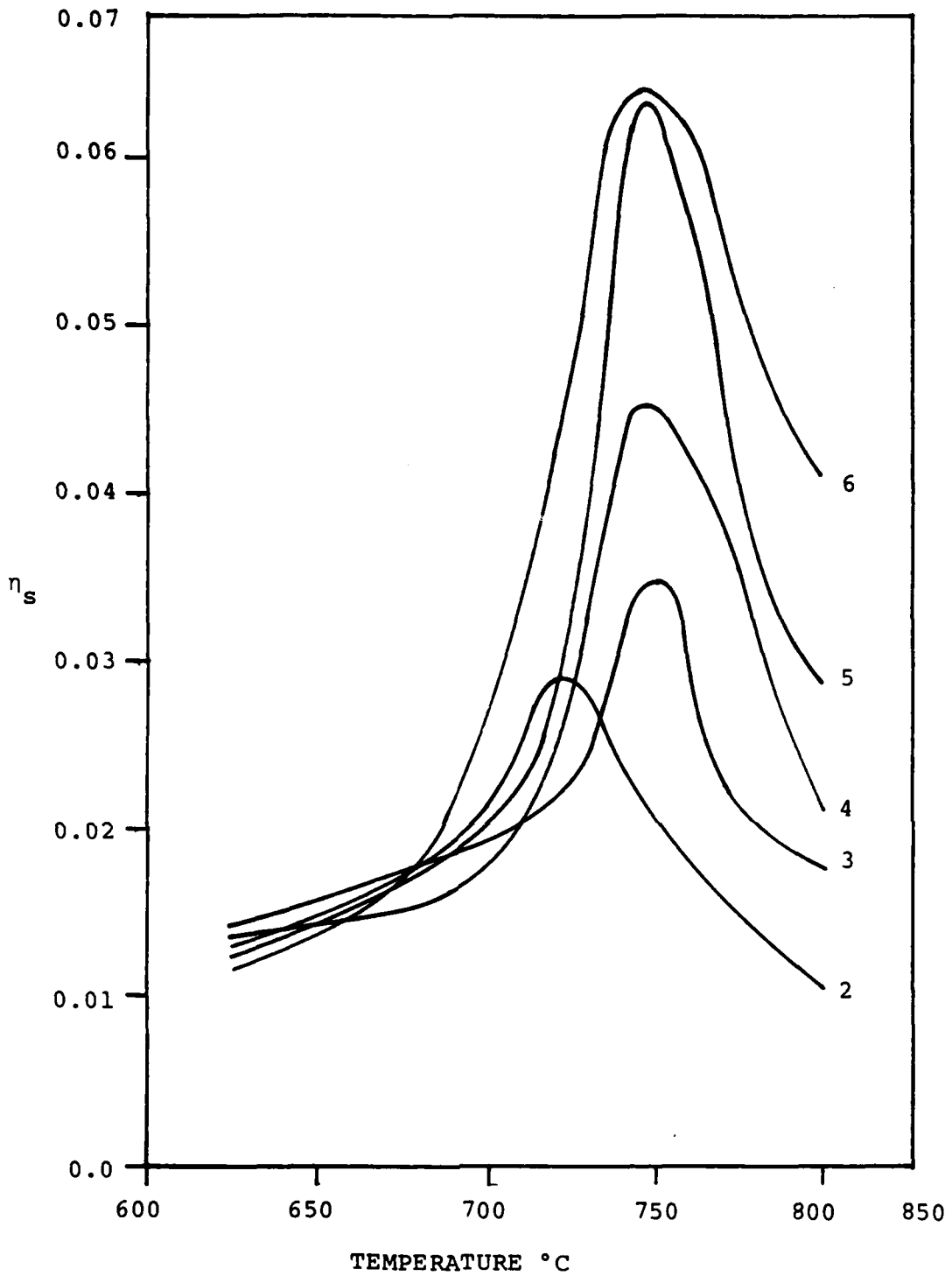


Figure 12. Modal Damping from Fluoride Material
 (Number Superimposed on the Curves
 Indicate Mode Number)

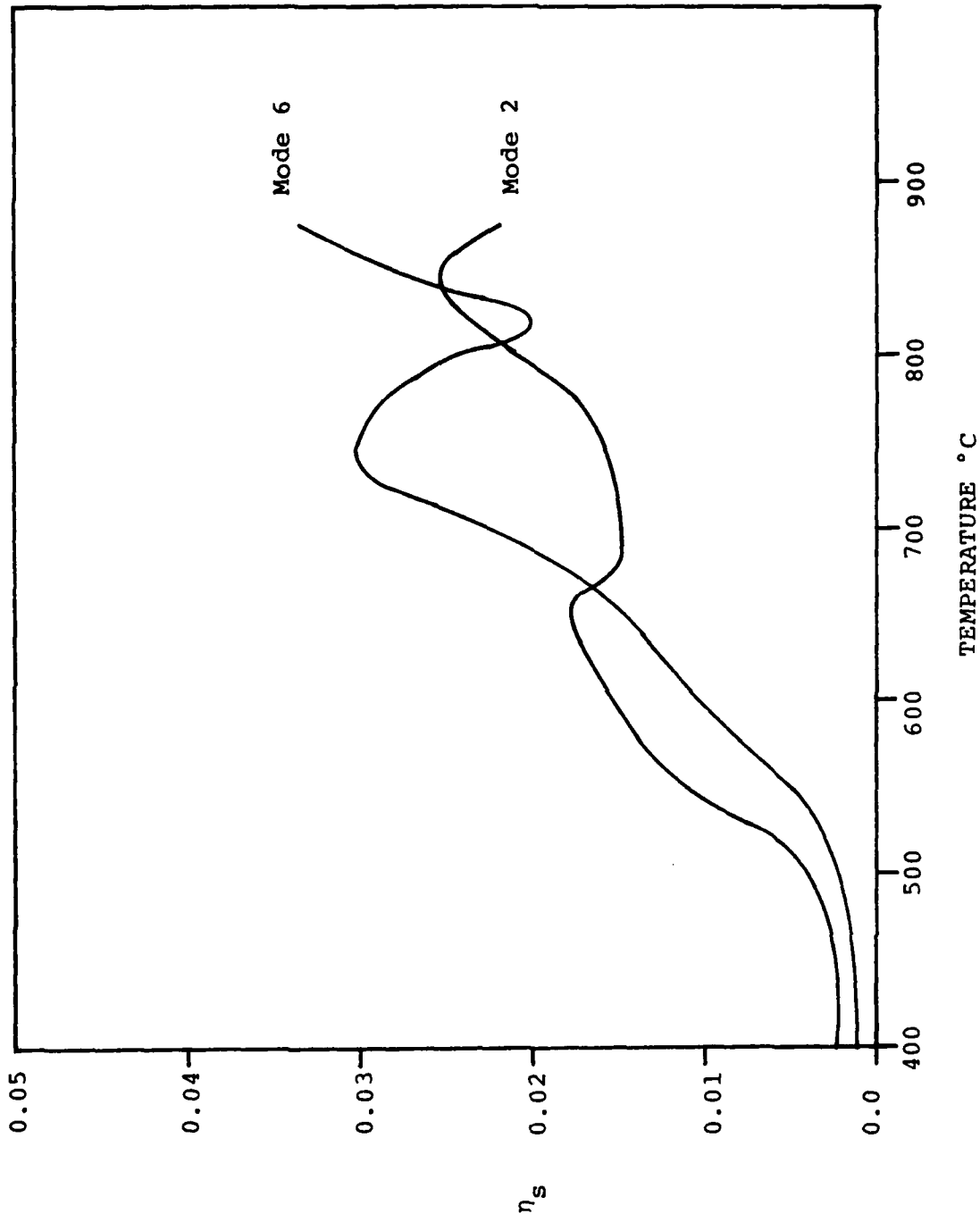


Figure 13. Modal Damping From Fluoride Material After Heat Treatment at 800°C for 20 Hours.

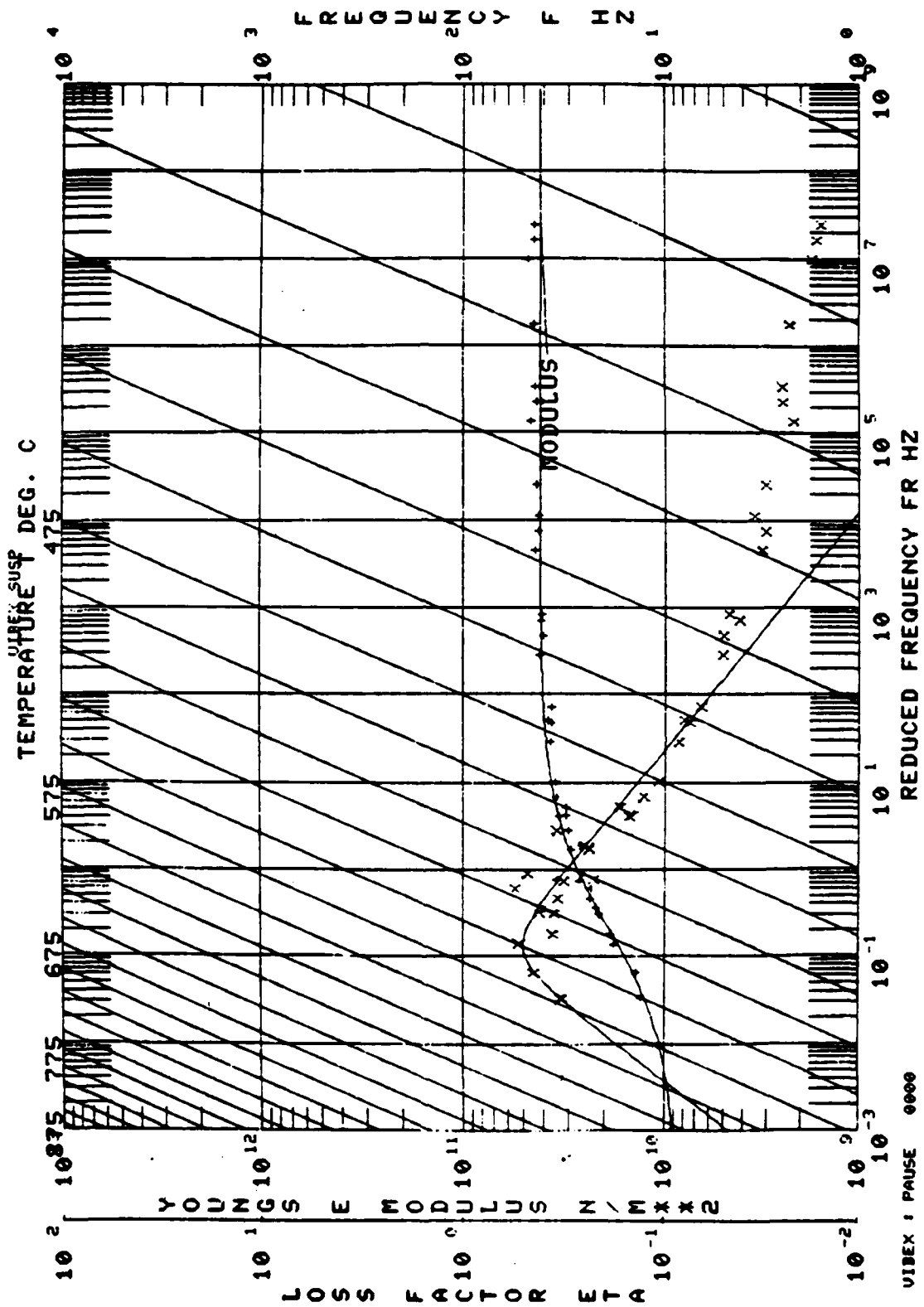
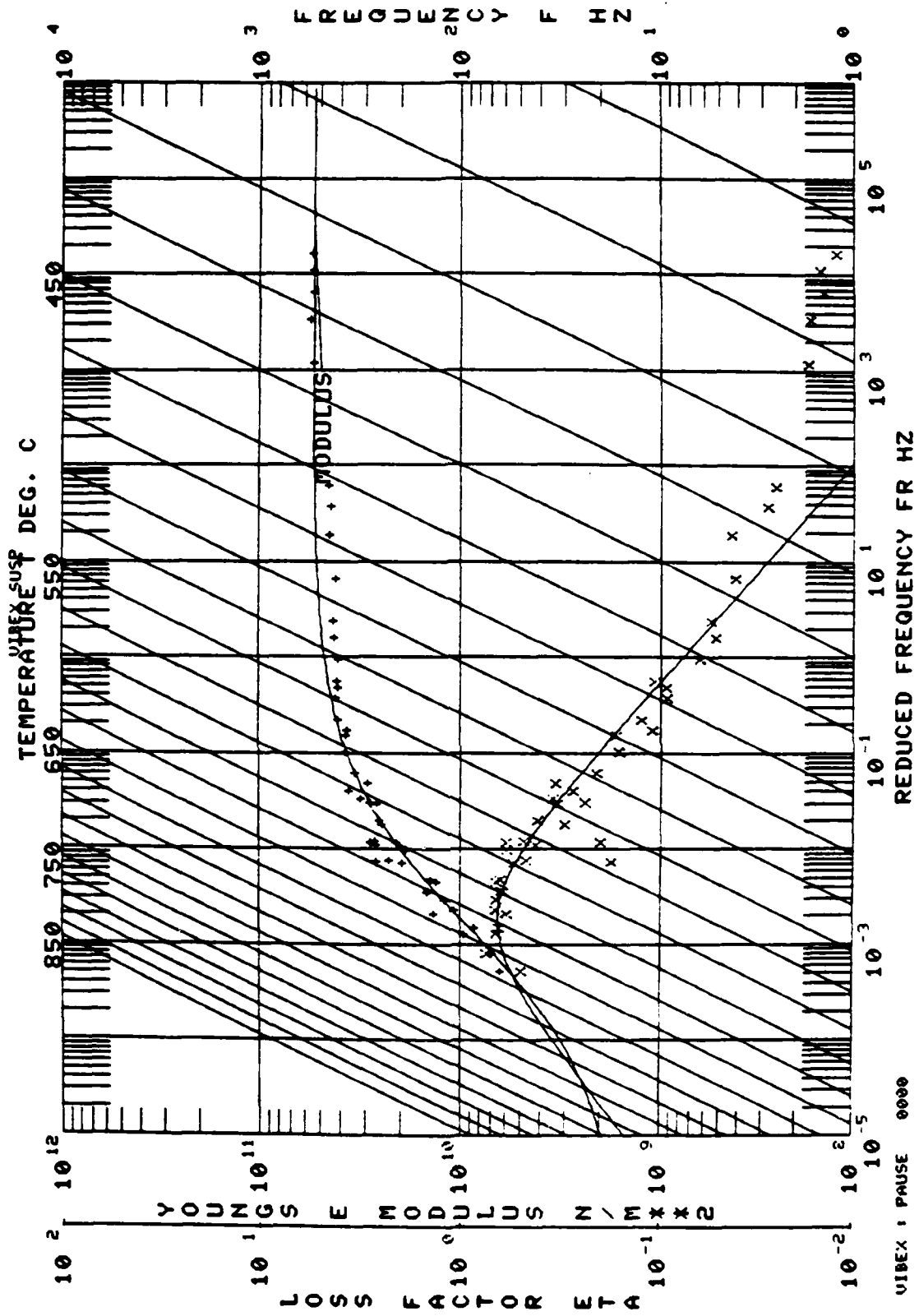


Figure 14. Reduced Nomogram for Composition III

TABLE 6
EXPERIMENTAL AND REDUCED DATA OF COMPOSITION III (AMB3)

NO.	MODULUS N/MT2	LOSS FACTOR	TEMP. DEG. C	FREQ. HZ	MODE NO.	BEAM NOF. N MT2	COMPOSITE LOSS FAC.	BEAM FREQ. HZ	LOSS MOD. N/MT2
1	1.3460E+10	.3401	593.3	38.9	2.	1.8926E+11	.0166	101.4	4.5774E+09
2	1.9034E+10	.3676	593.3	548.1	4.	1.9002E+11	.0246	556.3	6.9951E+09
3	2.2064E+10	.3602	593.3	913.5	5.	1.9120E+11	.0274	922.5	7.9616E+09
4	2.4101E+10	.3459	593.3	1371.5	6.	1.9262E+11	.0282	1380.6	8.3357E+09
5	2.4183E+10	.4529	579.4	99.2	2.	1.9050E+11	.0231	101.6	6.4241E+09
6	2.2490E+10	.4047	579.4	552.6	4.	1.9089E+11	.0313	557.6	9.1021E+09
7	2.3719E+10	.5632	579.4	918.0	5.	1.9207E+11	.0452	924.6	1.3477E+10
8	2.6562E+10	.4967	579.4	1380.2	6.	1.9354E+11	.0343	1383.9	1.3194E+10
9	1.8385E+10	.5429	565.6	100.3	2.	1.9197E+11	.0268	101.9	9.9819E+09
10	3.5061E+10	.2530	565.6	559.0	4.	1.8637E+11	.0258	551.7	8.1678E+09
11	2.6698E+10	.4283	565.6	1384.2	6.	1.9469E+11	.0258	1385.0	6.8931E+09
12	2.1581E+10	.4283	551.7	101.1	4.	1.9317E+11	.0216	102.2	9.2427E+09
13	2.9756E+10	.2460	551.7	562.4	4.	1.9315E+11	.0210	560.9	7.3196E+09
14	3.0836E+10	.3531	551.7	934.3	5.	1.9453E+11	.0353	930.5	1.0889E+10
15	3.1820E+10	.1484	551.7	1399.9	6.	1.9595E+11	.0151	1392.5	4.7100E+09
16	2.7069E+10	.3234	537.8	102.3	2.	1.9438E+11	.0259	102.6	8.7424E+09
17	3.4315E+10	.1545	537.8	568.2	4.	1.9440E+11	.0169	562.7	5.3415E+09
18	3.5146E+10	.1307	537.8	943.3	5.	1.9570E+11	.0145	933.3	4.5926E+09
19	3.5623E+10	.1102	537.8	1411.8	6.	1.9702E+11	.0123	1396.3	3.9257E+09
20	3.1769E+10	.1793	510.0	103.7	2.	1.9667E+11	.0173	103.1	5.4114E+09
21	3.7855E+10	.0775	510.0	573.8	4.	1.9626E+11	.0143	565.4	3.3132E+09
22	3.7100E+10	.0766	510.0	951.5	5.	1.9818E+11	.0058	939.2	2.8432E+09
23	3.7420E+10	.0670	510.0	1424.0	6.	1.9963E+11	.0077	1405.5	2.5065E+09
24	3.8903E+10	.0515	482.2	105.3	2.	1.9873E+11	.0097	103.7	3.1688E+09
25	4.2750E+10	.0521	482.2	580.8	4.	1.9835E+11	.0057	568.4	2.2253E+09
26	4.1465E+10	.0517	482.2	962.6	5.	2.0064E+11	.0054	945.0	2.1293E+09
27	4.2034E+10	.0424	482.2	1441.6	6.	2.0205E+11	.0050	1414.0	1.7802E+09
28	4.1630E+10	.0481	454.4	106.2	2.	2.0081E+11	.0050	101.4	2.0020E+09
29	4.5091E+10	.0323	454.4	585.5	4.	2.0045E+11	.0043	571.4	1.4550E+09
30	4.3244E+10	.0313	454.4	970.0	5.	2.0306E+11	.0040	950.7	1.3573E+09
31	4.3208E+10	.0355	454.4	1451.5	6.	2.0443E+11	.0045	1422.3	1.5344E+09
32	4.4517E+10	.0313	426.7	107.1	2.	2.0270E+11	.0041	104.7	1.3975E+09
33	4.7822E+10	.0226	426.7	589.9	4.	2.0249E+11	.0031	574.3	1.0687E+09
34	4.4944E+10	.0255	426.7	977.5	5.	2.0542E+11	.0033	956.2	1.1367E+09
35	4.5521E+10	.0234	386.9	1462.5	6.	2.0679E+11	.0033	1430.5	1.1465E+09
36	4.8654E+10	.0234	386.9	107.8	2.	2.0472E+11	.0031	105.2	1.0703E+09
37	4.8654E+10	.0180	388.9	593.7	4.	2.0454E+11	.0025	577.2	8.7423E+08
38	4.5305E+10	.0169	398.9	983.6	5.	2.0788E+11	.0022	961.9	7.6752E+08
39	4.5872E+10	.0161	398.9	1472.0	6.	2.0925E+11	.0021	1439.0	7.3838E+08

REDUC 1 PAUSE
REDUC SUSP



VIBEX : PAUSE 0000

Figure 15. Reduced Nomogram for Composition V

TABLE 7
EXPERIMENTAL AND REDUCED DATA OF COMPOSITION V (AMB5)

EXPERIMENTAL CODE :212
 MATERIAL :01-33-4; AM B5
 DATA SOURCES
 MANUFACTURER UDRI BEAM COATED ONE SIDE
 UDRI UDRI
 OTHER IN

NO.	MODULUS N/RYE2	LOSS FACTOR	TEMP. DEG. C	FREQ. HZ	MODE NO.	BEAM DIA. N. MINZ	COMPOSITE LOSS FAC.	BEAM FREQ. HZ	LOSS MOD. N/RYE2
1	6.44317E+09	.5072	676.7	96.0	2.	1.32323E+11	.0177	99.6	3.26791E+09
2	8.70944E+09	.6503	676.7	230.0	3.	1.21757E+11	.0307	278.4	5.75069E+09
3	1.22841E+10	.6752	676.7	534.6	4.	1.52121E+11	.0430	545.1	8.29477E+09
4	1.43353E+10	.6487	676.7	891.0	5.	1.82705E+11	.0472	905.6	9.29977E+09
5	2.68527E+10	.7815	676.7	1372.6	6.	1.84230E+11	.0235	1353.8	4.87431E+09
6	7.18260E+09	.7821	662.3	26.5	2.	1.83672E+11	.0298	99.9	5.41805E+09
7	1.10527E+10	.6879	662.3	212.6	3.	1.83065E+11	.0396	279.4	7.60324E+09
8	1.34876E+10	.6739	662.3	538.0	4.	1.83391E+11	.0464	542.0	9.08932E+09
9	2.30032E+10	.4817	662.3	912.5	5.	1.84451E+11	.0525	908.5	1.10862E+10
10	2.87067E+10	.2037	662.3	1382.6	6.	1.85511E+11	.0255	1358.5	5.84767E+09
11	3.86682E+09	.6793	648.9	97.5	4.	1.84702E+11	.0454	100.2	6.71532E+09
12	1.47122E+10	.6392	648.9	275.9	3.	1.84115E+11	.0474	230.2	9.40371E+09
13	1.98942E+10	.5489	648.9	538.1	4.	1.84453E+11	.0529	549.6	1.09192E+10
14	2.71981E+10	.4953	648.9	924.0	5.	1.85428E+11	.0617	911.0	1.34716E+10
15	2.52350E+10	.3083	643.9	1376.1	6.	1.86879E+11	.0359	1363.5	7.78054E+09
16	1.38398E+10	.5339	635.0	93.0	2.	1.86402E+11	.0414	100.7	8.25463E+09
17	2.14193E+10	.6041	635.0	522.0	4.	1.85876E+11	.0616	551.7	1.29386E+10
18	2.64654E+10	.3329	635.0	1383.8	6.	1.88069E+11	.0401	1367.8	8.81044E+09
19	1.50703E+10	.6199	621.1	99.5	2.	1.87551E+11	.0462	101.0	9.34241E+09
20	1.96873E+10	.5952	621.1	230.9	3.	1.87017E+11	.0548	282.4	1.13797E+10
21	2.58149E+10	.4221	621.1	559.5	4.	1.87226E+11	.0500	553.7	1.08967E+10
22	3.22346E+10	.3541	621.1	940.7	5.	1.88329E+11	.0499	918.0	1.14132E+10
23	2.95002E+10	.3745	621.1	1337.5	6.	1.89735E+11	.0432	1372.2	1.10177E+10
24	2.69567E+10	.4324	593.3	102.9	2.	1.89973E+11	.0525	101.6	1.16730E+10
25	3.45184E+10	.2125	593.3	238.8	3.	1.89499E+11	.0312	284.2	6.99839E+09
26	3.81715E+10	.1642	593.3	573.7	4.	1.89735E+11	.0314	557.4	7.23356E+09
27	3.76893E+10	.1699	593.3	957.8	5.	1.90716E+11	.0261	923.8	6.26653E+09
28	3.68501E+10	.2784	593.3	1431.2	6.	1.92152E+11	.0256	1382.6	6.40313E+09
29	4.1373E+10	.1281	565.6	105.7	2.	1.92127E+11	.0215	102.4	1.02047E+10
30	4.25425E+10	.0949	565.6	585.0	4.	1.92127E+11	.0215	560.0	5.20639E+09
31	4.18916E+10	.1494	565.6	1450.0	5.	1.94214E+11	.0184	1390.0	4.03859E+09
32	3.74495E+10	.1135	537.8	106.4	2.	1.94853E+11	.0175	102.9	4.25125E+09
33	4.1213E+10	.0957	537.8	299.9	3.	1.94373E+11	.0159	287.9	3.94839E+09
34	4.16425E+10	.0546	537.8	588.4	4.	1.94533E+11	.0108	564.4	2.69029E+09
35	4.30119E+10	.0539	537.8	977.7	5.	1.95533E+11	.0092	935.4	2.31936E+09
36	4.27802E+10	.0423	482.2	108.5	2.	1.90011E+11	.0071	104.0	1.81113E+09
37	4.54888E+10	.0444	482.2	295.0	3.	1.98445E+11	.0078	290.9	2.01740E+09
38	4.51643E+10	.0286	482.2	597.7	4.	1.98699E+11	.0050	570.4	1.29246E+09
39	4.60018E+10	.0261	482.2	991.7	5.	1.99697E+11	.0046	945.3	1.19945E+09
40	5.40580E+10	.0177	426.7	111.9	2.	2.02933E+11	.0035	105.1	9.72540E+08
41	5.71527E+10	.0172	426.7	294.3	3.	2.02532E+11	.0035	293.9	9.83380E+08
42	5.47760E+10	.0147	426.7	613.3	4.	2.02540E+11	.0039	575.9	8.0388E+08
43	5.52356E+10	.0151	426.7	1016.8	5.	2.03640E+11	.0039	954.5	8.36756E+08
44	6.50844E+10	.0126	426.7	1523.0	6.	2.05152E+11	.0025	1428.6	7.04300E+08
45	4.39409E+10	.0569	537.8	1464.5	6.	1.96990E+11	.0093	1399.9	2.49880E+09

REDUC 1 PAUSE 0000
REDUC SUSP

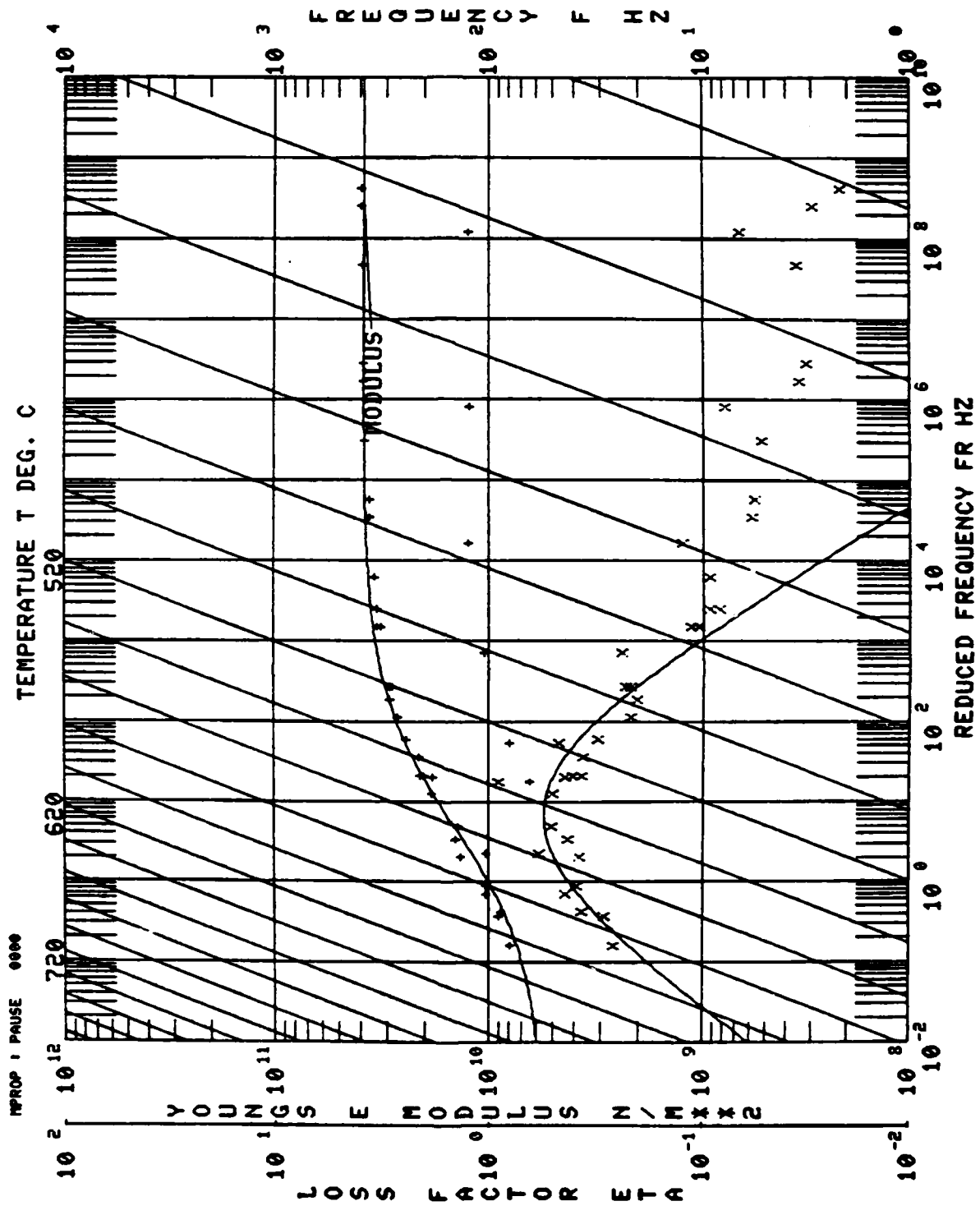


Figure 16. Reduced Nomogram for Composition VII

TABLE 8
EXPERIMENTAL AND REDUCED DATA OF COMPOSITION VII (AMB7)

EXPERIMENTAL CODE :215	MODULUS	LOSS	TEMP.	FREQ.	MODE	BEAM MOD.	COMPOSITE	BEAM FREQ.	LOSS MOD.
MATERIAL 101-40-3, AMB7	N/MI*2	FACTOR	DEG. C	HZ	NO.	(H, MI)*2	LOSS FMC.	HZ	N/MI*2
MANUFACTURER :UDRI									
UDRI :UDRI BEAM COATED ONE SIDE									
OTHER :H									
1	8.92369E+09	.3794	621.1	523.7	4.	1.30347E+11	.0237	548.5	3.38555E+09
2	1.05457E+10	.4591	621.1	881.1	5.	1.21739E+11	.0311	910.0	4.74655E+09
3	8.12439E+09	.2672	607.2	95.9	2.	1.29341E+11	.0147	921.0	2.17046E+09
4	2.13031E+10	.3754	555.6	921.3	5.	1.36394E+11	.0466	100.0	7.99680E+09
5	9.22967E+09	.2863	523.3	96.5	2.	1.94482E+11	.0182	100.0	2.73433E+09
6	1.38754E+10	.2887	593.3	540.4	4.	1.32784E+11	.0341	552.0	5.39346E+09
7	1.46859E+10	.4368	593.3	898.7	5.	1.94200E+11	.0399	916.0	6.40569E+09
8	1.05867E+10	.3922	579.4	97.3	2.	1.92200E+11	.0276	100.4	4.22601E+09
9	1.41670E+10	.5233	579.4	542.7	4.	1.94183E+11	.0464	554.0	7.41409E+09
10	1.05996E+10	.5974	565.6	98.0	2.	1.95081E+11	.0408	101.2	6.33277E+09
11	1.88223E+10	.5152	565.6	552.0	4.	1.95377E+11	.0530	555.7	9.69773E+09
12	2.04458E+10	.4171	565.6	919.0	5.	1.96394E+11	.0500	921.0	2.52786E+09
13	2.87410E+10	.2343	510.0	104.6	2.	2.00320E+11	.0363	102.6	6.73482E+09
14	3.25830E+10	.1164	510.0	580.0	4.	2.00473E+11	.0138	562.9	3.79309E+09
15	3.39138E+10	.0949	510.0	963.8	5.	2.01329E+11	.0166	932.5	3.21554E+09
16	3.5531E+10	.0535	454.4	103.1	2.	2.04049E+11	.0102	103.5	2.06274E+09
17	1.25565E+10	.0809	454.4	291.3	3.	2.03060E+11	.0062	289.1	1.01269E+09
18	3.91979E+10	.0350	454.4	525.6	4.	2.05345E+11	.0067	569.7	1.37358E+09
19	3.92175E+10	.0324	454.4	966.1	5.	2.06107E+11	.0062	943.5	1.26889E+09
20	6.57025E+09	.9277	551.7	271.4	3.	1.95959E+11	.0406	284.0	6.09547E+09
21	2.17598E+10	.3708	551.7	558.6	4.	1.96857E+11	.0467	557.8	8.06932E+09
22	1.83665E+10	.3160	551.7	933.6	5.	1.97675E+11	.0443	924.0	7.37936E+09
23	1.87534E+10	.4510	537.8	101.2	2.	1.98177E+11	.0500	102.0	8.45793E+09
24	8.18441E+09	.4839	537.8	273.7	3.	1.97342E+11	.0258	285.0	3.96032E+09
25	2.70749E+10	.2225	537.8	568.2	4.	1.97704E+11	.0333	559.0	6.02337E+09
26	2.96034E+10	.2076	537.8	947.1	5.	1.98532E+11	.0331	926.0	6.12393E+09
27	2.94540E+10	.2452	510.0	104.8	2.	2.00320E+11	.0353	102.6	6.58317E+09
28	1.07392E+10	.2452	510.0	277.0	3.	2.00266E+11	.0166	287.1	2.63345E+09
29	3.36265E+10	.1073	510.0	581.5	4.	2.00330E+11	.0187	562.7	3.61377E+09
30	3.39138E+10	.0848	482.2	963.8	5.	2.01329E+11	.0148	932.5	2.87536E+09
31	3.49308E+10	.0246	482.2	106.7	2.	2.02082E+11	.0159	103.0	3.30378E+09
32	1.28030E+10	.1270	482.2	280.5	3.	2.01518E+11	.0100	238.0	1.62656E+09
33	3.65620E+10	.0600	482.2	588.6	4.	2.02637E+11	.0110	566.0	2.19555E+09
34	3.65133E+10	.0582	482.2	974.9	5.	2.02711E+11	.0107	938.0	2.12672E+09
35	3.96355E+10	.0363	426.7	108.8	2.	2.06025E+11	.0070	104.0	1.43695E+09
36	1.27669E+10	.0625	426.7	284.1	3.	2.07155E+11	.0052	292.0	8.74942E+08
37	4.02447E+10	.0303	426.7	599.5	4.	2.07369E+11	.0052	572.5	1.21945E+09
38	4.06236E+10	.0223	426.7	933.2	5.	2.08077E+11	.0043	948.0	9.06280E+08

REDUC 1 PAUSE 0000
REDUC SUSP

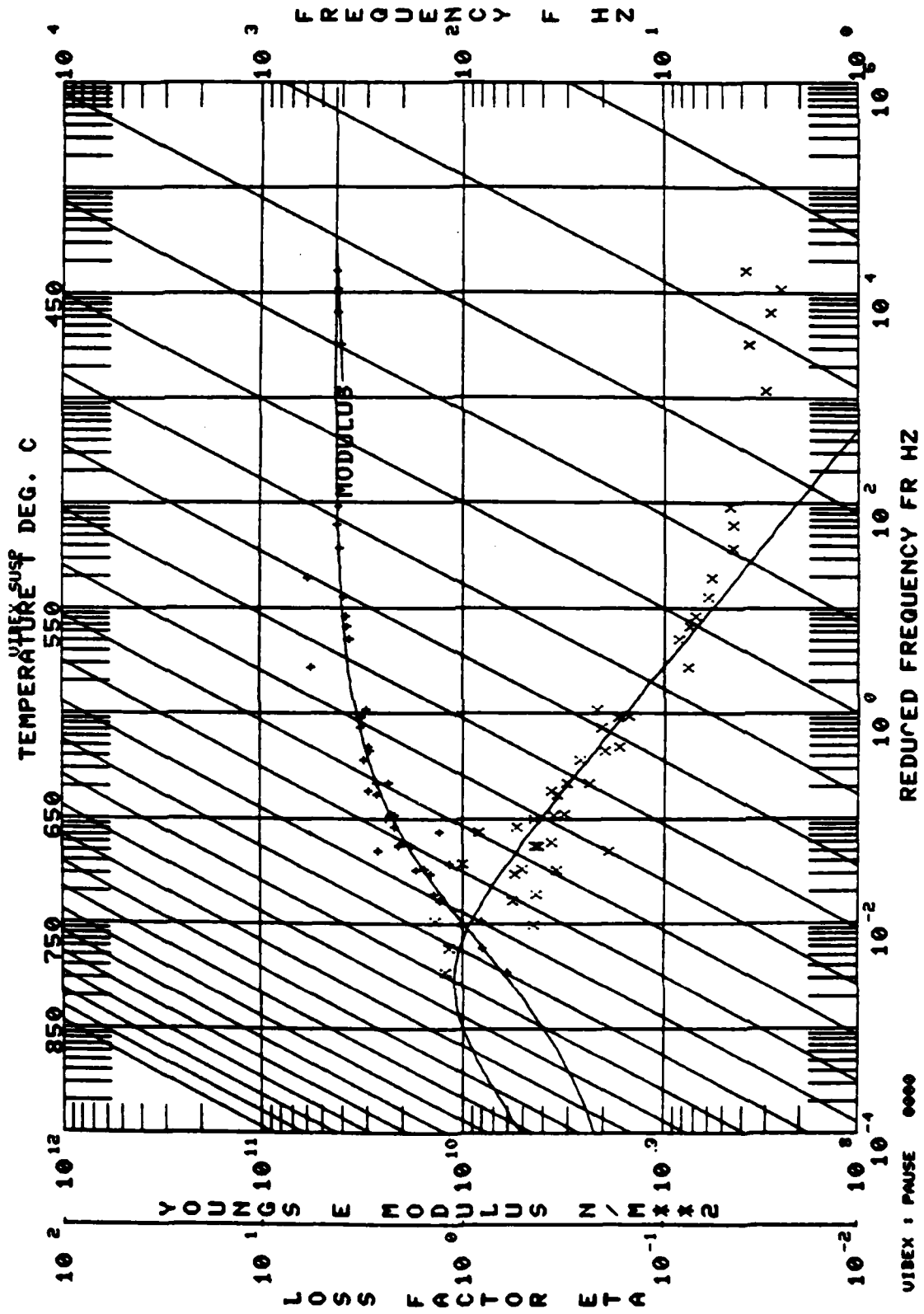


Figure 17. Reduced Nomogram for Composition VIII

TABLE 9
EXPERIMENTAL AND REDUCED DATA OF COMPOSITION VII (AMB8)

NO.	MODULUS N/MHz	LOSS FACTOR	TEMP. DEG. C	FFEQ. Hz	MODE NO.	BEAM IND. N/MHz	COMPOSITE LOSS FAC.	BEAM FREQ. Hz	LOSS MOD. N/MHz
1	6.11971E+09	1.2399	621.1	35.5	2.	1.87656E+11	.0534	100.6	7.58765E+09
2	1.04838E+10	.4575	621.1	271.2	3.	1.86691E+11	.0324	281.4	4.79628E+09
3	1.42622E+10	.4457	621.1	539.0	4.	1.87347E+11	.0413	552.4	6.35736E+09
4	1.74214E+10	.3547	621.1	902.3	5.	1.88391E+11	.0338	915.7	6.17898E+09
5	2.65794E+10	.1943	621.1	1388.3	6.	1.89705E+11	.0300	1370.1	5.22275E+09
6	3.16656E+10	1.1939	607.2	96.5	2.	1.86370E+11	.0671	140.9	9.79159E+09
7	1.33011E+10	.5254	607.2	274.6	3.	1.87954E+11	.0509	282.3	7.78654E+09
8	1.58597E+10	.5237	607.2	543.2	4.	1.88434E+11	.0529	554.0	8.36610E+09
9	2.14170E+10	.4316	607.2	916.0	5.	1.89586E+11	.0557	915.6	9.24281E+09
10	2.22460E+10	.5476	607.2	1374.0	6.	1.91119E+11	.0724	1375.2	1.21809E+10
11	8.28662E+09	1.3953	593.3	96.9	2.	1.89888E+11	.0537	101.4	1.15669E+10
12	1.48489E+10	.6653	593.3	277.0	3.	1.89488E+11	.0786	282.5	8.39344E+09
13	1.99518E+10	3.700	593.3	552.2	4.	1.90002E+11	.0450	556.3	7.38411E+09
14	2.45737E+10	.4522	593.3	928.0	5.	1.91200E+11	.0647	922.5	1.11111E+10
15	1.84762E+10	4.468	579.4	230.7	3.	1.9291E+11	.0509	284.1	8.55235E+09
16	2.32424E+10	3.188	579.4	558.3	4.	1.96891E+11	.0437	557.6	7.40927E+09
17	2.93769E+10	3.704	579.4	943.9	5.	1.92071E+11	.0614	924.6	1.10663E+10
18	1.19755E+10	1.0245	565.6	98.6	2.	1.91970E+11	.0797	101.9	1.22664E+10
19	2.2974E+10	.3638	565.6	284.5	3.	1.91364E+11	.0478	284.9	8.03995E+09
20	3.36830E+10	2.426	565.6	566.9	4.	1.91919E+11	.0377	559.1	6.65295E+09
21	3.15009E+10	2.587	565.6	951.0	5.	1.93361E+11	.0462	927.7	8.43745E+09
22	1.32761E+10	8.550	551.7	99.3	2.	1.93177E+11	.0722	102.2	1.13105E+10
23	2.36830E+10	3.106	551.7	286.7	3.	1.92710E+11	.0429	285.9	7.35681E+09
24	2.9622E+10	2.022	551.7	572.0	4.	1.93157E+11	.0332	560.9	5.99854E+09
25	3.3007E+10	2.110	551.7	957.0	5.	1.95370E+11	.0373	930.5	6.96218E+09
26	3.08518E+10	2.218	551.7	1423.0	6.	1.93958E+11	.0371	1392.5	6.84254E+09
27	2.71608E+10	3.470	537.8	103.8	2.	1.94389E+11	.0530	102.6	9.42459E+09
28	2.98895E+10	1.755	537.8	292.6	3.	1.9379E+11	.0284	286.8	5.15741E+09
29	3.26346E+10	1.550	537.8	578.2	4.	1.94405E+11	.0272	562.7	5.05961E+09
30	3.26964E+10	1.754	510.0	105.9	2.	1.96670E+11	.0302	103.1	5.66864E+09
31	5.71363E+10	.0776	510.0	314.4	3.	1.96230E+11	.0197	288.5	4.43475E+09
32	3.72132E+10	.0856	510.0	587.5	4.	1.96268E+11	.0164	565.4	3.18573E+09
33	3.85033E+10	.0708	510.0	978.2	5.	1.99634E+11	.0138	939.2	2.72615E+09
34	3.96124E+10	.0612	510.0	1466.9	6.	1.99637E+11	.0121	1405.5	2.42304E+09
35	3.82366E+10	.0755	482.2	107.9	2.	1.95773E+11	.0142	103.7	2.92365E+09
36	6.00508E+10	.0533	482.2	317.8	3.	1.95550E+11	.0154	290.2	3.56249E+09
37	4.14314E+10	.0459	482.2	596.3	4.	1.93357E+11	.0094	568.4	1.90007E+09
38	4.24924E+10	.0454	482.2	992.8	5.	2.00640E+11	.0094	345.0	1.93035E+09
39	4.17834E+10	.0477	482.2	1481.0	6.	2.00566E+11	.0097	1414.0	1.99103E+09
40	4.13622E+10	.0307	426.7	109.6	2.	2.02702E+11	.0062	104.7	1.27143E+09
41	4.09365E+10	.0375	426.7	306.8	3.	2.03091E+11	.0075	293.5	1.53519E+09
42	4.25849E+10	.0291	426.7	602.9	4.	2.02496E+11	.0060	574.3	1.24077E+09
43	4.28482E+10	.0259	426.7	1003.0	5.	2.05424E+11	.0053	956.6	1.10940E+09
44	4.33000E+10	.0394	426.7	1500.7	6.	2.06655E+11	.0053	1430.0	1.70756E+09

REDUC : PAUSE 0000
REDUC SUSP

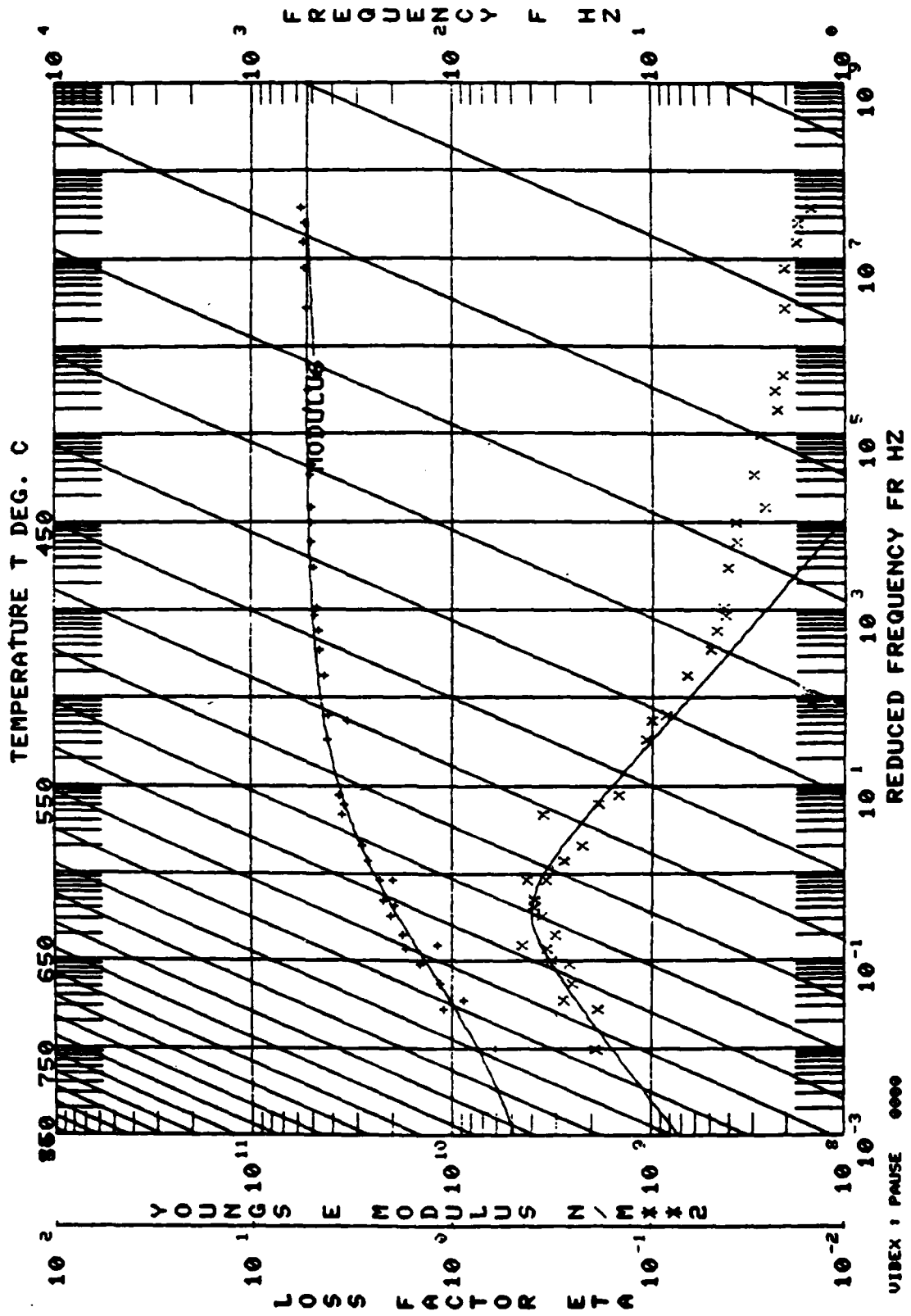


Figure 18. Reduced Nomogram for Composition IX

TABLE 10
EXPERIMENTAL AND REDUCED DATA OF COMPOSITION IX (AMB9)

EXPERIMENTAL CODE : 201
MATERIAL : AMB9, MAEIX
DATA SOURCES
MANUFACTURER : INONE
UDRI : UDRI
OTHER : INONE

NO.	MODULUS N/MSR2	LOSS FACTOR	TEMP. DEG. C	FREQ. HZ	MODE NO.	SEMI MOD. N/MSR2	COMPOSITE LOSS FACTOR	SEMI FREQ. HZ	LOSS MOD. N/MSR2
1	7.43939E+09	.1035	635.0	92.1	2	1.89007E+11	.0023	95.2	7.69741E+08
2	8.51814E+09	.1072	635.0	259.0	3	1.90654E+11	.0027	257.3	9.12864E+08
3	1.01326E+10	.1070	635.0	507.5	4	1.93110E+11	.0032	522.5	1.08459E+09
4	1.20407E+10	.1224	635.0	842.5	5	1.99666E+11	.0043	865.0	1.47400E+09
5	1.20661E+10	.2291	635.0	1261.2	6	1.91213E+11	.0080	1295.0	2.76320E+09
6	1.55571E+09	.1074	635.0	92.4	2	1.90200E+11	.0024	95.5	8.08542E+08
7	1.18431E+10	.112E	621.1	259.7	3	1.89202E+11	.0039	266.7	1.33261E+09
8	1.06538E+10	.1223	621.1	509.4	4	1.90270E+11	.0040	524.1	1.36695E+09
9	1.22692E+10	.1629	621.1	845.6	5	1.90934E+11	.0060	852.0	2.07237E+09
10	1.22813E+10	.2694	621.1	1266.3	6	1.92632E+11	.0095	1300.0	3.30918E+09
11	9.13735E+09	.1033	607.2	92.9	2	1.91397E+11	.0046	95.8	3.89671E+08
12	1.65249E+10	.0367	607.2	260.9	3	1.88351E+11	.0058	256.1	1.52803E+09
13	1.12263E+10	.1783	607.2	511.8	4	1.9198E+11	.0058	526.2	2.00215E+09
14	1.37222E+10	.2244	607.2	850.2	5	1.92307E+11	.0088	871.0	3.05328E+09
15	1.49315E+10	.3376	607.2	1273.5	6	1.93434E+11	.0143	1302.5	5.05328E+09
16	1.00195E+10	.1206	593.3	93.3	2	1.92597E+11	.0035	96.1	1.20646E+09
17	1.28383E+10	.3563	593.3	273.5	3	1.92966E+11	.0131	527.8	4.58045E+09
18	1.49410E+10	.2937	593.3	514.5	4	1.93545E+11	.0124	873.8	4.38779E+09
19	1.70597E+10	.4448	593.3	822.2	5	1.95011E+11	.0211	1307.8	7.58767E+09
20	9.39970E+09	.1913	579.4	93.5	2	1.93802E+11	.0052	96.4	1.79341E+09
21	1.23596E+10	.2723	579.4	263.0	3	1.93913E+11	.0096	270.0	3.36520E+09
22	1.62103E+10	.5338	579.4	518.1	4	1.93845E+11	.0243	520.0	8.5565E+09
23	1.79060E+10	.3077	579.4	859.9	5	1.94521E+11	.0153	876.0	5.50299E+09
24	2.20853E+10	.2657	579.4	1293.1	6	1.95688E+11	.0078	1310.0	7.2382E+09
25	1.25505E+10	.3855	565.6	264.2	3	1.9540E+11	.0133	271.2	4.82266E+09
26	1.95539E+10	.3939	565.6	521.9	4	1.94946E+11	.0212	530.5	7.70244E+09
27	2.1560E+10	.2974	565.6	866.8	5	1.95410E+11	.0179	878.0	6.58341E+09
28	2.40771E+10	.2352	565.6	1301.1	6	1.97164E+11	.0152	1315.0	5.6543E+09
29	1.57605E+10	.3597	537.8	95.1	2	1.97032E+11	.0157	97.2	5.6688E+09
30	2.03591E+10	.3583	537.8	262.1	3	1.97230E+11	.0198	272.3	7.29564E+09
31	2.51046E+10	.2608	537.8	520.1	4	1.97326E+11	.0174	534.0	6.54753E+09
32	2.99629E+10	.0205	537.8	880.5	5	1.97642E+11	.0016	882.0	6.14450E+08
33	3.14711E+10	.1920	510.0	1321.3	6	1.99571E+11	.0147	1323.0	5.72819E+09
34	3.76192E+10	.2022	510.0	96.6	2	1.99472E+11	.0190	97.8	7.15011E+09
35	3.54547E+10	.1129	510.0	272.3	3	1.9901E+11	.0150	274.0	5.75960E+09
36	3.64619E+10	.1165	510.0	891.3	4	1.9927E+11	.0101	883.0	4.00399E+09
37	3.19176E+10	.1428	482.2	1335.2	5	2.01107E+11	.0106	1339.0	4.24602E+09
38	3.47613E+10	.0972	482.2	98.1	2	2.01107E+11	.0116	98.2	4.55259E+09
39	3.60431E+10	.0744	482.2	275.7	3	2.01161E+11	.0085	275.0	3.3205E+09
40	3.90043E+10	.0646	482.2	541.7	4	2.01616E+11	.0067	539.5	2.6205E+09
41	3.62932E+10	.0595	482.2	909.3	5	2.02370E+11	.0052	893.5	2.51867E+09
42	4.05201E+10	.0722	454.4	1349.5	6	2.03786E+11	.0052	1356.9	2.42750E+09
43	3.97064E+10	.0596	454.4	93.1	2	2.0360E+11	.0065	98.7	2.62165E+09
44	4.31095E+10	.0454	454.4	278.6	3	2.0227E+11	.0059	278.0	2.41345E+09
45	4.45333E+10	.0378	454.4	546.9	4	2.03865E+11	.0044	542.5	1.80351E+09
46	3.99456E+10	.0434	426.7	908.9	5	2.04141E+11	.0040	898.0	1.66474E+09
47	4.45333E+10	.0378	426.7	1362.1	6	2.05957E+11	.0040	1344.0	1.68424E+09
48	3.99456E+10	.0434	426.7	100.0	2	2.05223E+11	.0042	99.2	1.7263E+09

TABLE 10 (continued)

50	4.19446E+10	.027	426.7	280.9	3.	2.05574E+11	.0043	278.0	1.79019E+09
51	4.23714E+10	.027	426.7	551.4	4.	2.06126E+11	.0029	545.5	1.17022E+09
52	4.53515E+10	.023	426.7	915.4	5.	2.06468E+11	.0026	902.5	1.10038E+09
53	4.70657E+10	.028	426.7	1372.5	6.	2.08105E+11	.0025	1351.0	1.07190E+09
54	4.78555E+10	.020	371.1	101.4	2.	2.08264E+11	.0022	100.1	9.38474E+08
55	4.58769E+10	.0169	371.1	553.4	4.	2.10074E+11	.0013	550.7	7.74349E+08
56	4.84851E+10	.0152	371.1	927.2	5.	2.10745E+11	.0013	911.8	7.93835E+08
57	5.02907E+10	.0158	371.1	1389.6	6.	2.12225E+11	.0012	1364.3	7.93455E+08
58	1.14128E+10	.2005	593.3	261.7	3.	1.92479E+11	.0096	269.0	2.26787E+09
59	3.05120E+10	.1422	510.0	535.7	4.	1.99752E+11	.0112	537.0	4.35282E+09

REDUC 1 PAUSE 0000

REDUC SUSP

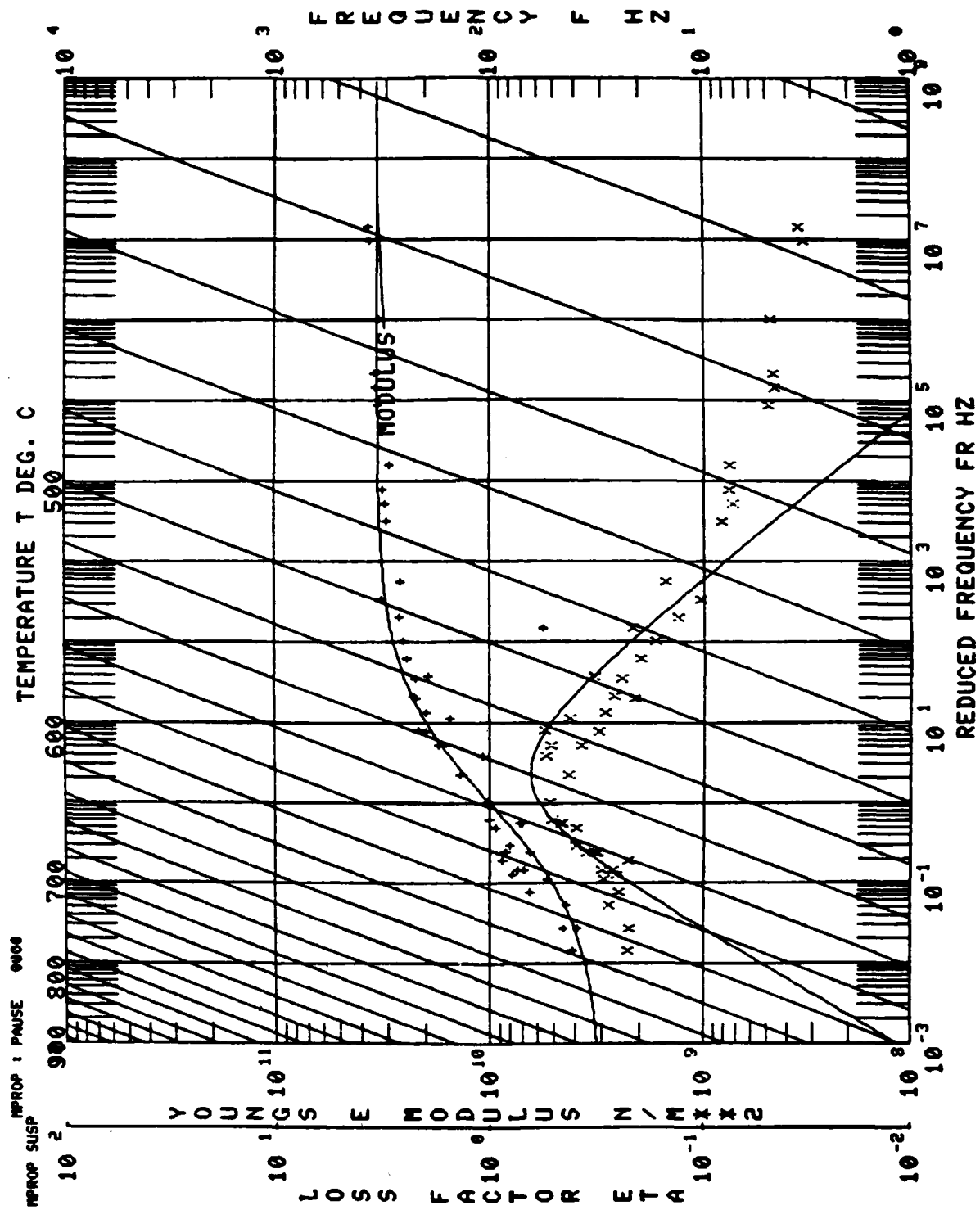


Figure 19. Reduced Nomogram for Composition X

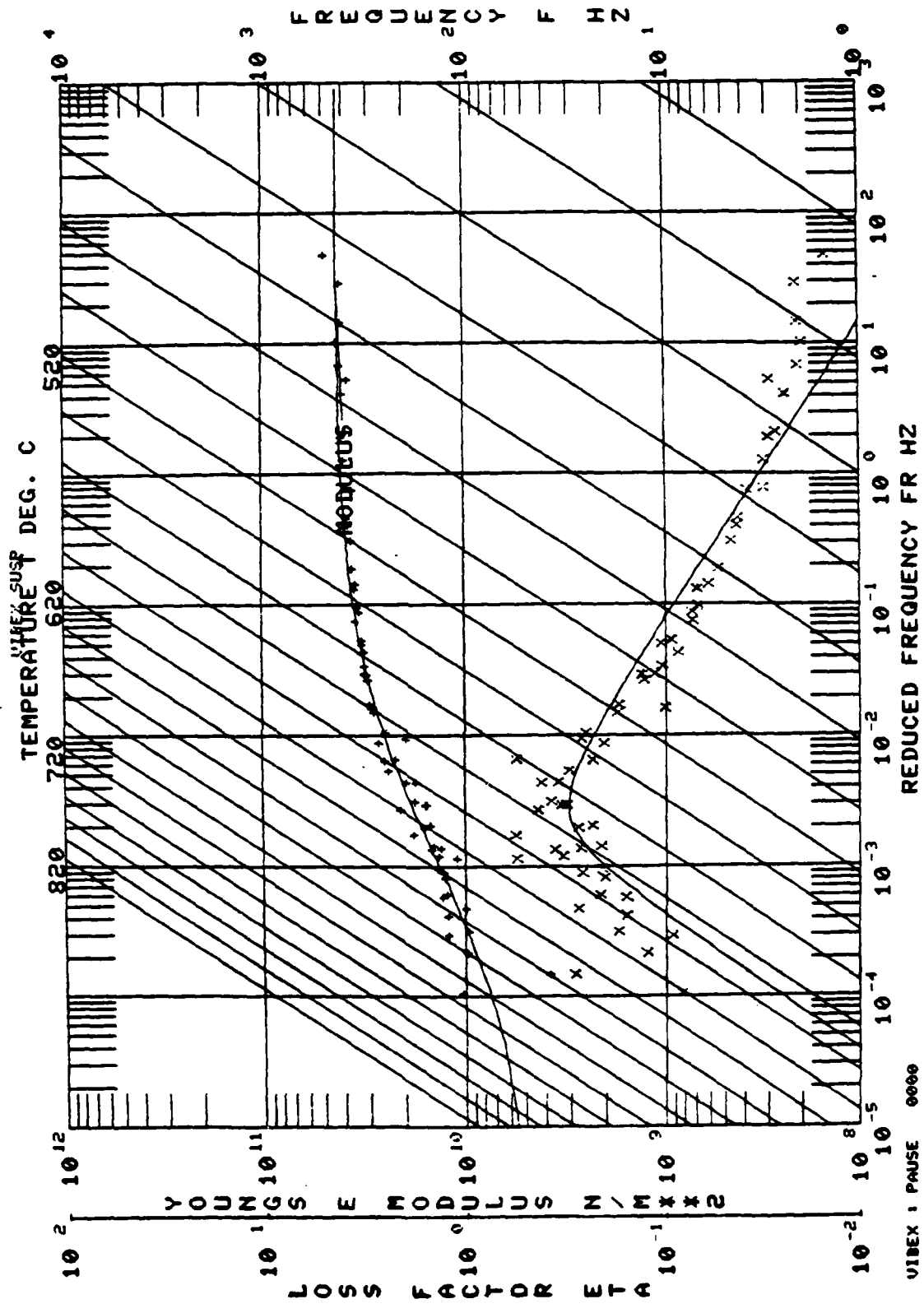
TABLE 11
EXPERIMENTAL AND REDUCED DATA OF COMPOSITION X (AMB10)

EXPERIMENTAL CODE :217
MATERIAL :01-77-1; AMB10
DATA SOURCES
MANUFACTURER :UDRI BEAM COATED ONE SIDE
UDRI :UDRI
OTHER :NONE

NO.	MODULUS N/MTX2	LOSS FACTOR	TEMP. TEG. C	FREQ. HZ	MODE NO.	BEAM MID. N/MTX2	COMPOSITE LOSS FAC.	BEAM FREQ. HZ	LOSS MOD. N/MTX2
1	1.09961E+10	.5532	531.8	95.1	2.	1.51618E+11	.0181	96.9	6.13780E+09
2	2.32208E+10	.2676	537.8	531.7	4.	1.52208E+11	.0173	532.5	6.21324E+09
3	2.25681E+10	.2466	537.8	873.3	5.	1.52518E+11	.0155	381.5	5.56497E+09
4	7.19854E+09	.4767	555.6	94.0	2.	1.49942E+11	.0104	96.4	3.42732E+09
5	1.76517E+10	.5324	565.6	869.0	5.	1.50959E+11	.0270	877.0	9.39709E+09
6	5.51283E+09	.2996	593.3	93.3	2.	1.48381E+11	.0051	95.9	1.65127E+09
7	1.02530E+10	.5209	593.3	516.2	4.	1.48678E+11	.0161	526.5	5.34045E+09
8	1.03989E+10	.5346	593.3	354.2	5.	1.49140E+11	.0157	871.7	5.55939E+09
9	2.69043E+10	.3324	510.0	367.7	2.	1.53187E+11	.0183	97.4	6.51106E+09
10	3.23671E+10	.1851	510.0	536.8	4.	1.53515E+11	.0099	535.0	3.64444E+09
11	4.61737E+09	.2573	621.1	390.4	5.	1.52255E+11	.0091	880.7	3.40299E+09
12	7.11138E+09	.2722	621.1	92.6	2.	1.46348E+11	.0073	95.2	1.04966E+09
13	8.70833E+09	.3221	631.1	510.4	4.	1.46706E+11	.0060	523.0	1.93605E+09
14	4.22333E+09	.2302	635.0	847.2	5.	1.47195E+11	.0086	866.0	2.80511E+09
15	6.62572E+09	.2561	635.0	503.6	4.	1.45386E+11	.0053	521.5	1.69675E+09
16	8.05343E+09	.2607	635.0	943.5	5.	1.46178E+11	.0055	863.0	2.09952E+09
17	8.93222E+09	.2722	635.0	123.4	2.	1.47149E+11	.0053	1291.0	2.05632E+09
18	4.97128E+09	.2845	607.2	92.3	2.	1.47269E+11	.0040	95.5	1.27942E+09
19	8.21270E+09	.4015	607.2	513.2	4.	1.47830E+11	.0101	525.0	3.30038E+09
20	9.64452E+09	.4122	607.2	950.9	5.	1.48047E+11	.0115	868.5	3.88755E+09
21	1.42111E+10	.3646	607.2	1283.4	6.	1.49192E+11	.0051	1300.0	1.73466E+09
22	6.62204E+09	.4322	579.4	93.7	2.	1.49125E+11	.0073	96.1	2.38756E+09
23	1.46211E+10	.3722	579.4	361.5	5.	1.49228E+11	.0170	874.0	6.15763E+09
24	6.62204E+09	.2646	579.4	529.3	4.	1.51648E+11	.0349	531.0	1.23615E+10
25	2.13779E+10	.5650	551.7	274.2	5.	1.51228E+11	.0073	879.0	6.01239E+09
26	2.03191E+10	.2959	551.7	1312.1	6.	1.52778E+11	.0136	1315.5	4.88955E+09
27	2.32975E+10	.2170	551.7	36.0	2.	1.52559E+11	.0194	97.2	6.75667E+09
28	1.56259E+10	.4324	523.9	534.2	4.	1.52942E+11	.0137	534.0	4.97742E+09
29	2.47140E+10	.2014	523.9	825.4	5.	1.53378E+11	.0121	584.0	4.42539E+09
30	2.56626E+10	.1724	523.9	1286.8	6.	1.54291E+11	.0037	1322.0	1.24552E+09
31	7.1276E+09	.2180	482.2	93.1	2.	1.54764E+11	.0111	97.9	4.10873E+09
32	2.66034E+10	.1544	482.2	541.8	4.	1.54953E+11	.0068	537.5	2.56331E+09
33	3.06974E+10	.0335	482.2	308.7	5.	1.55317E+11	.0061	891.0	2.31731E+09
34	3.13443E+10	.0730	482.2	1344.5	6.	1.56634E+11	.0065	1332.0	2.48737E+09
35	3.26667E+10	.0776	454.4	99.1	2.	1.56349E+11	.0061	98.4	2.31195E+09
36	3.06787E+10	.0769	454.4	516.2	4.	1.56688E+11	.0044	540.5	1.69637E+09
37	3.38122E+10	.0502	454.4	906.4	5.	1.57219E+11	.0042	895.0	1.63001E+09
38	3.4740E+10	.0469	454.4	1356.5	6.	1.58235E+11	.0042	1339.0	1.68278E+09
39	3.56645E+10	.0477	454.4	39.9	2.	1.57974E+11	.0042	98.9	1.62712E+09
40	3.56645E+10	.0490	426.7	550.9	4.	1.05257E+11	.0032	443.0	1.84505E+09
41	3.32053E+10	.0103	426.7	913.1	5.	1.58653E+11	.0034	890.1	1.26518E+09
42	1.79603E+11	.0339	426.7	1366.5	6.	1.59909E+11	.0034	1345.1	1.35463E+09
43	3.72867E+10	.0359	426.7	94.1	2.	1.49909E+11	.0105	96.4	3.46407E+09
44	3.77015E+10	.0681	565.6	262.0	5.	1.50959E+11	.0135	377.0	6.41543E+09
45	7.40034E+09	.3809	565.6	1302.9	6.	1.51505E+11	.0133	1310.0	6.46707E+09
46	1.60450E+10	.3180	621.1	510.8	2.	1.46348E+11	.0029	95.2	9.19695E+08
47	2.03760E+10	.2297	621.1	92.8	4.	1.46706E+11	.0029	523.0	2.32864E+09
48	4.00340E+09	.3065	621.1	510.8	4.	1.46706E+11	.0029	523.0	2.32864E+09
49	7.59720E+09	.3065	621.1	510.8	4.	1.46706E+11	.0029	523.0	2.32864E+09

TABLE 11 (continued)

50	8.61519E+09	.3292	621.1	847.1	5.	1.47196E+11	.0087	866.0	2.83648E+09
51	1.2669E+10	.1323	579.4	1286.6	6.	1.51041E+11	.0049	1308.0	1.66782E+09
52	8.25035E+09	.5200	621.1	1265.9	5.	1.48053E+11	.0131	1295.0	4.29081E+09
	REDUC : PAUSE	.0006							
	REDUC SUSP								



VIBEX : PAUSE 0000

Figure 20. Reduced Nomogram for Composition XI

TABLE 12
EXPERIMENTAL AND REDUCED DATA OF COMPOSITION XI (AMBII)

EXPERIMENTAL CODE 1226
 MATERIAL AMBII-MEXII
 DATA SOURCES
 MANUFACTURER INOME
 UDRI
 OTHER INOME

NO.	MODULUS N/MS ²	LOSS FACTOR	TEMP. DEG. C	FREQ. HZ	MODE NO.	BEAM MOD. N/MS ²	COMPOSITE LOSS FAC	BEAM FREQ. HZ	LOSS MOD. N/MS ²
1	1.05863E+10	.0E+5	704.4	90.6	2.	1.81998E+11	.0032	93.2	8.94763E+08
2	1.24970E+10	.0968	704.4	254.3	3.	1.82330E+11	.0042	261.2	1.19964E+09
3	1.3555E+10	.1634	704.4	520.7	4.	1.82734E+11	.0076	512.5	2.18293E+09
4	1.39519E+10	.2123	704.4	829.3	5.	1.83139E+11	.0103	948.0	2.96233E+09
5	1.45943E+10	.2176	704.4	1243.1	6.	1.83544E+11	.0041	1270.0	3.17506E+09
6	1.45943E+10	.2981	690.6	90.0	2.	1.83556E+11	.0070	93.7	1.11939E+09
7	1.24542E+10	.1617	690.6	255.9	3.	1.84009E+11	.0093	262.4	2.01325E+09
8	1.29824E+10	.2086	690.6	502.7	4.	1.84582E+11	.0126	515.0	2.70829E+09
9	1.34956E+10	.2721	690.6	833.3	5.	1.85305E+11	.0126	853.0	3.67279E+09
10	1.51834E+10	.2369	690.6	1249.9	6.	1.86513E+11	.0122	1276.0	3.59712E+09
11	1.00208E+10	.1282	676.7	91.3	2.	1.86175E+11	.0045	94.0	1.28433E+09
12	1.25303E+10	.2199	676.7	256.7	3.	1.85132E+11	.0095	263.2	2.75579E+09
13	1.37564E+10	.3115	676.7	504.8	4.	1.85659E+11	.0157	516.5	4.57706E+09
14	1.62346E+10	.2801	676.7	839.5	5.	1.86393E+11	.0153	855.5	4.54776E+09
15	1.57471E+10	.3216	676.7	1254.8	6.	1.87685E+11	.0170	1280.0	5.06357E+09
16	1.01938E+10	.2728	648.9	92.0	2.	1.88102E+11	.0098	94.7	2.84206E+09
17	1.43632E+10	.3681	648.9	259.6	3.	1.87957E+11	.0184	265.2	5.47569E+09
18	2.12765E+10	.4440	648.9	514.4	4.	1.88133E+11	.0307	520.0	9.44760E+09
19	2.02089E+10	.3537	648.9	850.8	5.	1.89236E+11	.0230	862.0	7.07651E+09
20	2.24749E+10	.5378	648.9	1278.0	6.	1.90629E+11	.0405	1290.0	1.26712E+10
21	9.92937E+09	.1773	622.8	91.6	2.	1.86715E+11	.0061	94.4	1.76073E+09
22	1.30911E+10	.2687	622.8	257.9	3.	1.86542E+11	.0120	264.2	3.51811E+09
23	1.63126E+10	.5761	622.8	509.7	4.	1.86450E+11	.0351	517.6	1.05532E+10
24	1.61136E+10	.372	622.8	842.6	5.	1.8921E+11	.0182	859.0	5.43518E+09
25	1.79810E+10	.4262	622.8	1263.2	6.	1.88860E+11	.0215	1284.0	7.66331E+09
26	1.12310E+10	.5881	621.1	92.8	2.	1.90772E+11	.0215	95.4	6.38027E+09
27	2.54004E+10	.2344	621.1	251.1	4.	1.90725E+11	.018	523.5	5.97623E+09
28	2.5257E+10	.2530	621.1	503.5	5.	1.91830E+11	.0295	868.0	6.54033E+09
29	2.95117E+10	.3037	621.1	844.1	6.	1.93003E+11	.0092	1298.0	3.02041E+09
30	1.82646E+10	.2074	593.3	94.6	2.	1.93094E+11	.0175	96.2	7.00745E+09
31	2.73272E+10	.2074	593.3	268.2	3.	1.93651E+11	.0159	268.8	5.66682E+09
32	3.02303E+10	.1733	593.3	529.6	4.	1.94097E+11	.0159	527.5	5.23913E+09
33	3.12685E+10	.1346	593.3	876.1	5.	1.94912E+11	.0127	873.0	4.20744E+09
34	2.43782E+10	.0981	593.3	1322.0	6.	1.95387E+11	.0095	1306.0	2.33240E+09
35	2.43782E+10	.3133	579.4	95.8	2.	1.94912E+11	.0277	96.4	7.63751E+09
36	2.89447E+10	.1367	579.4	269.6	3.	1.94245E+11	.0159	269.6	5.21147E+09
37	2.2245E+10	.1167	579.4	531.1	4.	1.94336E+11	.0139	522.2	1.76143E+09
38	3.20162E+10	.1071	579.4	881.0	5.	1.94333E+11	.015	876.0	3.52527E+09
39	3.5392E+10	.1871	579.4	1322.1	6.	1.96676E+11	.0077	1310.3	5.36575E+09
40	1.96799E+10	.2701	565.6	96.2	2.	1.99997E+11	.0166	97.7	2.63445E+09
41	3.08956E+10	.1312	565.6	271.2	3.	1.95472E+11	.0122	270.5	3.11565E+09
42	3.2887E+10	.0948	565.6	533.0	4.	1.9513E+11	.0073	530.0	2.53203E+09
43	3.38172E+10	.0749	565.6	884.9	5.	1.96774E+11	.0075	879.0	2.53203E+09
44	3.19538E+10	.1074	565.6	1325.8	6.	1.9788E+11	.0073	1314.0	2.51487E+09
45	3.4001E+10	.0599	537.8	97.6	2.	1.98159E+11	.0071	97.2	2.43283E+09
46	3.68014E+10	.0599	537.8	274.2	3.	1.97715E+11	.0071	272.0	2.44202E+09
47	3.68014E+10	.0553	537.8	538.5	4.	1.97710E+11	.0059	533.0	2.03095E+09
48	3.73110E+10	.0472	537.8	893.7	5.	1.98794E+11	.0051	883.5	2.75986E+09
49	3.93893E+10	.0436	537.8	1339.5	6.	1.99901E+11	.0049	1321.0	1.71744E+09

TABLE 12 (continued)

50	3.95221E+10	510.0	4.	1.99342E+11	.0036	536.0	1.27406E+09
51	4.04168E+10	510.0	5.	2.00824E+11	.0037	838.0	1.30153E+09
52	4.13829E+10	510.0	9.	2.02177E+11	.0035	1328.5	1.24964E+09
53	3.68508E+10	482.2	2.	2.02050E+11	.0041	98.2	1.45303E+09
54	3.93879E+10	482.2	3.	2.01511E+11	.0030	274.8	1.08408E+09
55	4.09146E+10	482.2	4.	2.01312E+11	.0028	538.5	1.01264E+09
56	4.18404E+10	482.2	5.	2.02637E+11	.0025	892.0	8.97590E+08
57	4.35055E+10	482.2	6.	2.03855E+11	.0024	1314.0	8.75672E+08
58	3.87708E+10	454.4	3.	2.04112E+11	.0032	98.7	1.15577E+09
59	4.15423E+10	454.4	3.	2.03577E+11	.0025	276.0	8.85377E+08
60	4.20078E+10	454.4	4.	2.04142E+11	.0025	541.6	9.10953E+08
61	5.01500E+10	454.4	5.	2.00372E+11	.0021	827.0	7.66555E+08
62	3.80219E+10	510.0	3.	1.99760E+11	.0046	273.4	1.69552E+09
63	3.53224E+10	510.0	2.	1.99997E+11	.0063	97.7	2.18266E+09

REINC 1 PAUSE 0000
 REDUC SUSP

3.1.4. Low Temperature Glasses

Six low melting materials were formulated for damping measurements. Compositions of these materials are shown in Table 13. Reduced nomograms for loss factor and loss modulus are shown in Figure 21 through 30, with experimental and reduced data in Tables 12,13,14,15, and 16. As expected, these compositions exhibit peak damping in the range of 600°F to 800°F (315°C to 427°C) All these compositions exhibited slight tendency towards devitrification; nonetheless, composition LT-3 appears to be the most stable composition. Contrary to expectation, composition LT-5 shows decreased loss factor and increased peak damping temperature as compared to LT-1 and LT-3. It is most probable that there has been a greater degree of devitrification in composition LT-5.

TABLE 13

COMPOSITIONS OF LOW TEMPERATURE GLASSES.

<u>Ident. No.</u>	<u>PbO</u>	<u>PbF₂</u>	<u>B₂O₃</u>	<u>2.0</u>
LT-1	84.0	--	9.0	7.0
LT-2	80.4	3.6	9.0	7.0
LT-3	76.4	7.2	9.0	7.0
LT-4	73.2	10.8	9.0	7.0
LT-5	69.6	14.4	9.0	7.0
LT-6	66.0	18.0	9.0	7.0

The composition LT-2 exhibited flat loss factor vs frequency and temperature curves indicating that the composition has completely crystallized during the measurement.

These low temperature compositions were designed to cover the damping temperature range of 600°F to 800°F, which is normally considered to be the range of high temperature polymers.

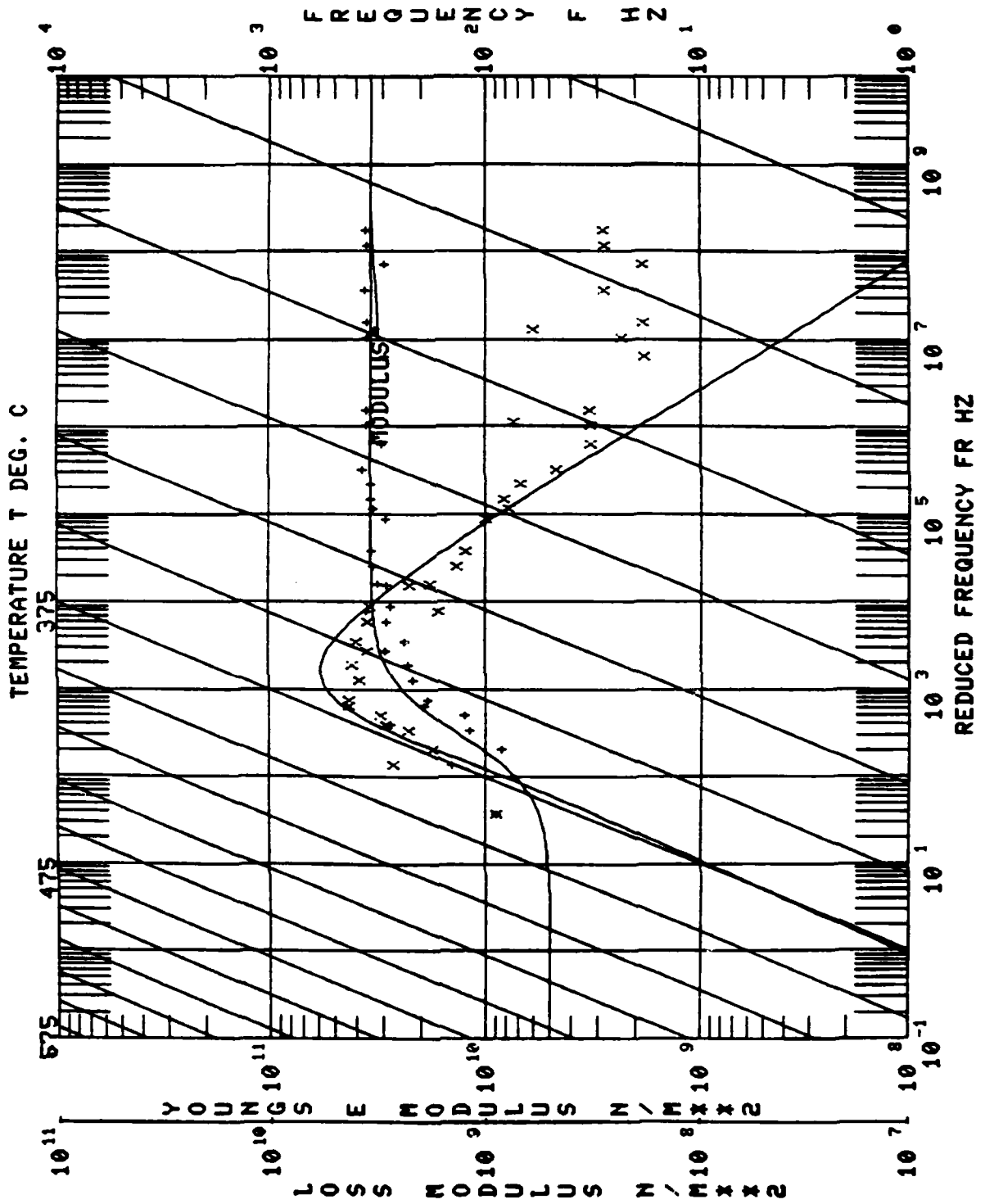


Figure 21. Reduced Nomogram Displaying Loss Factor for LT-1.

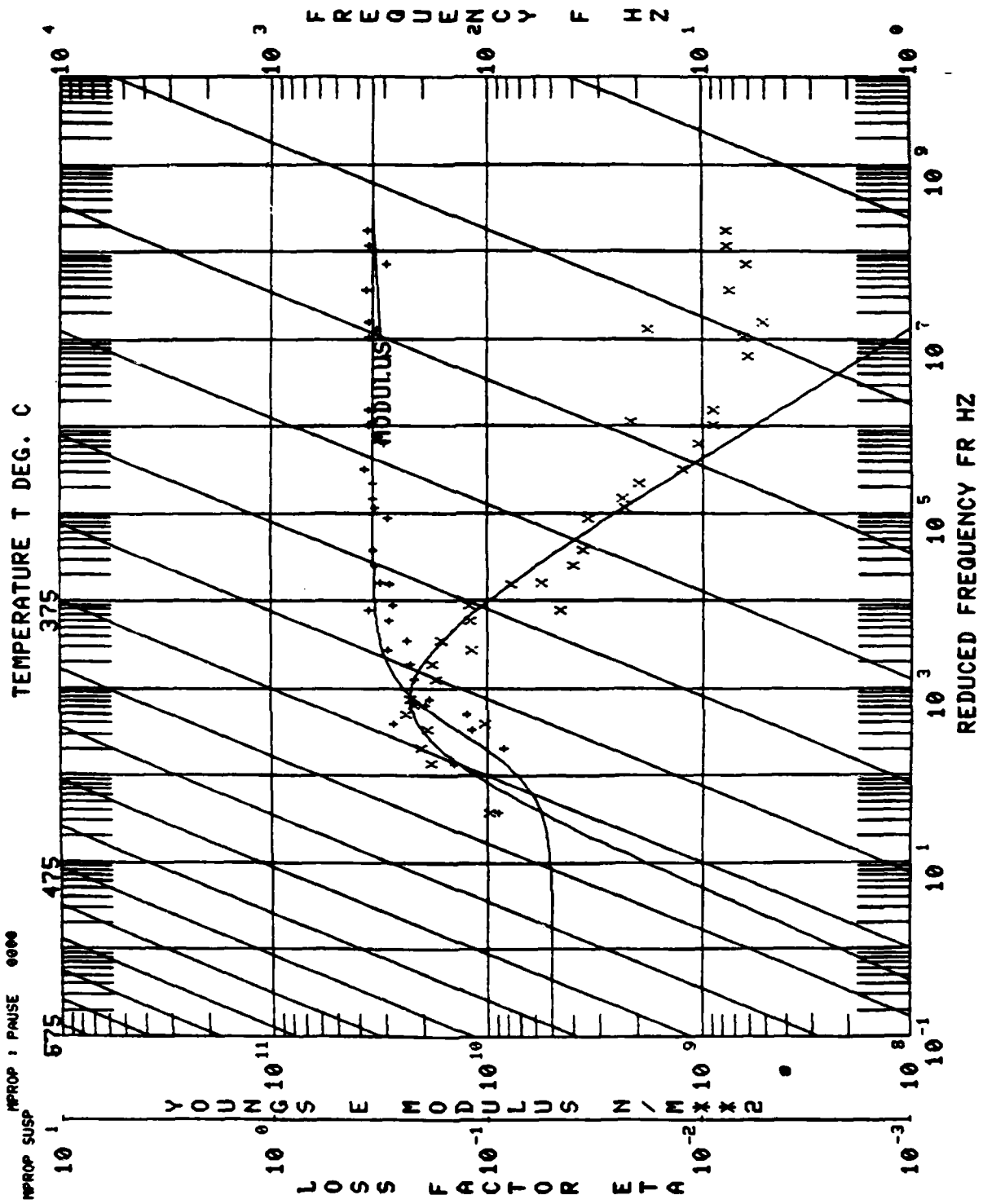


Figure 22. Reduced Nomogram Displaying Loss Modulus for LT-1.

TABLE 14
EXPERIMENTAL AND REDUCED DATA OF COMPOSITION LT-1.

EXPERIMENTAL CODE :232
MATERIAL :LT1,015501
MANUFACTURER DATA SOURCES
UDRI :NONE
OTHER :NONE

NO.	MODULUS N/MHz	LOSS FACTOR	TEMP. DEG. C	FREQ. HZ	MODE NO.	BEAM MOD. N/MHz	COMPOSITE LOSS FAC.	BEAM FREQ. HZ	LOSS MOD. N/MHz
1	9.0894E+02	.1001	385.0	35.3	2.	2.0839E+11	.0022	99.2	9.0963E+08
2	1.2859E+10	.1930	385.0	87.5	5.	2.1112E+11	.0055	306.1	2.3278E+09
3	1.4650E+10	.1863	371.1	96.9	2.	2.1075E+11	.0064	99.8	2.7291E+09
4	2.8027E+10	.1055	371.1	278.0	3.	2.1125E+11	.0056	279.8	2.9578E+09
5	1.8884E+10	.2324	371.1	538.3	4.	2.1380E+11	.0100	551.6	4.3827E+09
6	2.2667E+10	.1763	371.1	530.1	5.	2.1219E+11	.0089	908.4	3.9250E+09
7	2.3061E+10	.1832	371.1	1332.1	6.	2.1346E+11	.0100	100.1	4.2244E+09
8	1.9613E+10	.2226	356.1	97.3	2.	2.1198E+11	.0090	553.5	4.0487E+09
9	2.4161E+10	.1676	356.1	543.3	4.	2.1528E+11	.0079	910.9	3.5864E+09
10	2.9164E+10	.1230	356.1	899.3	5.	2.1336E+11	.0079	1362.2	3.4543E+09
11	2.8095E+10	.1234	356.1	1342.9	6.	2.1463E+11	.0076	100.4	3.5912E+09
12	2.9634E+10	.1202	343.3	99.2	2.	2.1325E+11	.0079	281.4	1.6748E+09
13	3.5931E+10	.0465	343.3	279.9	3.	2.1367E+11	.0036	555.0	1.2583E+09
14	2.9032E+10	.0792	343.3	547.6	4.	2.1645E+11	.0050	913.1	1.2901E+09
15	3.3522E+10	.0410	343.3	906.0	5.	2.1440E+11	.0030	1365.4	1.2583E+09
16	3.4186E+10	.0369	343.3	1354.3	6.	2.1563E+11	.0027	915.4	3.3975E+08
17	3.4694E+10	.0243	329.4	908.8	5.	2.1548E+11	.0018	1368.3	7.0379E+08
18	3.4023E+10	.0202	329.4	1358.9	6.	2.1671E+11	.0015	101.0	7.9252E+08
19	3.3088E+10	.0233	315.6	100.2	2.	2.1581E+11	.0017	283.0	4.7229E+08
20	3.7596E+10	.0126	315.6	281.8	3.	2.1611E+11	.0010	558.4	3.2712E+08
21	3.0659E+10	.0107	315.6	551.7	4.	2.1911E+11	.0007	917.7	3.2981E+08
22	3.6241E+10	.0091	315.6	912.5	5.	2.1655E+11	.0007	1372.2	3.3158E+08
23	3.6367E+10	.0091	315.6	1364.3	6.	2.1779E+11	.0007	101.3	7.5005E+08
24	3.4071E+10	.0220	301.1	100.5	2.	2.1709E+11	.0016	560.2	1.8750E+08
25	3.0622E+10	.0062	301.1	553.0	4.	2.2052E+11	.0004	920.1	2.3647E+08
26	3.5941E+10	.0056	301.1	914.4	5.	2.1770E+11	.0005	1375.6	1.9015E+08
27	3.6938E+10	.0053	301.1	1367.1	6.	2.1893E+11	.0004	101.6	6.1168E+08
28	3.3503E+10	.0183	287.8	100.7	2.	2.1859E+11	.0013	284.7	2.8625E+08
29	3.7399E+10	.0077	287.8	283.3	3.	2.1871E+11	.0006	561.8	1.3853E+08
30	2.9511E+10	.0063	287.8	554.4	4.	2.2178E+11	.0006	922.4	2.5545E+08
31	3.6453E+10	.0078	287.8	917.0	5.	2.1899E+11	.0006	1379.1	2.3697E+08
32	3.6613E+10	.0078	287.8	1371.0	6.	2.1998E+11	.0006	100.7	1.8015E+09
33	8.6129E+09	.2092	385.0	529.3	4.	2.1642E+11	.0013	1355.1	3.1140E+09
34	1.2713E+10	.2150	329.4	99.7	2.	2.1239E+11	.0010	556.7	1.0131E+09
35	3.1907E+10	.0577	329.4	549.4	4.	2.1777E+11	.0022	99.2	9.0963E+08
36	2.9409E+10	.0346	329.4	87.5	5.	2.1112E+11	.0055	306.1	2.3278E+09

REDUC 1 PAUSE 0000
REDUC SUSP

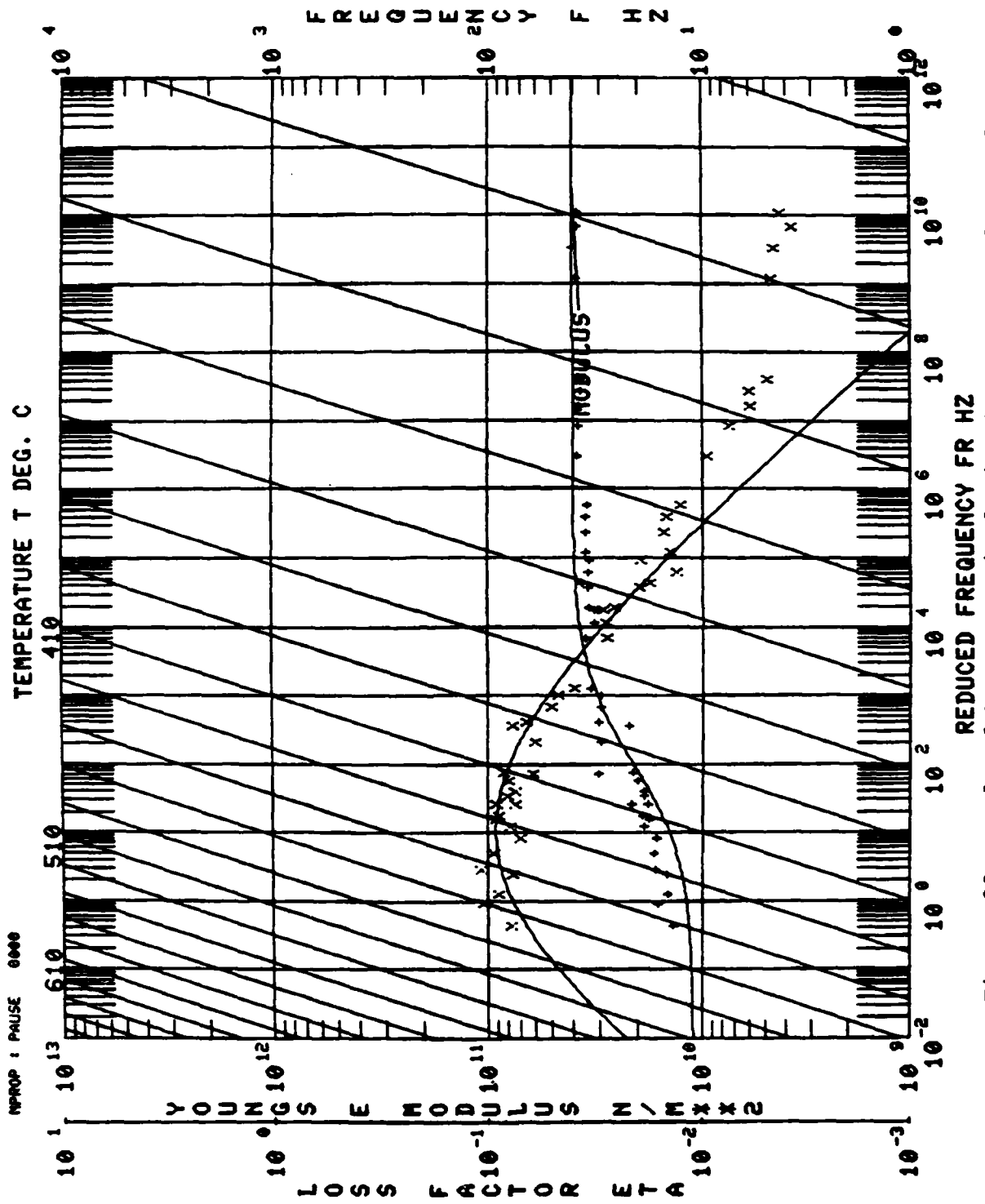


Figure 23. Reduced Nomogram Displaying Loss Factor for LT-3.

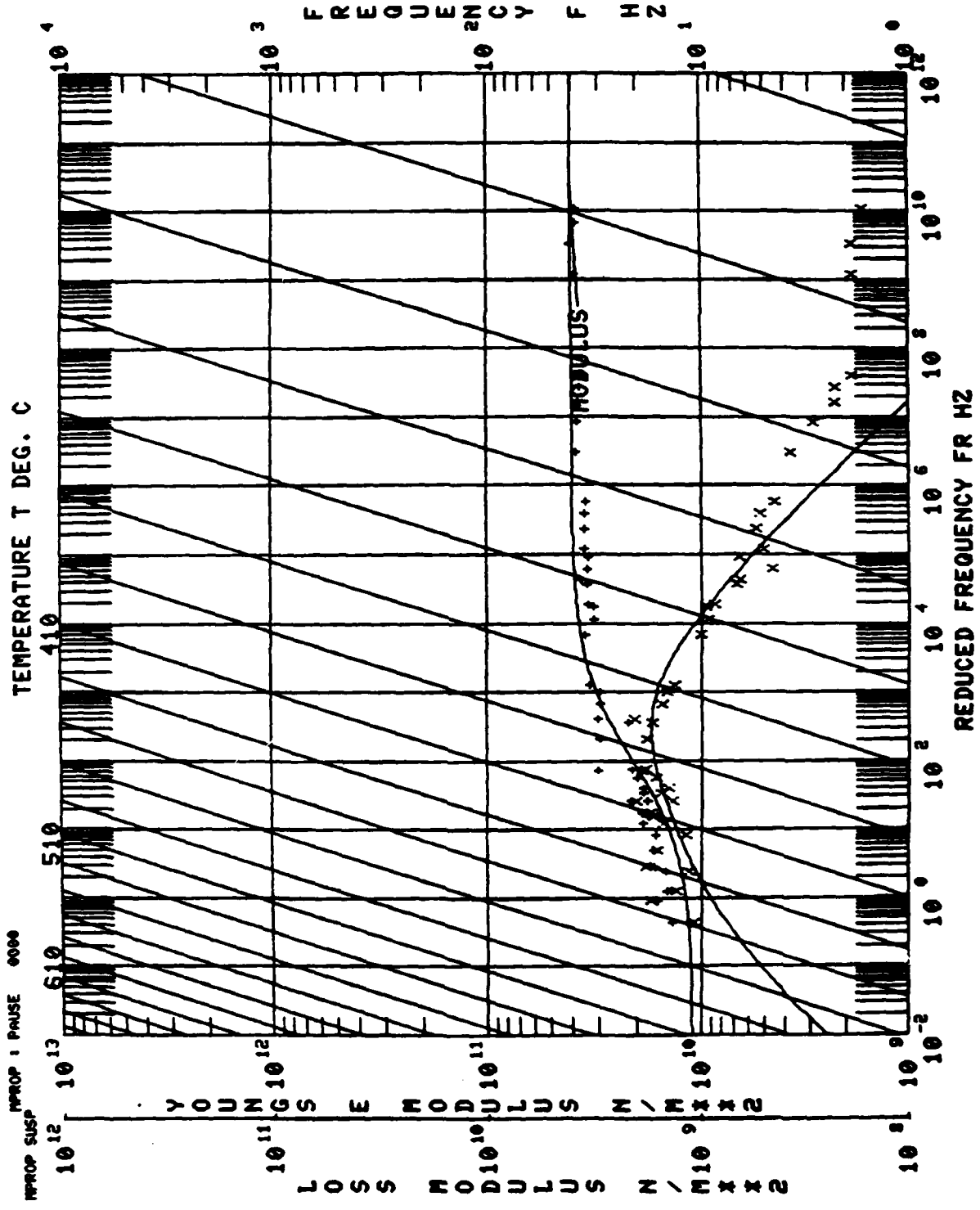


Figure 24. Reduced Nomogram Displaying Loss Modulus for LT-3.

TABLE 15
EXPERIMENTAL AND REDUCED DATA OF COMPOSITION LT-3.

EXPERIMENTAL CODE : 241
MATERIAL : UDLT 3
DATA SOURCES
MANUFACTURER : UDRI.01-84-01
UPRI : KUMAR
OTHER INHNE

NO.	MODULUS N/M/12	LOSS FACTOR	TEMP. DEG. C	FREQ. MC	MODE NO.	BEAM MOD. N/M/12	COMPOSITE LOSS FAC	BEAM FREQ. MC	LOSS MOD. N/M/12
1	1.39817E+10	.0797	479.4	93.5	2.	1.39451E+11	.0067	97.9	1.11393E+09
2	1.47178E+10	.0911	479.4	262.6	3.	1.39913E+11	.0080	274.3	1.34128E+09
3	1.49553E+10	.0785	479.4	514.5	4.	1.39527E+11	.0070	537.0	1.17404E+09
4	1.64999E+10	.1065	468.3	94.4	2.	2.30471E+11	.0103	98.1	1.75768E+09
5	1.72665E+10	.0956	468.3	519.5	4.	2.30793E+11	.0096	538.7	1.65116E+09
6	1.67895E+10	.0713	468.3	860.6	5.	2.32369E+11	.0070	894.0	1.20713E+09
7	1.92478E+10	.0803	468.3	1290.4	6.	2.31704E+11	.0088	1330.8	1.54483E+09
8	1.70042E+10	.1034	451.7	94.8	2.	2.31699E+11	.0108	98.4	1.86061E+09
9	1.82063E+10	.0938	451.7	522.3	4.	2.31987E+11	.0098	540.3	1.70752E+09
10	1.84646E+10	.0733	451.7	867.8	5.	2.33957E+11	.0080	897.5	1.40843E+09
11	1.90719E+10	.0764	451.7	1293.0	6.	2.30560E+11	.0082	1341.5	1.45691E+09
12	1.94122E+10	.0912	441.7	268.3	3.	2.34387E+11	.0089	278.7	1.77047E+09
13	1.91633E+10	.0824	441.7	526.5	4.	2.34387E+11	.0089	543.5	1.57873E+09
14	2.04115E+10	.0816	441.7	873.0	5.	2.34184E+11	.0093	898.0	1.66526E+09
15	2.20574E+10	.0936	423.9	96.6	2.	2.37548E+11	.0114	98.9	2.06519E+09
16	2.15727E+10	.0865	423.9	270.7	3.	2.3752E+11	.0095	271.6	1.86610E+09
17	2.25003E+10	.0779	423.9	1318.7	6.	2.37565E+11	.0095	1350.0	1.75268E+09
18	3.11324E+10	.0627	412.8	99.1	2.	2.34579E+11	.0100	99.1	1.95201E+09
19	3.2953E+10	.0610	412.8	277.5	3.	2.35490E+11	.0095	278.1	1.84882E+09
20	3.19880E+10	.0579	412.8	544.5	4.	2.35140E+11	.0108	544.5	2.11203E+09
21	3.03210E+10	.0516	412.8	901.6	5.	2.30922E+11	.0080	904.0	1.66554E+09
22	3.38793E+10	.0484	412.8	1349.3	6.	2.38489E+11	.0075	1353.0	1.78447E+09
23	3.5203E+10	.0493	385.0	100.4	2.	2.38757E+11	.0047	908.0	9.43725E+08
24	3.26985E+10	.0238	385.0	210.4	2.	2.10343E+11	.0048	1359.0	9.68209E+08
25	3.26840E+10	.0256	385.0	436.7	6.	2.10343E+11	.0050	90.8	1.02174E+09
26	3.58213E+10	.0235	371.1	100.0	2.	2.37480E+11	.0050	90.8	8.89609E+08
27	3.41801E+10	.0251	371.1	291.6	3.	2.38011E+11	.0044	278.8	8.89609E+08
28	3.47647E+10	.0179	371.1	552.9	4.	2.38165E+11	.0034	548.5	6.91061E+08
29	3.48288E+10	.0135	371.1	915.2	5.	2.38757E+11	.0023	908.0	4.68691E+08
30	3.42277E+10	.0197	371.1	1360.4	6.	2.11272E+11	.0033	1368.0	6.75509E+08
31	3.72083E+10	.0178	357.2	101.4	2.	2.38520E+11	.0032	100.1	6.63032E+08
32	3.5922E+10	.0144	357.2	283.2	3.	2.39053E+11	.0025	286.5	5.1287E+08
33	3.59054E+10	.0155	357.2	555.0	4.	2.39305E+11	.0027	556.0	5.55654E+08
34	3.58558E+10	.0150	357.2	920.0	5.	2.39305E+11	.0025	911.0	5.26451E+08
35	3.54252E+10	.0129	357.2	1376.0	6.	2.12204E+11	.0022	1368.0	4.55877E+08
36	3.91694E+10	.0097	330.6	102.3	2.	2.10400E+11	.0018	102.5	3.80750E+08
37	3.85767E+10	.0076	330.6	285.7	3.	2.09790E+11	.0014	281.0	2.94271E+08
38	3.79760E+10	.0061	330.6	558.1	4.	2.10230E+11	.0011	552.0	2.31035E+08
39	3.79046E+10	.0061	330.6	927.2	5.	2.11525E+11	.0011	914.0	2.31567E+08
40	3.79011E+10	.0050	330.6	1387.4	6.	2.13449E+11	.0009	1369.0	1.80631E+08
41	3.98964E+10	.0048	301.7	102.9	2.	2.14098E+11	.0009	101.0	1.92733E+08
42	4.14015E+10	.0047	301.7	287.4	3.	2.05508E+11	.0009	280.0	1.92845E+08
43	3.81004E+10	.0038	301.7	563.4	4.	2.18360E+11	.0007	554.0	1.49073E+08
44	3.91809E+10	.0044	301.7	932.3	5.	2.12916E+11	.0008	917.0	1.70691E+08

REDUC : PAUSE
0000

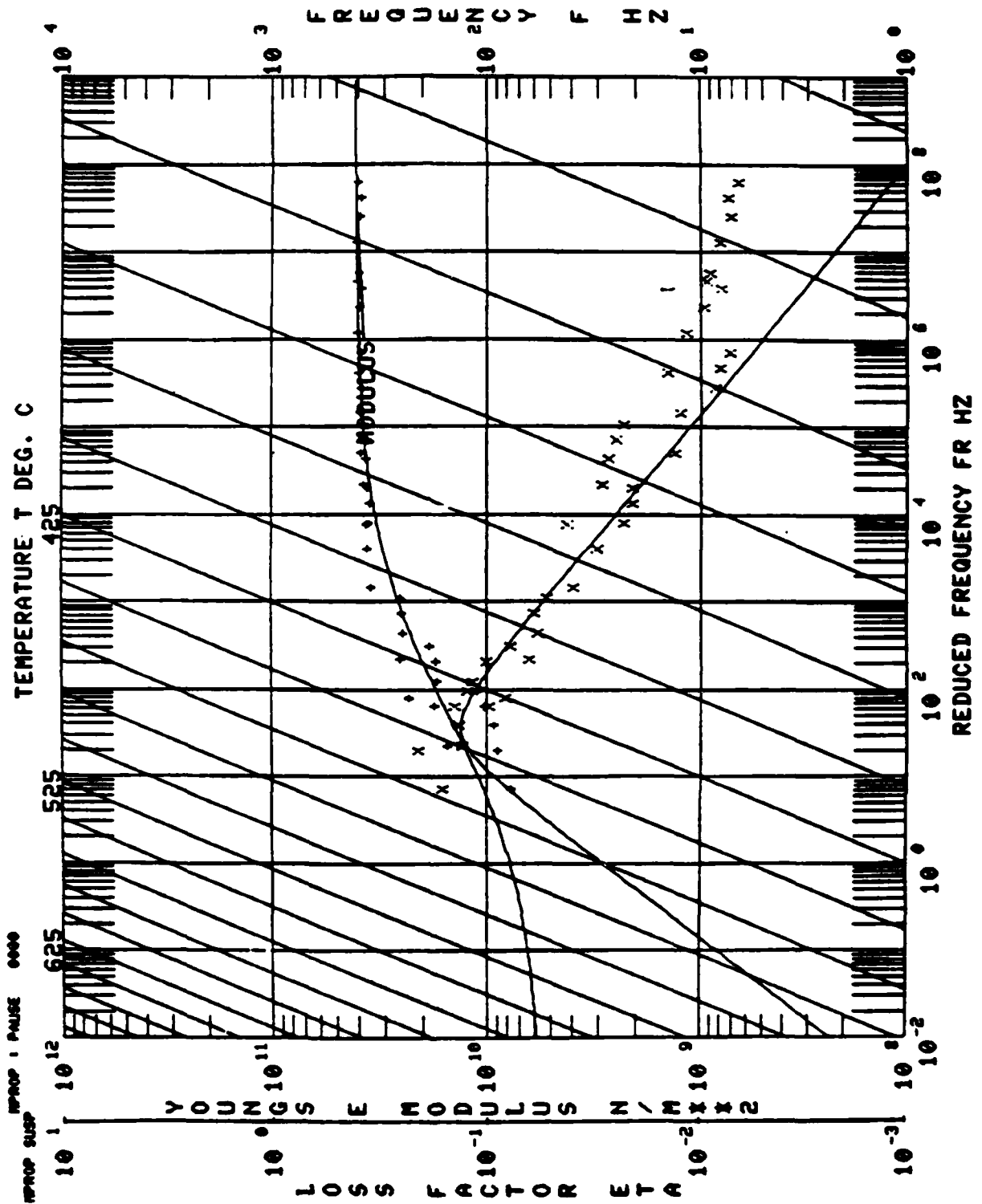


Figure 25. Nomogram for LT-4 with Modulus and Loss Factor

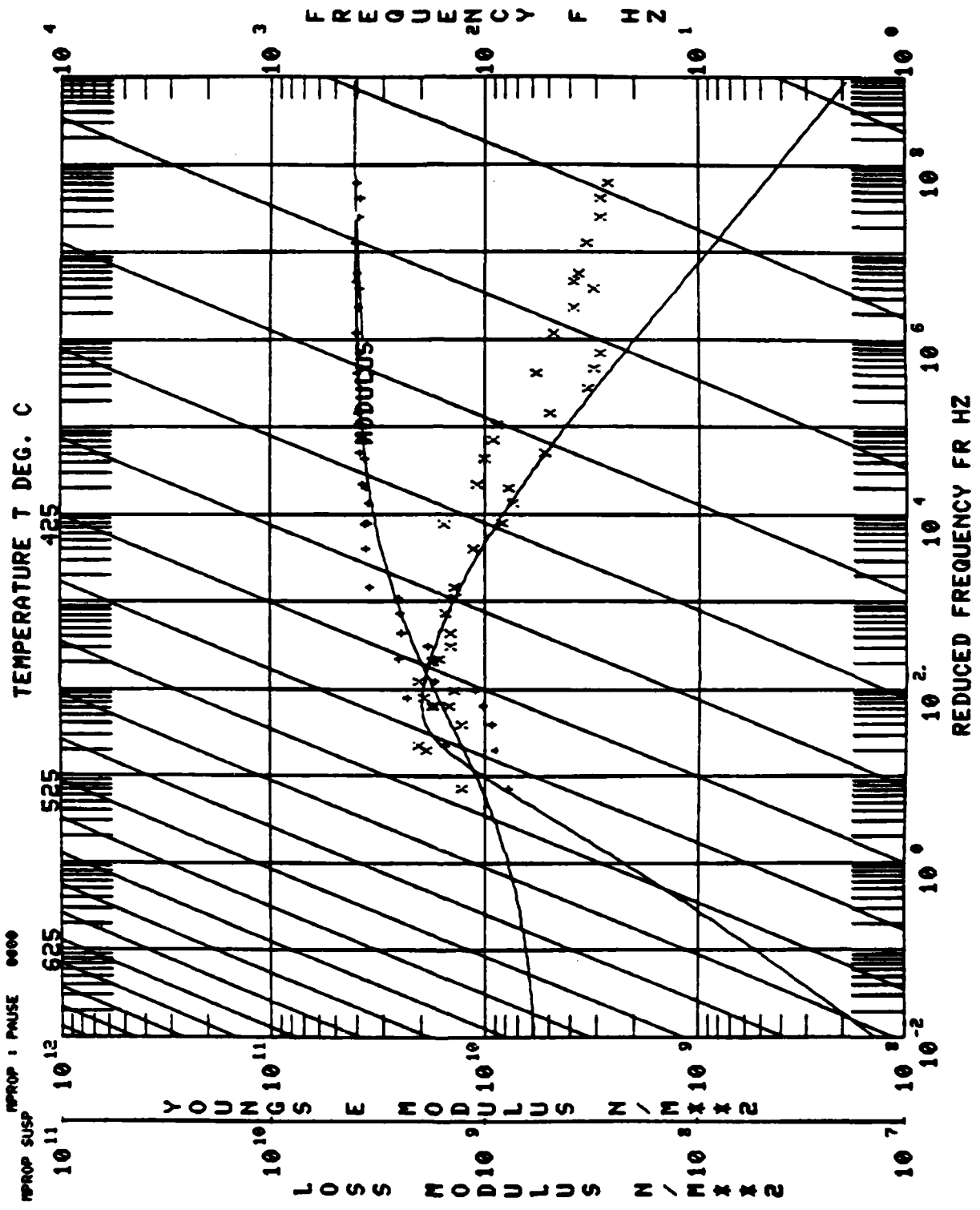


Figure 26. Nomogram for LT-4 with Loss Modulus and Modulus

TABLE 16
EXPERIMENTAL AND REDUCED DATA OF COMPOSITION LT-4.

EXPERIMENTAL CODE :233
MATERIAL :UDLT4
DATA SOURCES
MANUFACTURER :HOME
UDRI :KUNIPAP 01-81-01
OTHER :3-9-82

NO.	MODULUS N/MS2	LOSS FACTOR	TEMP. DEG. C	FREQ. HZ	MODE NO.	BEAM HOP. N/MS2	COMPOSITE LOSS FAC.	BEAM FREQ. HZ	LOSS MOD. N/MS2
1	7.89672E+09	.1657	454.4	92.4	2.	2.04123E+11	.0069	98.1	1.30273E+09
2	9.09099E+09	.2121	454.4	359.3	3.	2.03614E+11	.0101	274.2	1.92860E+09
3	9.44990E+09	.1383	454.4	510.5	4.	2.05667E+11	.0068	539.5	1.31181E+09
4	1.04695E+10	.1439	454.4	849.0	5.	2.06727E+11	.0077	895.0	1.50662E+09
5	1.13203E+10	.1258	454.4	1271.8	6.	2.07318E+11	.0072	1338.0	1.42453E+09
6	1.55705E+10	.1336	440.6	94.5	2.	2.05374E+11	.0102	28.4	2.07973E+09
7	1.78373E+10	.0999	440.6	265.8	3.	2.04304E+11	.0087	275.0	1.78128E+09
8	1.75017E+10	.1187	440.6	522.3	4.	2.07652E+11	.0101	541.0	2.07708E+09
9	1.76140E+10	.1222	440.6	855.0	5.	2.08751E+11	.0071	897.0	1.80002E+09
10	1.87821E+10	.0344	426.7	129.8	6.	2.08719E+11	.0092	1341.0	1.48798E+09
11	2.35321E+10	.0344	426.7	96.6	2.	2.06419E+11	.0077	98.6	1.97364E+09
12	2.56499E+10	.0552	426.7	271.4	3.	2.05922E+11	.0068	275.7	1.67315E+09
13	2.51395E+10	.0538	426.7	533.2	4.	2.07556E+11	.0077	542.5	1.48268E+09
14	2.54791E+10	.0611	426.7	883.9	5.	2.02998E+11	.0071	899.0	1.55736E+09
15	2.59797E+10	.0537	426.7	1323.4	6.	2.02998E+11	.0063	1345.0	1.39435E+09
16	3.52903E+10	.0405	398.9	99.6	2.	2.08519E+11	.0051	99.1	1.42773E+09
17	3.68922E+10	.0313	398.9	279.3	3.	2.07793E+11	.0049	277.0	1.15573E+09
18	3.61474E+10	.0235	393.9	548.4	4.	2.09474E+11	.0036	545.0	8.50257E+08
19	3.56443E+10	.0212	398.9	908.2	5.	2.10906E+11	.0032	904.0	7.57205E+08
20	3.69423E+10	.0214	392.9	1366.5	6.	2.11876E+11	.0033	1351.0	7.90249E+08
21	3.71156E+10	.0429	385.0	100.2	2.	2.09572E+11	.0067	99.4	1.59286E+09
22	3.81346E+10	.0294	385.0	280.5	3.	2.08544E+11	.0047	277.5	1.12050E+09
23	3.72686E+10	.0275	385.0	550.8	4.	2.10436E+11	.0043	546.2	1.06860E+09
24	3.68331E+10	.0254	385.0	912.6	5.	2.12074E+11	.0039	906.5	9.33951E+08
25	3.90791E+10	.0235	385.0	1366.7	6.	2.12975E+11	.0037	1354.5	8.95956E+08
26	3.94931E+10	.0135	371.1	100.9	2.	2.10628E+11	.0022	99.6	5.33015E+08
27	3.93175E+10	.0127	371.1	282.2	3.	2.09673E+11	.0021	278.2	5.08420E+08
28	3.87795E+10	.0082	371.1	553.6	4.	2.11400E+11	.0014	547.5	3.38598E+08
29	3.82165E+10	.0075	371.1	915.5	5.	2.12766E+11	.0012	908.0	2.14844E+08
30	3.93567E+10	.0075	371.1	1372.4	6.	2.13766E+11	.0012	1357.0	2.9735E+08
31	4.0446E+10	.0145	357.2	101.3	2.	2.11686E+11	.0024	99.9	5.87150E+08
32	4.10167E+10	.0119	357.2	283.2	3.	2.10427E+11	.0020	273.7	4.88977E+08
33	3.97899E+10	.0098	357.2	555.6	4.	2.12173E+11	.0016	543.5	3.99491E+08
34	3.91380E+10	.0081	357.2	919.9	5.	2.13715E+11	.0013	910.0	3.1725E+08
35	4.03746E+10	.0092	357.2	1377.8	6.	2.14708E+11	.0015	1360.0	3.7027E+08
36	4.07266E+10	.0097	343.3	101.6	2.	2.1246E+11	.0016	100.1	3.93595E+08
37	4.14531E+10	.0083	343.3	284.0	3.	2.1246E+11	.0014	279.3	3.4242E+08
38	4.00799E+10	.0073	343.3	556.9	4.	2.13141E+11	.0012	549.7	2.94417E+08
39	3.91899E+10	.0075	343.3	922.2	5.	2.14890E+11	.0012	912.5	2.94592E+08
40	4.06479E+10	.0057	343.3	1381.1	6.	2.15556E+11	.0011	1353.0	2.73227E+08

REDUC : PAUSE 0000
REDUC SUSP

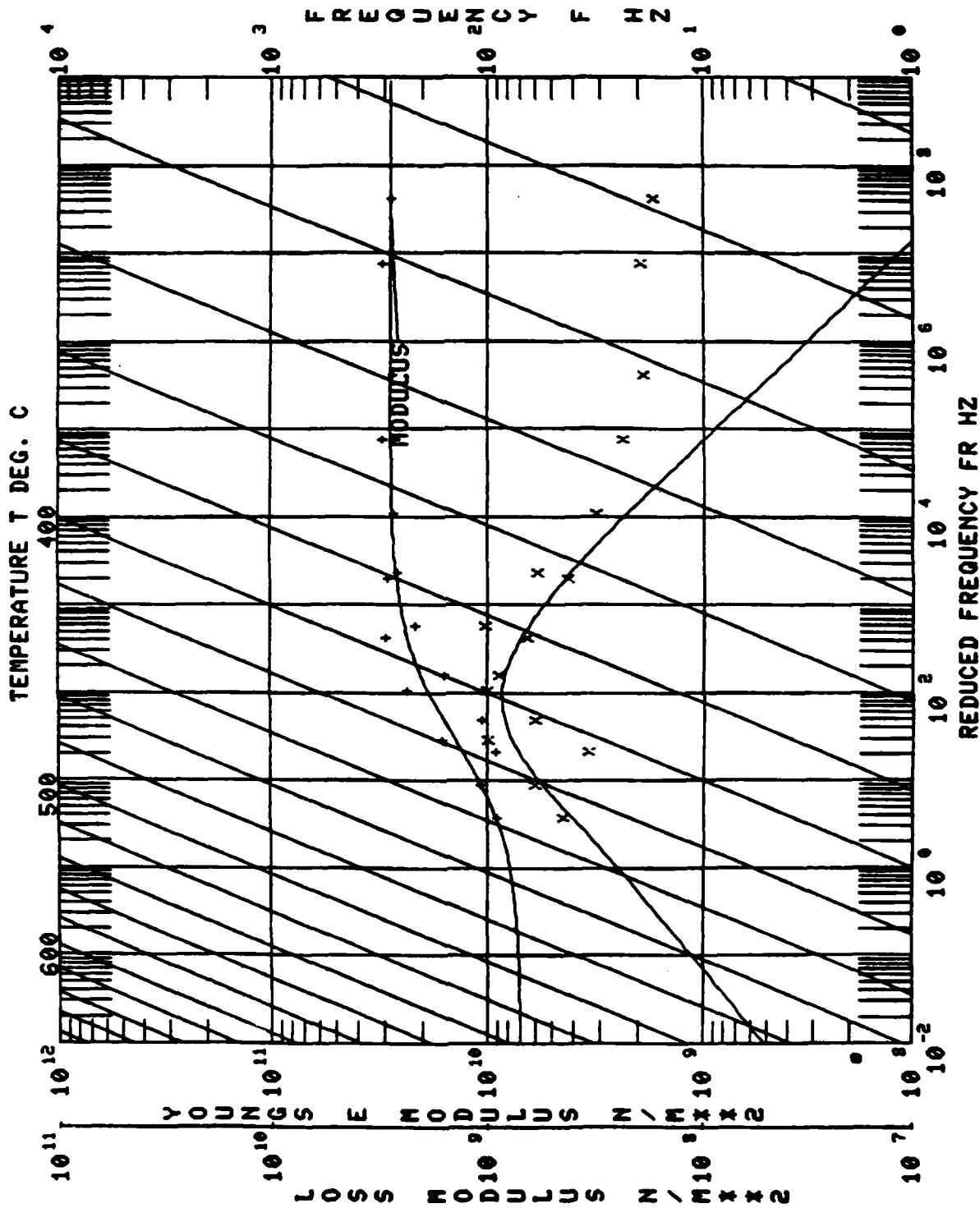


Figure 27. Reduced Nomogram Displaying Loss Factor for LT-5.

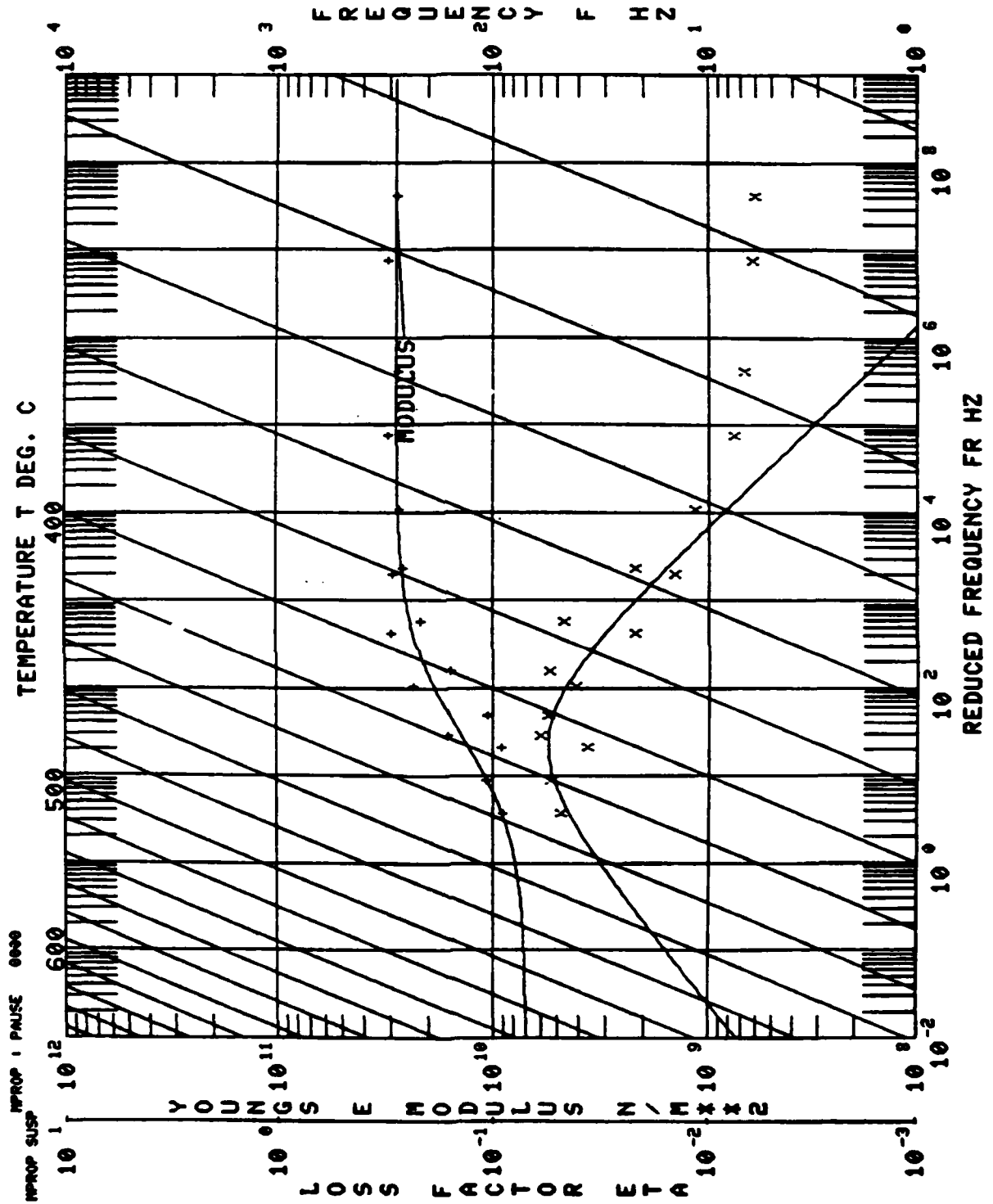


Figure 28. Reduced Nomogram Displaying Loss Modulus for LT-5.

TABLE 17
EXPERIMENTAL AND REDUCED DATA OF COMPOSITION LT-5.

EXPERIMENTAL CODE 1240	MATERIAL IDULT 5	DATA SOURCES	MANUFACTURER IUDRI	OTHER INONE					
NO.	MODULUS N/MSI2	LOSS FACTOR	TEMP. DEG. C	FREQ. HZ	MODE NO.	EEMV HGD. N. MSI2	COMPOSITE LOSS FAC.	BEAM FREQ. HZ	LOSS MOD. N/MSI2
1	9.22790E+09	.0394	437.8	93.4	2.	2.02129E+11	.0025	98.3	4.55626E+06
2	9.39279E+09	.0370	437.8	513.0	4.	2.02420E+11	.0019	542.5	3.47235E+08
3	1.10465E+10	.0555	426.7	94.0	2.	2.02948E+11	.0033	99.0	6.12404E+08
4	1.08555E+10	.0554	426.7	515.4	4.	2.03541E+11	.0033	544.0	6.13204E+08
5	1.64569E+10	.0213	412.8	95.6	2.	2.03769E+11	.0052	99.2	1.00954E+02
6	1.60204E+10	.0558	412.8	523.8	4.	2.04665E+11	.0046	545.5	3.93566E+02
7	2.38472E+10	.0423	398.9	97.5	2.	2.04592E+11	.0049	99.4	1.00201E+09
8	2.19291E+10	.0474	398.9	534.5	4.	2.06169E+11	.0051	547.5	1.04189E+09
9	2.98753E+10	.0224	355.0	99.1	2.	2.05416E+11	.0031	99.6	6.67731E+08
10	2.66469E+10	.0223	355.0	541.8	4.	2.07300E+11	.0023	549.0	5.93974E+08
11	2.97432E+10	.0146	371.1	99.4	2.	2.07111E+11	.0020	100.0	4.33212E+08
12	2.74733E+10	.0117	371.1	544.2	4.	2.08434E+11	.0015	550.5	3.2145E+02
13	3.11890E+10	.0078	343.3	100.0	2.	2.08313E+11	.0011	100.3	2.41754E+02
14	3.81014E+10	.0069	343.3	547.1	4.	2.10332E+11	.0009	553.0	1.95143E+08
15	3.14066E+10	.0053	315.6	100.4	2.	2.09978E+11	.0009	100.7	1.99329E+08
16	2.83561E+10	.0062	315.6	549.6	4.	2.12238E+11	.0008	555.5	1.75032E+08

REDUC : PAUSE 0000

REDUC SUSP

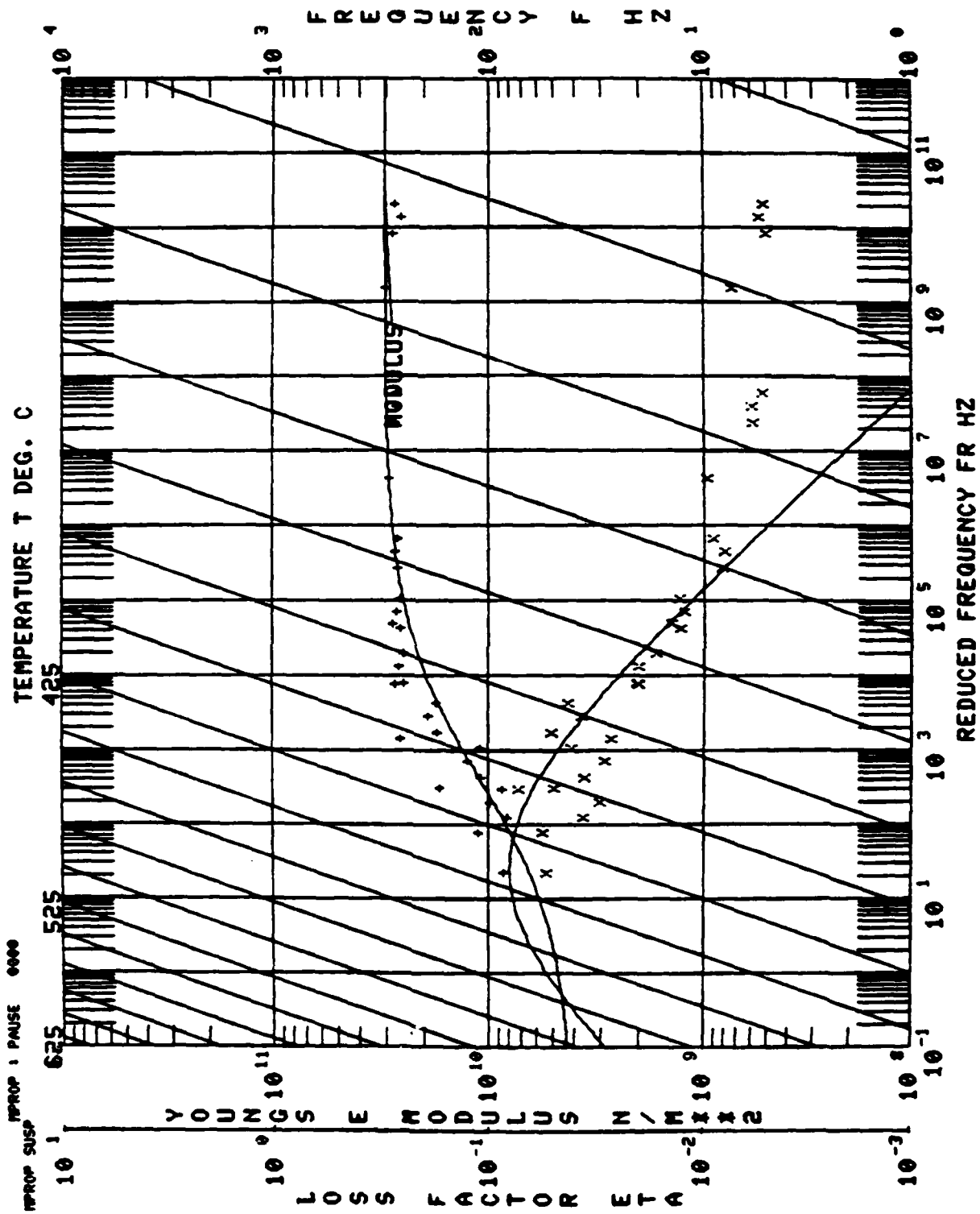


Figure 29. Nomogram for LT-6 with Modulus and Loss Factor

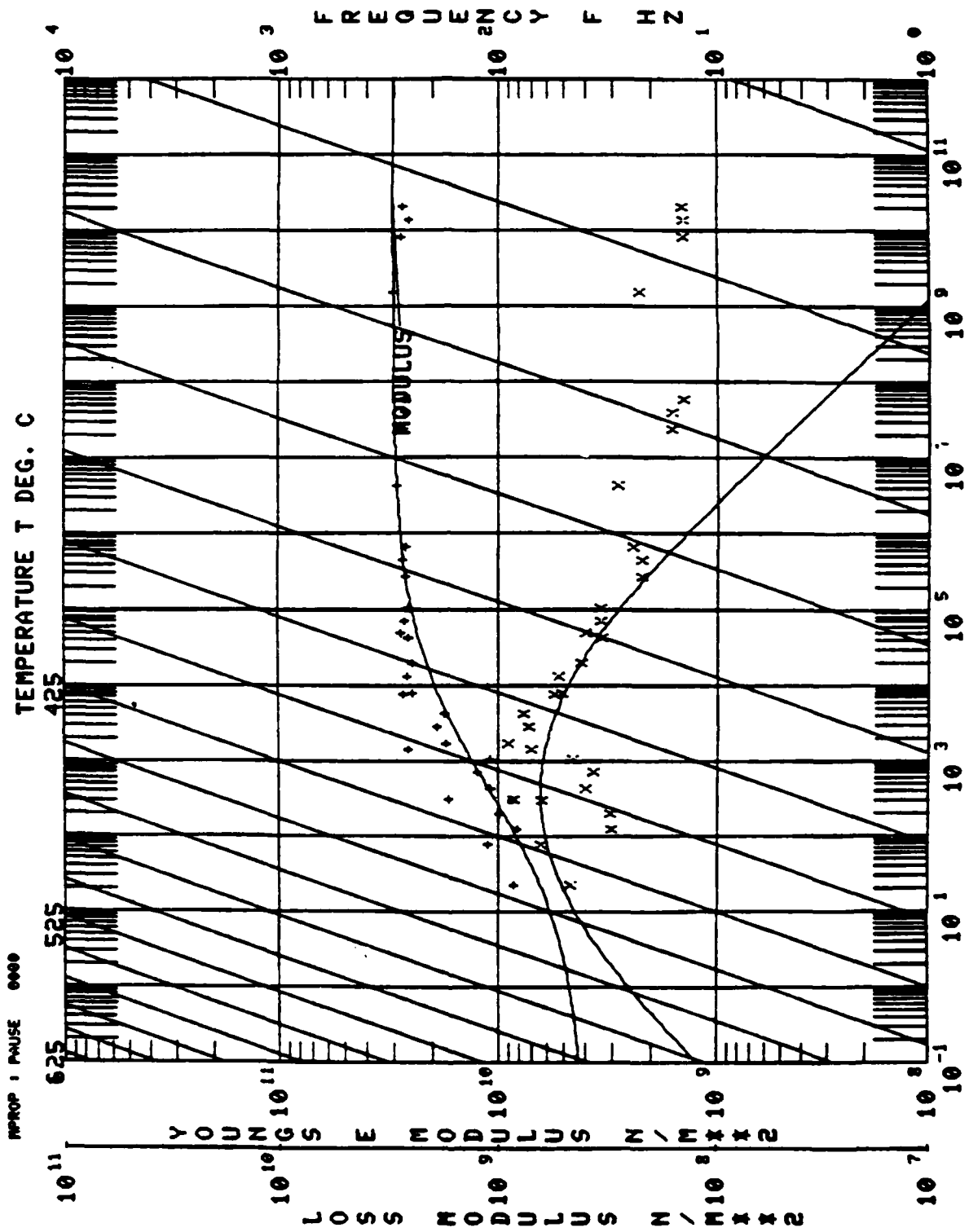


Figure 30. Nomogram for LT-6 with Loss Modulus and Modulus

TABLE 18
EXPERIMENTAL AND REDUCED DATA OF COMPOSITIONS LT-6

EXPERIMENTAL CODE 12-2
MATERIAL UDM16
DATA SOURCES
MANUFACTURER INCHIE
UDRI KUMAR 01-82-01
OTHER 13-9-82

NO.	MODULUS N/MHz	LOSS FACTOR	TEMP. DEG. C	FREQ. HZ	MODE NO.	BEAM MOD. N/MHz	COMPOSITE LOSS FAC.	LEHM FREQ. HZ	LOSS MOD. N/MHz
1	8.78336E+09	.0551	440.6	92.3	2.	2.0325E+11	.0028	98.5	4.83861E+08
2	8.39689E+09	.0371	440.6	510.1	4.	2.0432E+11	.0018	542.0	3.11698E+08
3	1.00931E+10	.0312	440.6	845.6	5.	2.0349E+11	.0018	894.0	3.14808E+08
4	8.80374E+09	.0735	440.6	1266.0	6.	2.06870E+11	.0037	1344.0	6.50099E+08
5	1.15128E+10	.0571	426.7	93.8	4.	2.0428E+11	.0023	92.7	6.56919E+08
6	1.11081E+10	.0365	426.7	515.4	2.	2.0552E+11	.0021	543.5	3.77292E+08
7	1.28283E+10	.0294	426.7	854.2	5.	2.0454E+11	.0021	896.3	3.77292E+08
8	1.12158E+10	.0416	426.7	1278.2	6.	2.0810E+11	.0026	1348.0	4.68354E+08
9	1.7199E+10	.0509	412.8	95.4	2.	2.0489E+11	.0047	98.9	8.75523E+08
10	1.77304E+10	.0520	412.8	525.7	4.	2.0622E+11	.0049	544.5	9.21947E+08
11	1.95435E+10	.0330	412.8	871.8	5.	2.0555E+11	.0039	898.5	7.41892E+08
12	1.77939E+10	.0439	412.8	1304.2	6.	2.0918E+11	.0041	1351.5	7.31170E+08
13	2.61439E+10	.0276	392.9	97.8	2.	2.0571E+11	.0036	99.1	7.20359E+08
14	2.51789E+10	.0207	392.9	537.2	4.	2.0742E+11	.0026	546.0	5.2006E+08
15	2.65885E+10	.0205	392.9	889.8	5.	2.0663E+11	.0027	901.0	5.4429E+08
16	2.51989E+10	.0169	392.9	1332.1	6.	2.1027E+11	.0021	1355.0	4.24763E+08
17	2.75307E+10	.0206	385.0	98.3	2.	2.0655E+11	.0028	99.3	5.6787E+08
18	2.61265E+10	.0132	385.0	539.5	4.	2.0833E+11	.0017	547.2	3.43610E+08
19	2.73205E+10	.0127	385.0	893.3	5.	2.0770E+11	.0017	903.2	3.45791E+08
20	2.61213E+10	.0133	385.0	1337.7	6.	2.1120E+11	.0017	1358.0	3.4742E+08
21	2.84935E+10	.0144	371.1	98.7	2.	2.0717E+11	.0020	99.4	4.09475E+08
22	2.67135E+10	.0084	371.1	541.4	4.	2.0935E+11	.0011	548.5	2.24150E+08
23	2.76867E+10	.0021	371.1	896.5	5.	2.0899E+11	.0011	906.0	2.25453E+08
24	2.67115E+10	.0093	371.1	1342.2	6.	2.1213E+11	.0012	1361.0	2.47159E+08
25	2.96266E+10	.0098	343.3	99.2	2.	2.0863E+11	.0014	99.8	2.92594E+08
26	2.74986E+10	.0060	343.3	544.2	4.	2.1085E+11	.0008	550.5	1.64910E+08
27	2.73763E+10	.0050	343.3	901.0	5.	2.1173E+11	.0008	912.0	1.6531E+08
28	2.71765E+10	.0054	343.3	1348.9	6.	2.1401E+11	.0007	1367.0	1.45638E+08
29	3.0667E+10	.0075	315.6	99.7	2.	2.0989E+11	.0011	100.1	2.31024E+08
30	2.82333E+10	.0052	315.6	546.3	4.	2.1238E+11	.0007	552.5	1.4594E+08
31	2.60735E+10	.0056	315.6	905.4	5.	2.1573E+11	.0007	920.5	1.4547E+08
32	2.79342E+10	.0053	315.6	1355.6	6.	2.1558E+11	.0007	1372.0	1.47343E+08

REDUC 1 PAUSE 0000
REDUC SUSP

3.2 RELATIONSHIP BETWEEN THE DAMPING TEMPERATURE AND GLASS TRANSITION TEMPERATURE

Figure 31 shows a plot of the maximum loss factor at 100 Hz versus the glass transition temperature (T_g) of test matrix glasses whose damping properties were reported earlier (10). The glass transition temperatures for the compositions are also shown in Table 19. It is obvious from the figure that there is a linear relationship between the loss factor peak temperature and T_g . Regression analysis of the data provided a relationship between the damping peak temperature, T_η at 100 Hz and the glass transition temperature as expressed by equation (6). The correlation coefficient for this relationship is 0.96.

$$T_\eta = 166.02 + 1.10T_g \quad (6)$$

where: T_η and T_g are in °C.

The relationship is useful in predicting the damping peak temperature if the glass transition temperature is known. This suggests that the loss factor peak temperature T_η is determined by the viscosity of the glass just as T_g corresponds to a given viscosity (approximately 10^{13} poise). Also, increasing T_g indicates general stiffening of the glass structure and, therefore, one can expect a decrease in the η_D peak height. However, an attempt to correlate the η_D peak height with the glass transition temperature was not successful.

An estimate of the viscosity corresponding to the η_D peak temperature can be made because the viscosity-temperature relationship of the Corning 0010 glass is known. Figure 32 shows the viscosity-temperature relationship of the glass. The loss factor peak temperature for the glass at 100 Hz is 650°C, which corresponds to a viscosity of 10^7 poise. Similarly, at 1000 Hz, the loss factor peak corresponds to a viscosity of $10^{6.5}$ poise. It is, therefore, noted that the observed damping occurs when the glass temperature is near the softening point (viscosity = $10^{7.6}$). Also, the damping temperature is about 200°C above the glass transition temperature. The glass transition temperature of the

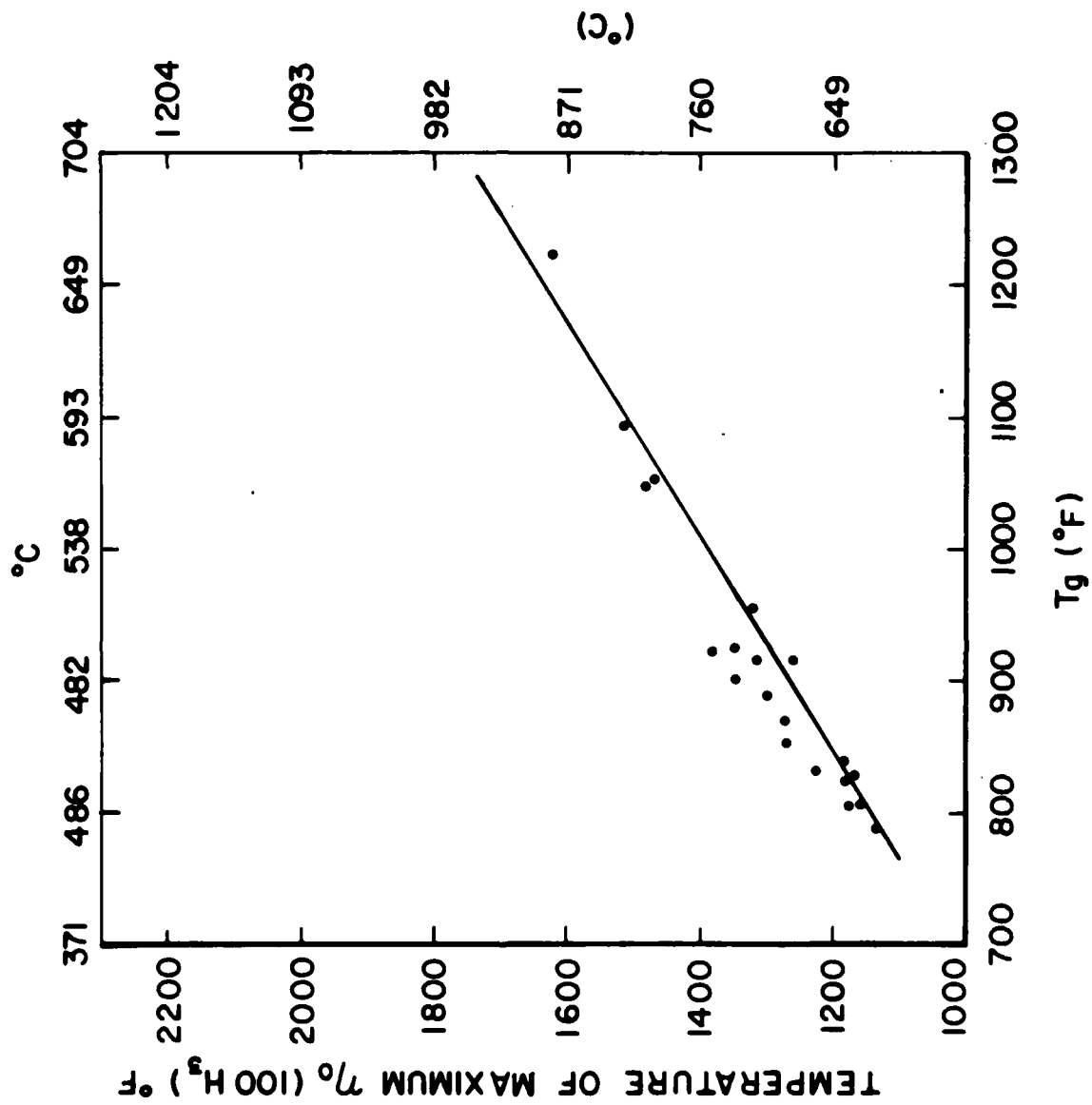


Figure 31. Maximum Loss Factor (η_D) Temperature Versus the Glass Transition Temperature (T_g).

TABLE 19
 GLASS TRANSITION TEMPERATURES (T_g) OF TEST
 MATRIX GLASS COMPOSITIONS

Specimen Number	T_g ($^{\circ}$ C)
M30	429
M1	532
M36	601
M2	441
M19	408
M17	491
M29	583
M49	475
M32	568
M26	441
M12	496
M21	662
M35	466
M24	494
M11	489
M22	511
M14	447
M48	421
M5	456
M27	482
M41	541
M31	466
M4	590
M45	491
M46	564
M6	447
M7	431

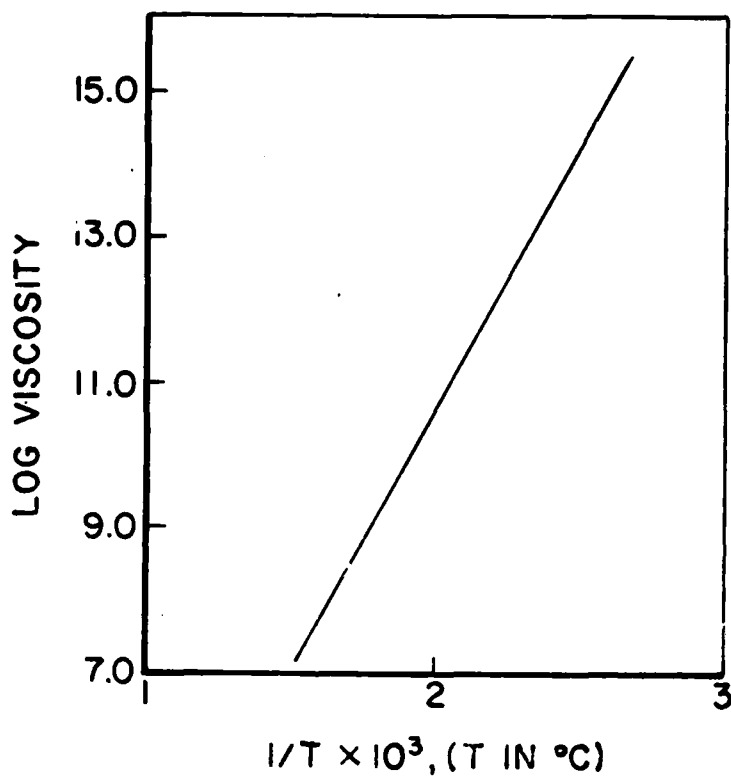


Figure 32. Log Viscosity Versus 1/T for Corning 0010 Glass (viscosity in poise).

Corning 0010 glass is approximately 430°C. At the damping temperature, the glass can be characterized as a viscous, rather than a viscoelastic, material.

3.3 EFFECT OF NUCLEATION AND CRYSTALLIZATION ON THE VISCOELASTIC DAMPING

In the previous section, it has been shown that the viscosity of the vitreous enamel ranges from 10^6 to 10^7 poise in the damping range. The viscosity range is favorable for processes like nucleation and crystallization. It has also been observed that when a vitreous enamel is aged in the damping range, generally there is a reduction in the loss factor (Q^{-1}). The structural mechanisms leading to the reduction are not understood. It has been hypothesized that the reduction is related to the devitrification, but no experimental data exist to support this hypothesis. In view of this lack of understanding of the effects of thermal aging on the damping properties, this work was undertaken.

Figure 33 illustrates a typical viscosity versus temperature relationship for silicate glasses. The viscoelastic damping range is indicated by a shaded area in the figure. Included schematically in the figure are nucleation and growth rate curves for silicate glasses. It should be noted that the damping range approximately coincides with the crystal growth range. A glass coating containing nucleating sites would be expected to crystallize in the damping range. This assumption can be justified if the real situation is examined. These vitreous enamel coatings are generally applied on superalloys substrates. Diffusion of the metallic ions into the coating can enhance the nucleation and growth processes. Prolonged exposure of the coating in the damping range would be expected to transform the vitreous enamel coating into a crystalline coating. A consequence of the transformation would be a significant change in the damping properties.

In view of the background provided above, two glass compositions were thermally aged in the damping temperature range. Their damping properties and microstructural development were

characterized as a function of heat treatment time. Optical microscope, scanning electron microscope (SEM), and x-ray diffraction were the primary analytical tools for microstructural characterization.

Compositions of the two glasses designated as A and B with the heat treatment conditions are shown in Table 20. Composition A is Al_2O_3 free, whereas composition B contains 5.70 percent Al_2O_3 . Heat treatment temperatures approximately correspond to the respective peak damping temperatures. Heat treatment times were arbitrarily chosen.

TABLE 20
COMPOSTIONS IN WEIGHT PERCENT

	A	Heat Treatment Conditions	B	Heat Treatment Conditions
SiO_2	74.65	at 760°C	70.40	at 815°C
Al_2O_3	--	I no heat treatment	5.70	I no heat treatment
Na_2O	12.78	II 100 hours	12.05	II 112 hours
CaO	10.77	III 314 hours	10.15	III 309 hours
CoO	1.80		1.70	

The loss factor of these glasses as a function of temperature and heat treatment are shown in Figures 34 and 35. The loss factor decreased with increasing heat treatment time near the peak damping for both compositions. Composition B, in general, has a lower loss factor than composition A. This can be explained on the basis of the Al_2O_3 concentration in the glass. It has been shown that the addition of Al_2O_3 decreases the loss factor (6) significantly.

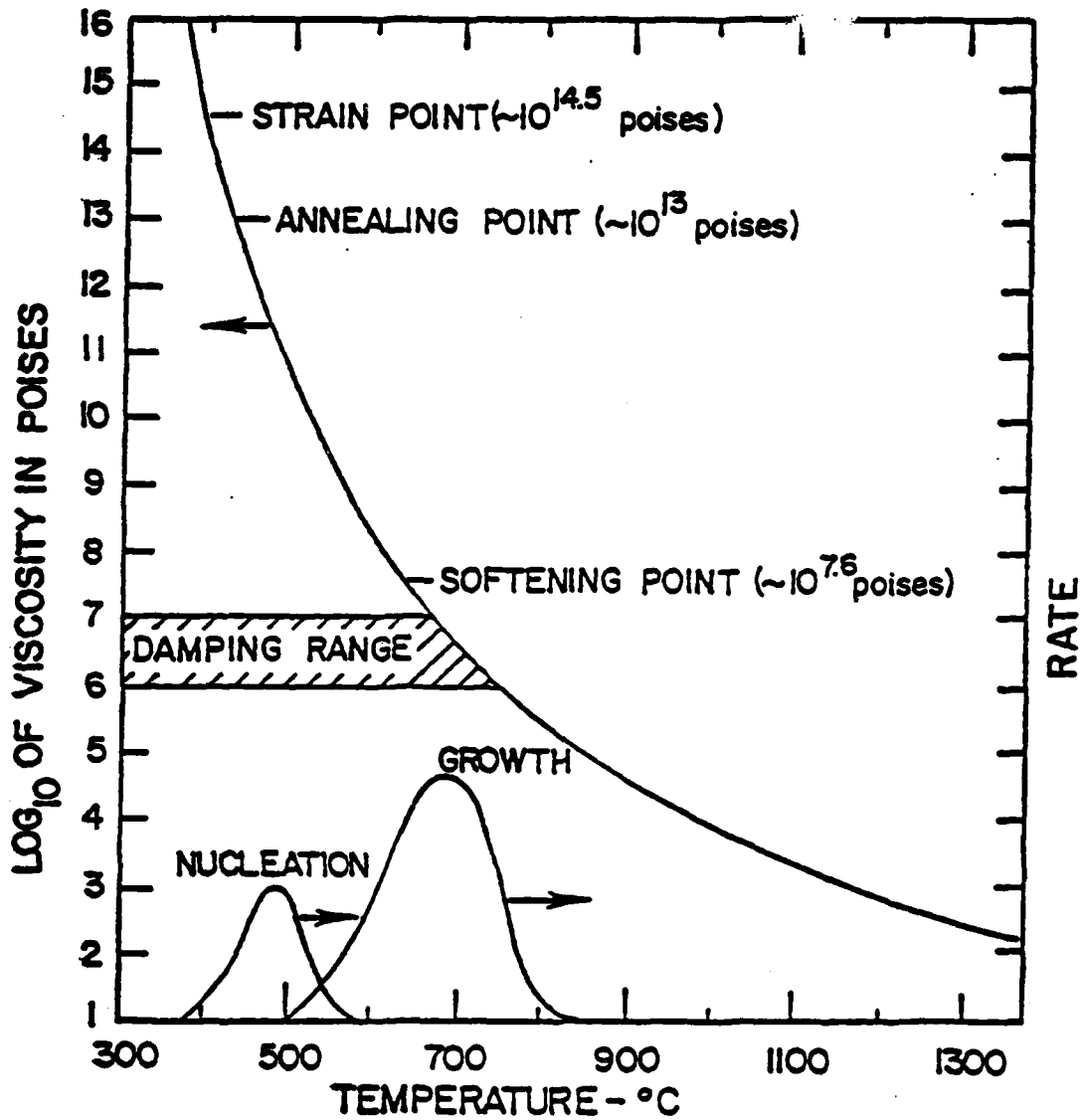


Figure 33. Typical Viscosity Curve for Glass Showing Common Reference Points.

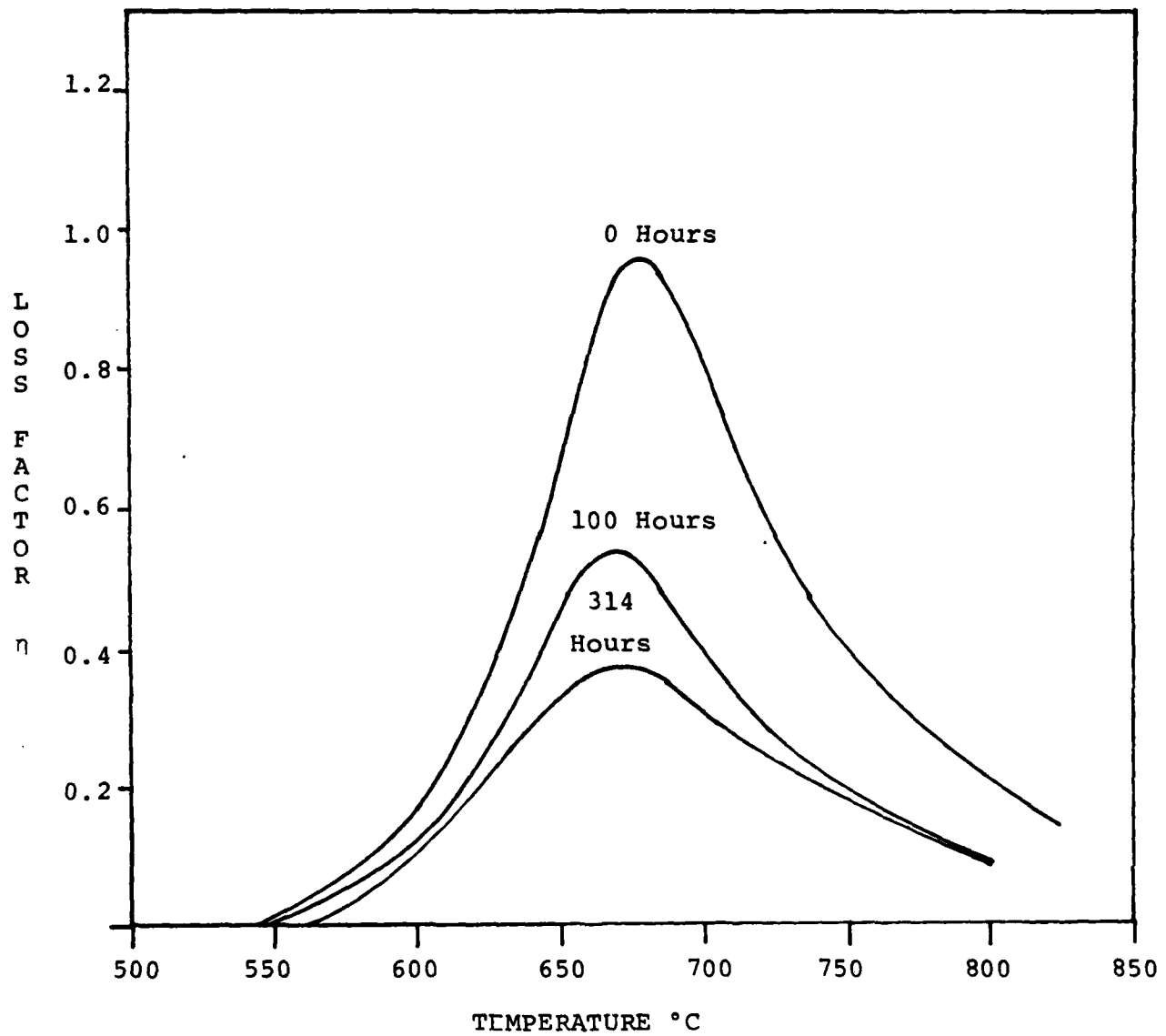


Figure 34. Loss Factor as a Function of Temperature and Heat Treatment Time at 760°C for Composition A.

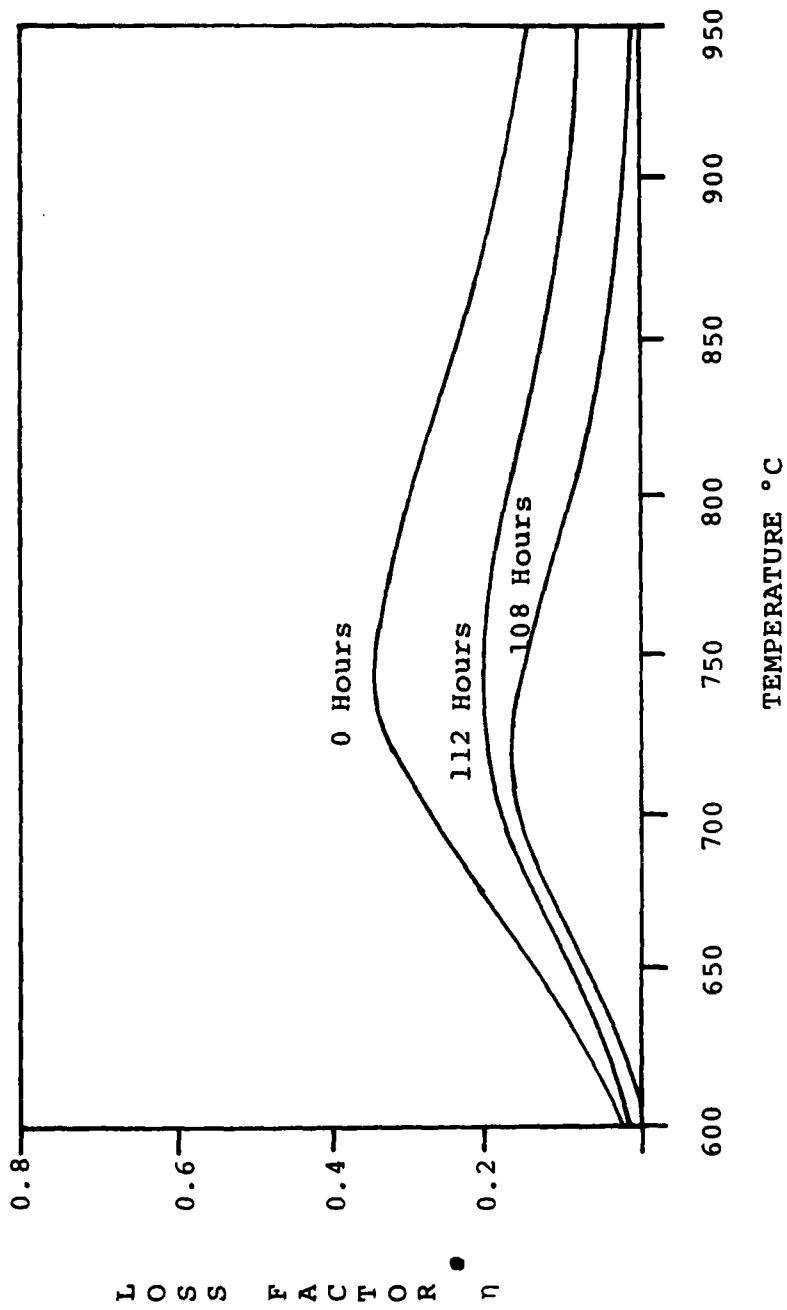


Figure 35. Loss Factor as a Function of Temperature and Heat Treatment Time at 815°C for Composition B.

Figure 36 shows the optical micrographs of the enamel-metal interface of "as-fired" and "heat treated" (112 hours at 815°F or 435°C) specimens obtained from composition B. Both specimens exhibited seeds and bubbles at the interface. No crystalline phase or microstructure was present in the as-fired enamel coating. However, after the heat treatment, a crystalline phase in the vitreous enamel coating appeared. The crystalline phase was noted to originate from the seeds and bubbles in most instances, and appears in the micrograph as elongated needles. There was also a marked variation in the grain sized distribution of the metal at the interface. It appears that the metallic grains at the interface have been fragmented into smaller sizes due to chemical reaction with the vitreous enamel coating. The fragmentation of the metallic grain is much more pronounced after heat treatment (Figure 36b).

The evidence of crystallization from the optical microscopy and possibility of glass-metal interaction at the interface promoted further microscopic examination. Several specimens were examined under SEM and the observations are described in the following paragraphs.

Figures 37 shows the glass-metal interface for composition A after various heat treatments. All these micrographs have similar magnification. It should be noted that the fragmentation of the metallic grains at the interface increases with increasing heat treatment time. Also the degree of crystallization of the vitreous enamel coating increases with progressive heat treatment. No change in the size and distribution of the pores at the interface was noted.

Figure 38 shows morphology of the vitreous enamel coating "A" at varying magnifications after a heat treatment of 100 hours. The appearance of crystals of hexagonal habit can be noted in micrographs 38b and 38c.

Figure 39 demonstrates the microstructure of the vitreous enamel coating "A" at varying magnifications after 314 hours of heat treatment. As expected, the degree of crystallinity has increased when compared to the 100 hour specimen (Figure 38a, 38b, 38c).

Figure 40 shows the metal-glass interface for composition "B" as a function of heat treatment time. Fragmentation of the metallic grains at the interface is similar to the one observed in Figure 37. There is no evidence of crystallinity in the vitreous enamel coating in the as-fired specimen (Figure 40a). After heat treatment the coating crystallized as evidenced by micrographs 40b and 40c.

Figure 41 shows the enamel coating for the composition "B" at various magnifications after heat treatment for 112 hours. All three micrographs show the existence of a predominately glassy phase. After heat treatment for 309 hours, there is a significant increase in the degree of crystallinity, as shown in Figure 42. However, in this case, characteristics of the crystals appear to be different from those of the composition "A" for similar heat treatment (Figure 39). The crystalline phase is present as elongated needles rather than in a hexagonal habit.

The crystalline phases for both compositions which appeared after heat treatment were identified by x-ray diffraction. Table 21 summarizes the x-ray diffraction results. After heat treatment, composition "A" developed α -quartz and devitrite ($\text{Na}_2\text{O}\cdot 3\text{CaO}\cdot 6\text{SiO}_2$) crystals; α -quartz being the major crystalline phase. The hexagonal crystals shown in Figures 38 and 39 can now be identified as α -quartz. After heat treatments of composition "B", α -cristobalite and devitrite ($\text{Na}_2\text{O}\cdot 3\text{CaO}\cdot 6\text{SiO}_2$) appear as crystalline phases; α -cristobalite being the major crystalline phase. The elongated crystals observed in Figure 42 are therefore α -cristobalite.

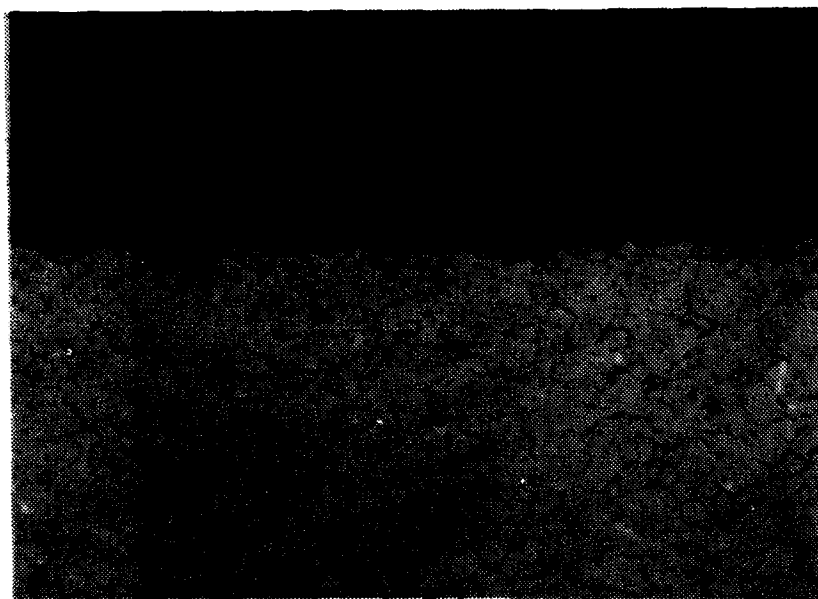
Prolonged heat treatment of the vitreous enamel coatings "A" and "B" in the viscoelastic range progressively reduced the loss factors as shown in Figures 2 and 3. Microstructural analysis by optical microscopy, SEM, and x-ray diffraction revealed crystallization of the coatings. The degree of crystallinity for both compositions was related to the heat treatment time. It is suggested that the crystallization of the glass coatings is primarily responsible for the reduced loss factor. This suggestion can further be justified by considering the fundamental origin of



(a)

Glass

Metal

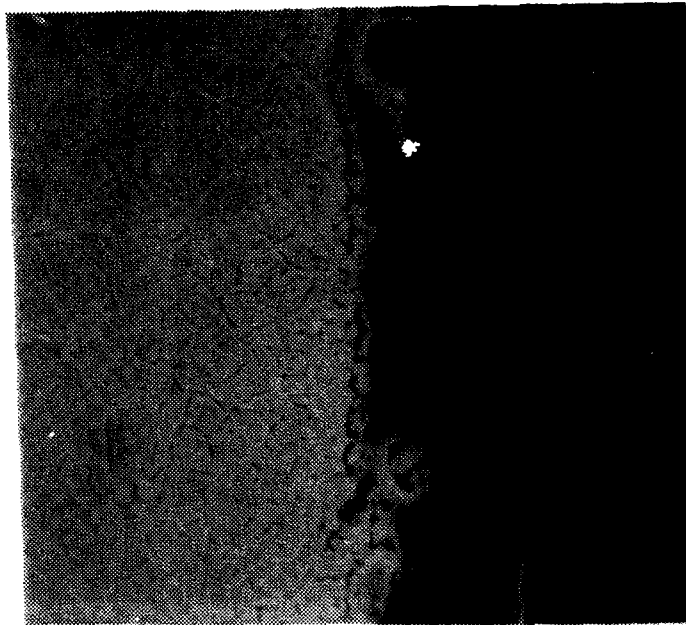


(b)

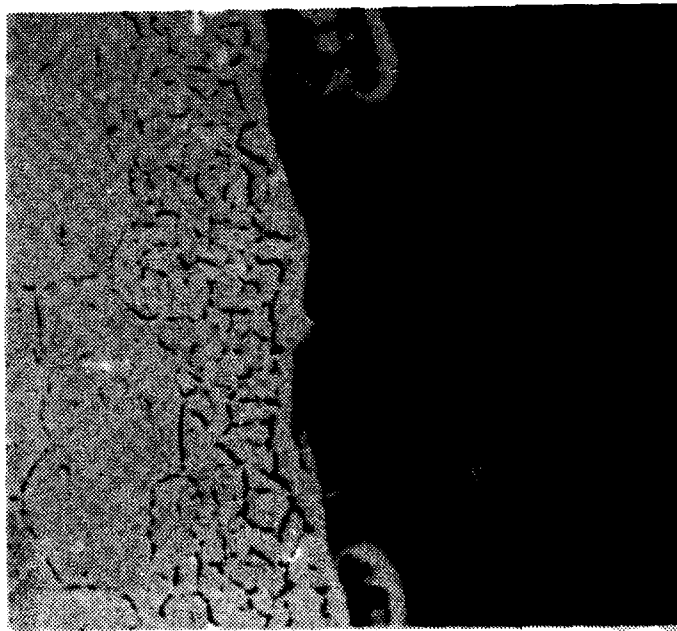
Glass

Metal

Figure 36. Optical Micrographs: (a) As Fired Specimen (150X); (b) Heat Treated for 112 Hours at 1,500°F (150X).



(a) As Fired
(1000X)



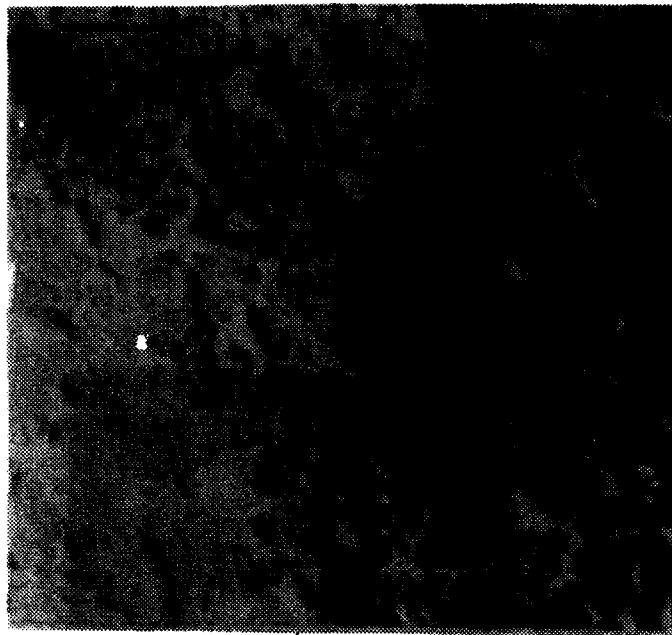
(b) At 100 Hours
(1000X)

Figure 37. Glass-Metal Interface for Composition "A"
After Various Heat Treatments (continued).



(c) At 314 Hours
(1000X)

Figure 37. Glass-Metal Interface for Composition "A"
After Various Heat Treatments (concluded).



(a) 100X



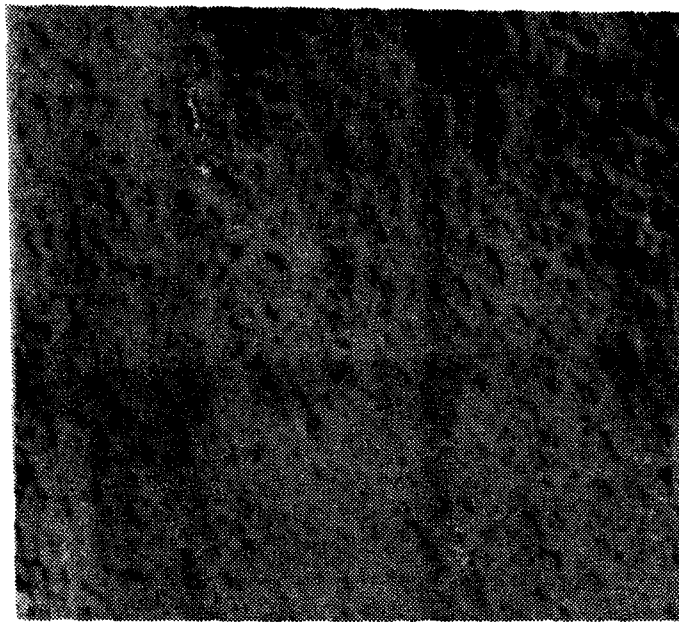
(b) 300X

Figure 38. Morphology of Vitreous Enamel Coating "A"
After Heat Treatment of 100 Hours (continued).

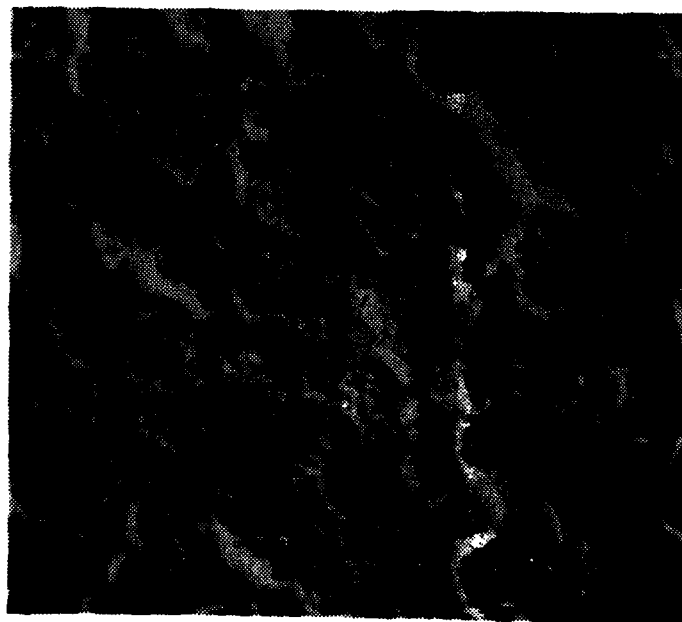


(c) 1000X

Figure 38. Morphology of Vitreous Enamel Coating "A"
After Heat Treatment of 100 Hours (concluded).



(a) 100X



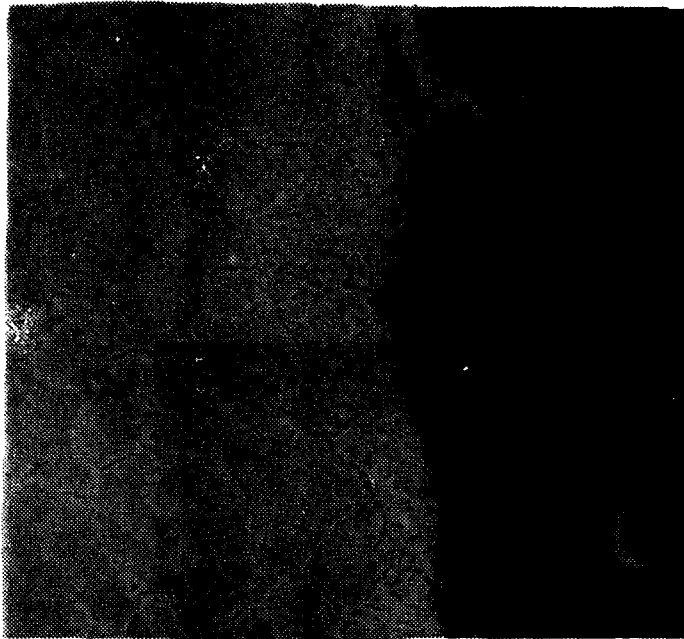
(b) 300X

Figure 39. Microstructure of Vitreous Enamel "A" After 314 Hours of Heat Treatment (continued).

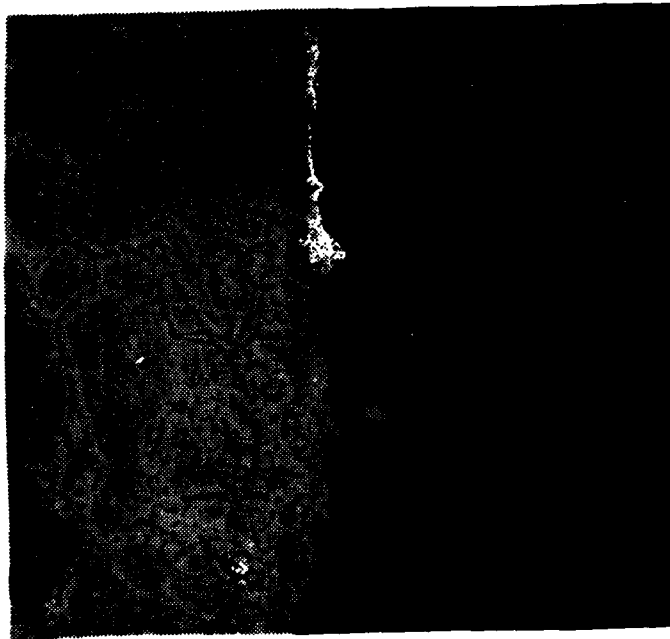


(c) 1000X

Figure 39. Microstructure of Vitreous Enamel "A" After 314 Hours of Heat Treatment (concluded).

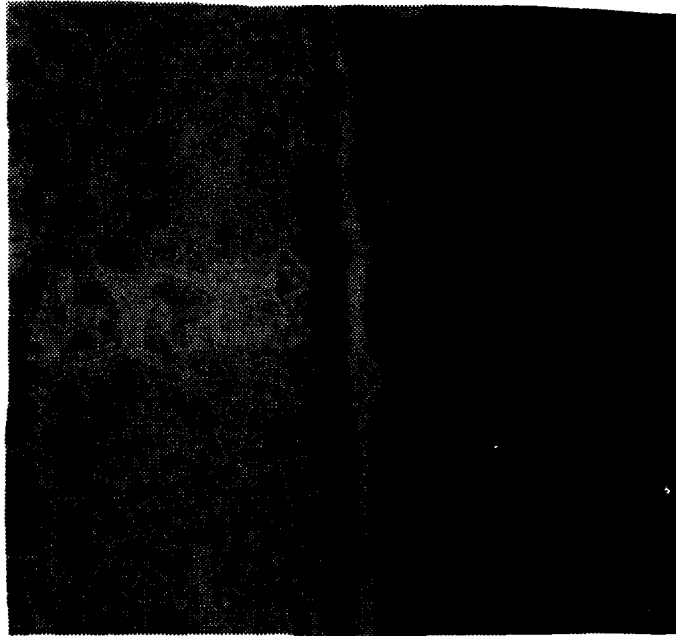


(a) As Fired
(1000X)



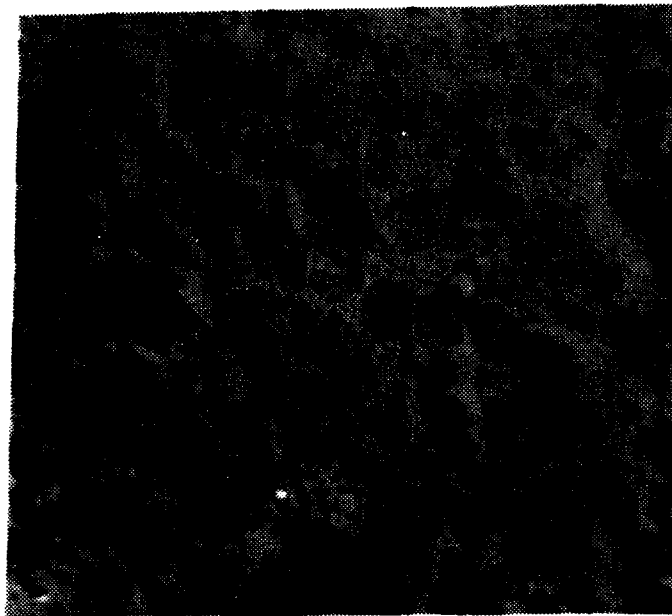
(b) At 112 Hours
(1000X)

Figure 40. Metal-Glass Interface for Composition "B"
as a Function of Heat Treatment Time (continued).

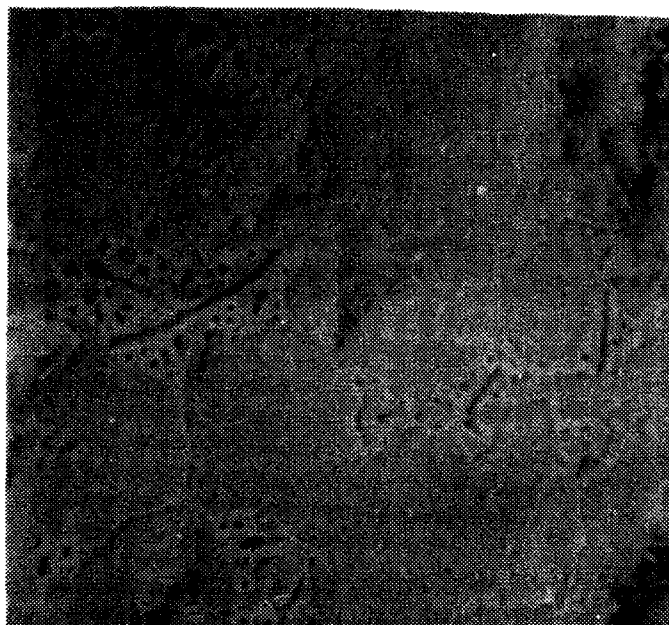


(c) At 309 Hours
(1000X)

Figure 40. Metal-Glass Interface for Composition "B"
as a Function of HEat Treatment Time (concluded).

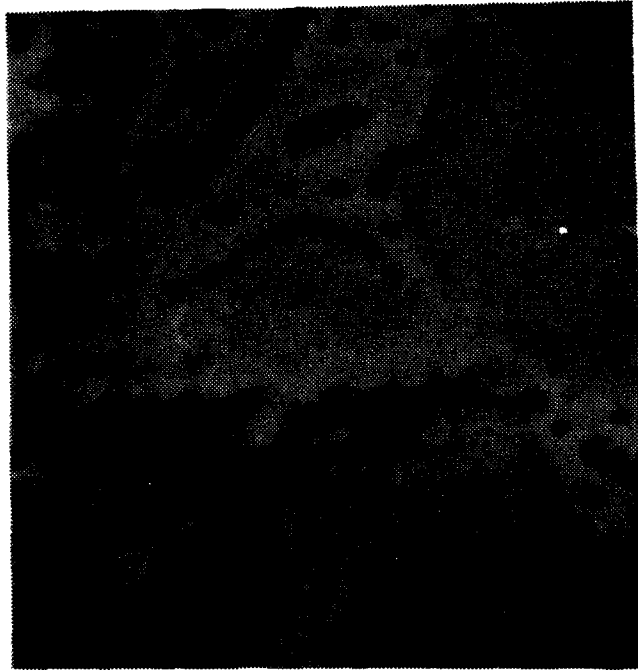


(a) 100X



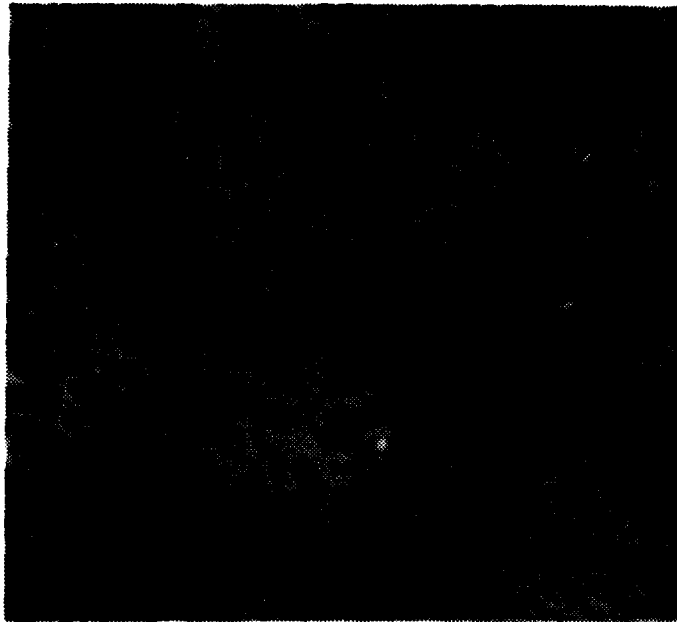
(b) 300X

Figure 41. Enamel Coating "B" at Various Magnifications After Heat Treatment for 112 Hours (continued).



(c) 1000X

Figure 41. Enamel Coating "B" at Various Magnifications
After Heat Treatment for 112 Hours (concluded).



(a) 100X



(b) 300X

Figure 42. Enamel Coating "B" at Various Magnification
After Heat Treatment for 309 Hours (continued).



(c) 1000X

Figure 42. Enamel Coating "B" at Various Magnifications
After Heat Treatment for 309 Hours (concluded).

TABLE 21

CRYSTALLINE PHASES AFTER VARIOUS HEAT TREATMENTS

Compositions	Heat Treatment	Crystalline Phases
A	I as fired	no crystalline phase
	II heat treated at 760°C for 100 hours	major - α -quartz minor - devitrite
	III heat treated at 760°C for 314 hours	major - α -quartz minor - devitrite
B	I as fired	no crystalline phase
	II heat treated at 815°C for 112 hours	major - α -cristobalite minor - possibly devitrite and mullite
	III heat treated at 815°C for 309 hours	major - α -cristobalite minor - possibly devitrite

α -quartz - hexagonal

α -cristobalite - tetragonal

the viscoelastic damping. The viscoelastic damping originates from the vitreous nature of a material in the proper viscosity range. Any deviation from the vitreous nature would affect the damping properties. Crystallization of the coating is such a deviation where the amount of a vitreous material is progressively reduced. Number of relaxation units and sites which give rise to the damping are directly proportional to the amount of vitreous material in the coating. Crystallization reduces the number of relaxation units and sites and therefore the loss factor.

One would expect a shift in the loss factor peak temperatures of Figures 34 and 35 with progressive crystallization. With crystallization the viscosity of the residual glass would change and therefore shift the damping peak. No shift in the peak temperatures would indicate that the viscosity of the residual glass was similar to the parent glass. Compositions used in this investigation provide such a situation. During crystallization crystalline SiO_2 (α -quartz and cristobalite were major phases for both compositions) precipitate thereby making the residual glass richer in Na_2O and CaO . Na_2O would make the glass softer whereas CaO has the opposite effect and the overall effect being neutral. No shift in the loss factor peak temperatures (Figures 33 and 34) suggest a neutral effect of the crystallization on the viscosity.

The general observation on the microstructural development suggests that increasing heat treatment or aging time leads to a progressive increase in the crystallinity of the vitreous enamel coating. There is also a significant microstructural change of the metallic substrate microstructure. These two processes independently or in combination alter the damping properties. However, it is well known that metals have much lower damping than the vitreous enamel at these temperatures, and any microstructural change in the metallic substrate would not be expected to influence the damping properties significantly. Therefore, the variations in the damping data (as shown in Figures 34 and 35) must be related to the microstructural change in the vitreous enamel coating. This leads to the conclusion that the reduction in damping capacity of

the enamel coating is related to the increasing degree of crystallinity. This does not mean that vitreous enamel coatings cannot be used as a vibration damping material. However, care must be taken when developing and utilizing enamel compositions in view of the fact that the conditions during the viscoelastic damping are favorable for nucleation and growth processes.

3.4. CONSTRAINED LAYER DAMPING WITH VITREOUS ENAMEL

For many years, vitreous enamels have been known to exhibit high loss modulus in the transition range. As a result, many of the research and application efforts to date that have utilized vitreous enamels as vibration damping materials have been directed toward free layer damping designs. In previous publications (6, 11, and 12), the viscosity temperature relationship of a vitreous enamel in the damping range and its influence on the damping properties had been discussed. Areas of concern have developed after consideration of viscosity within the damping range and practical application. Some areas of concern are; flow under gravity and centrifugal force, weathering and reaction with atmospheric gases, and volatilization of components from the vitreous enamel. All of these potential problems can be controlled by applying a protective layer over the damping material. A protective layer over an enamel damping layer has been used successfully in several applications (2, 3, and 13). In cases where a protective layer was needed, an interesting phenomenon was recorded. Enamel damping materials in a constrained layer damping design exhibited an increased temperature range of effective system damping in contrast to a free layer damping system. In addition to this gain, the handling of vitreous enamel constraining layer damping designs would be less cumbersome as the enamel could be coated onto a constraining layer of desired size and shape. The enamel could then be soldered or spot welded into place. Several constrained layer vitreous enamel treatments were evaluated both to better view their advantages and to determine the mechanism involved. This section discusses the results and mechanisms involved in the vitreous enamel constrained layer damping treatment.

AD-A124 290

VITREOUS ENAMEL DAMPING MATERIAL DEVELOPMENT(U) DAYTON
UNIV OH RESEARCH INST B KUMAR NOV 82 UDR-TR-82-105
AFWAL-TR-82-4162 F33615-79-C-5108

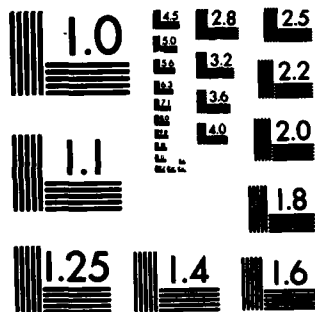
22

UNCLASSIFIED

F/G 11/3 . NL



END
DATE
FILMED
83
DTIC



MICROCOPY RESOLUTION TEST CHART
NATIONAL BUREAU OF STANDARDS-1963-A

The damping material used in this experiment was Corning composition 1990*. The 1990 was applied to: 1) test beams in partial and full coverage (see Figure 43); and 2) iron and stainless steel foils. All foil applications were done using the plasma spray technique. The coated constraining layers were welded onto cantilever beams. A photograph of the coated iron foil and the composite beam is shown in Figure 44. The damping of the four composite beams was determined using the standard resonant beam technique described in Reference . The experimental results are presented in Table 22. Modal loss factors were determined by the half power bandwidth method. Verification test measurements were carried out on the free layer and iron constrained specimens. Reproducibility was excellent at lower temperatures. At high temperatures (above 700°C), there were minor discrepancies which are believed to be related to the devitrification of the vitreous enamel. Oxidation of the iron foil was noted during the damping tests at elevated temperature. The stainless steel foil exhibited little or no oxidation under similar conditions.

The modal loss factor versus temperature plots for a free layer damping treatment, a constrained layer damping treatment, and the bare beam itself, are shown in Figure 45. The free layer treatment shows a loss factor of .018 at 480°C, whereas the constrained layer treatment exhibits a loss factor of .0318 at 710°C. The temperature range where the modal loss factor (η_s) is above .01 for the free layer treatment is 440°C to 525°C. The constrained layer treatment has η_s of .01 from 475°C to 850°C where the experiment was terminated. The temperature range of effective damping for the constrained layer treatment is of significant interest. Although a broadening of the modal damping peak with the constrained layer polymer materials is anticipated, a peak broadening which extends several hundred degrees centigrade is unusual. Analysis of the origin of broadness will be discussed in detail in the following paragraphs.

Like the polymeric materials, vitreous enamels span three distinct modulus regions with increasing temperature. However, unlike the polymeric materials which have a rubbery region above

*SiO₂-41, Li₂O-2, Na₂O-5, K₂O-12, PbO-40

TABLE 22
EXPERIMENTAL TEST MATRIX

Beam Configuration	Damping Material Thickness	Constraining Layer Thickness	Maximum System η	Temperature Range Where $\eta_s \geq .01$
Free layer beam full coated	.031 cm	----	.025	427°-538°C
Free layer beam partially coated	.031 cm	----	.019	432°-524°C
Iron constrained layer beam	.023 cm	.013 cm	.032	480°->840°C
Stainless steel constrained layer beam	.028 cm	.013 cm	.055	470°->850°C

T_g , the vitreous enamel becomes a liquid when heated above T_g . A typical modulus and loss factor versus temperature plot for a viscoelastic material is illustrated in Figure 46. Region I is the design range for a free layer damping treatment. Region II is the design range for a constrained layer damping treatment. The mechanisms of damping for these two regions are well understood. In polymeric materials, Region III is the rubbery region and is the design region for tuned viscoelastic dampers. A proposed mechanism in enamels above T_g follows.

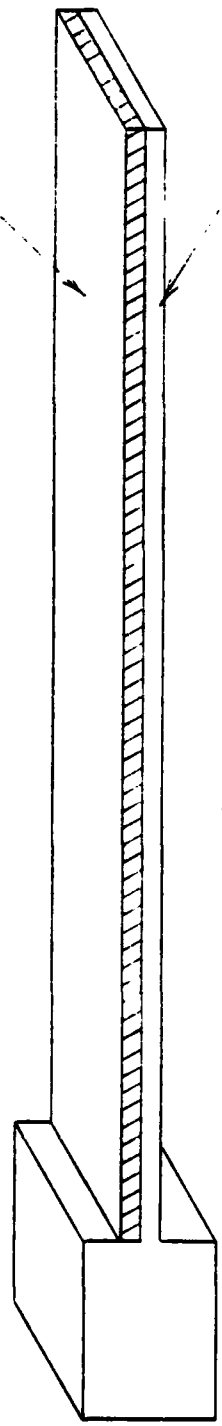
The broad damping peak of the constrained layer system shown in Figure 45 covers all three regions. The addition of a constraining layer to a free layer damping material should result in a decreased effectiveness of the damping system in the temperature region of Figure 46 as a result of the reduction in extensional deformation in the damping material. This is demonstrated in the test results in Figure 45. The free layer effectiveness is reduced, but the material loss modulus is sufficiently high to contribute significant damping at approximately 475°C. As the temperature continues to increase, the material loss factor and modulus begin to decrease. Ordinarily, this would result in decreased system damping as shown in the free layer curve in Figure 45; however, a new phenomenon now takes control of the damping. As the modulus begins to drop, significant shear caused by the constraining layer begins to be established in the damping layer. As a result, the system damping continues to increase with temperature to a peak value. This damping trend continues throughout the temperature range of the experiment. A review of the characteristics of vitreous enamels above T_g sheds light on this phenomenon.

Most of the vitreous enamels behave like Newtonian liquid at temperature beyond the glass transition range. The static viscosity of the enamel decreases continuously as the temperature is increased. The static viscosity for the Corning 1990 glass in the temperature range of interest exhibits typical behavior and is shown in Figure 47. The rate of decrease is higher at lower temperatures than those at the high temperatures.

Damping Material

Beam

Full Coverage



Damping Material

Beam

Partial Coverage

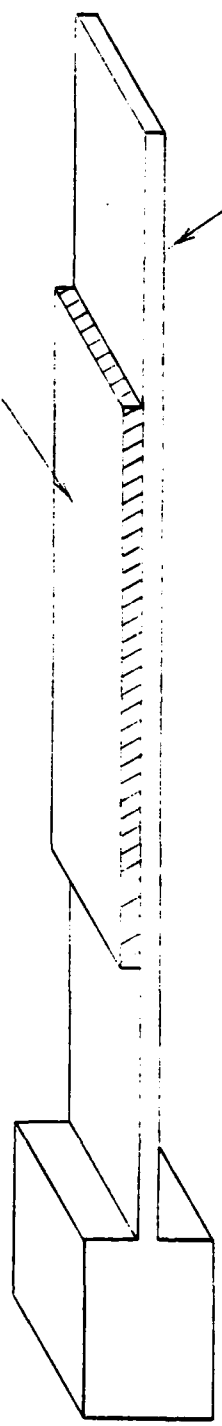


Figure 43 Test Beams for Corning Composition 1990.



(A)



(B)

Figure 44. (A) Vitreous enamel coated iron foil.
(B) Spot welded iron foil on beam.

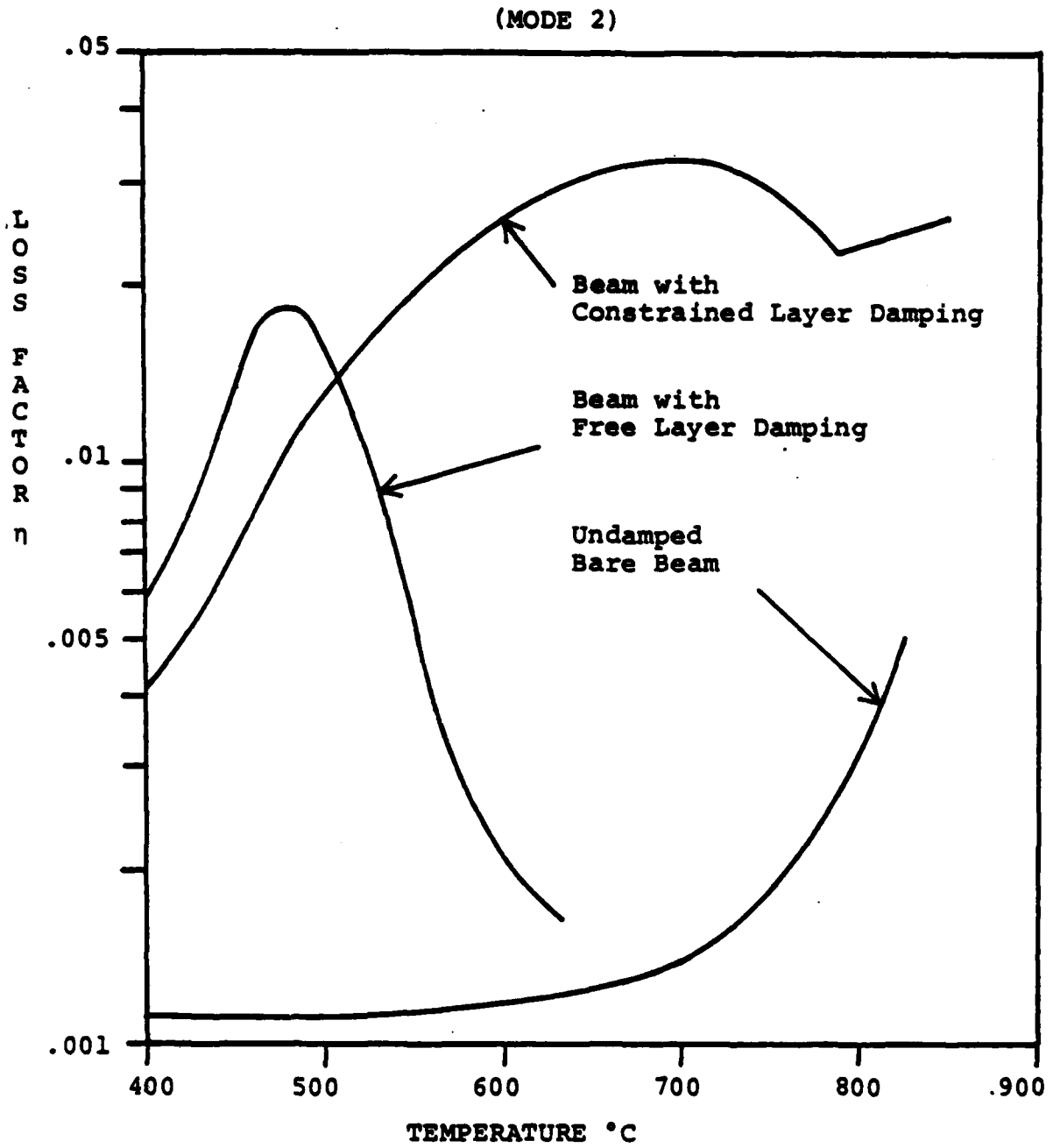


Figure 45. Loss Factor Versus Temperature Comparison for Undamped, Free Layer Damped, and Constrained Layer Damped.

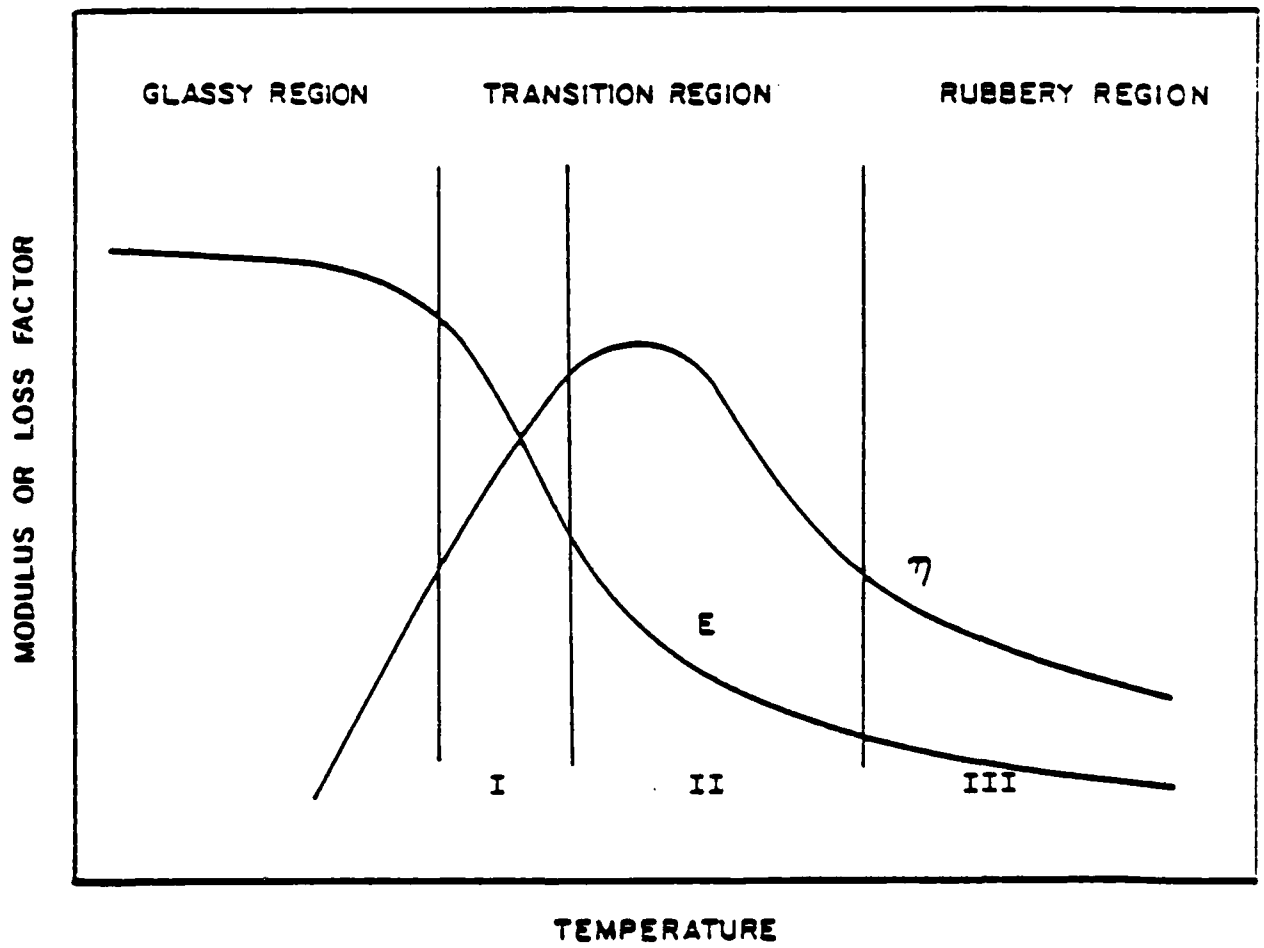


Figure 46. Typical Temperature Dependence of Polymer Viscoelasticity.

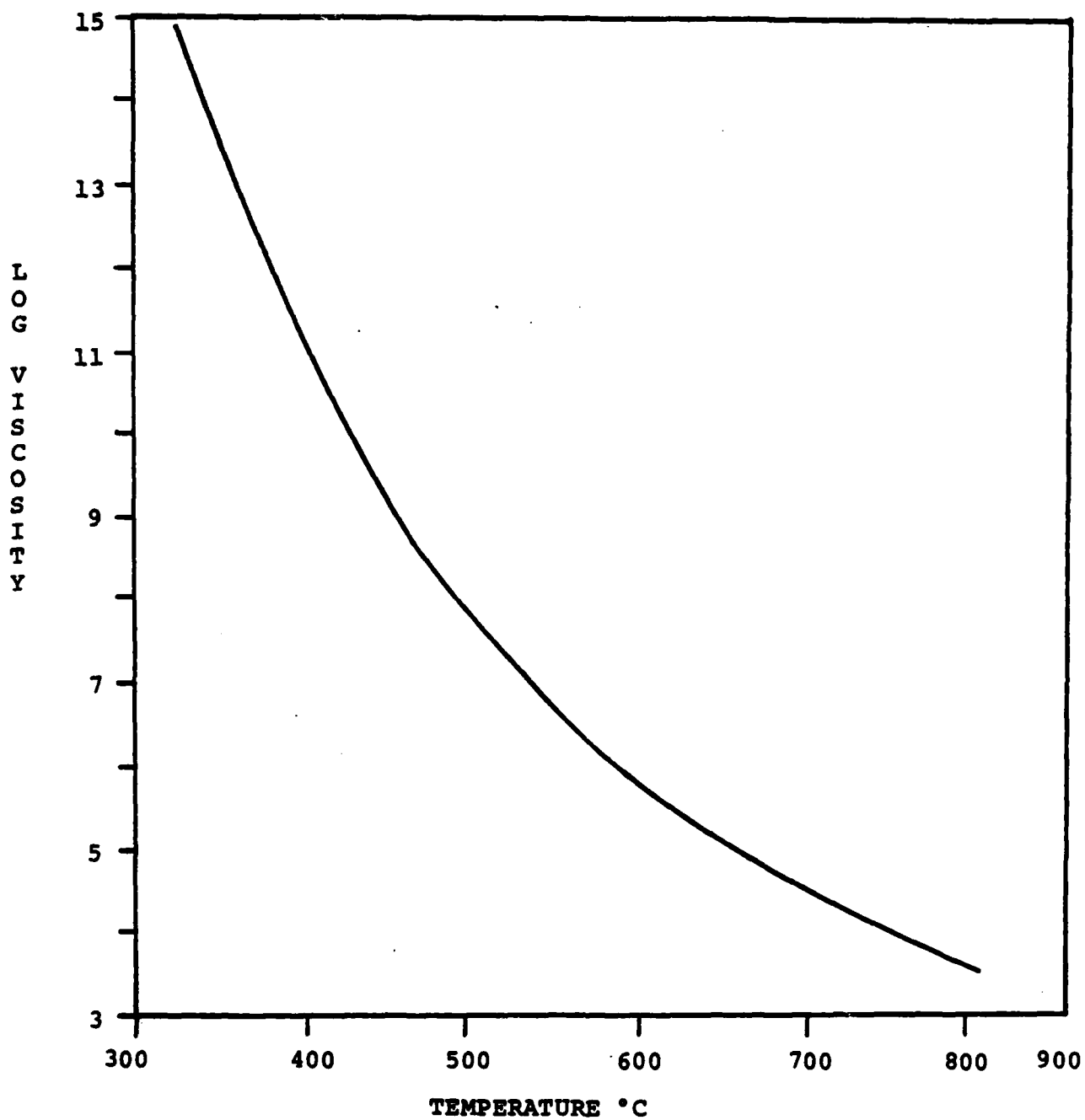


Figure 47. Static Viscosity Versus Temperature of Corning Glass 1990 Composition.

Plots of $\log \frac{\eta}{\phi}$ and experimentally determined $\log \eta_s$ are shown in Figure 48. There is a good correlation between the measured η_s and the calculated $\frac{\eta}{\phi}$ for the constrained system at lower temperatures (up to 700°C). Table 23 gives values of $\frac{\eta}{\phi}$ at various temperatures.

A minimum for the modal loss factor of the constrained layer system that is centered around 790°C can be seen in Figure 45. The second measurement of a similar constrained layer specimen did not reproduce the minimum. Only speculative explanation can be provided for this behavior as further characterization continues. Two possible explanations for the behavior are possible. Any defect arising from the spot welding of the enamel coated iron foil could contribute to the unexpected damping behavior. Also, it is known that the crystallization of the vitreous enamel coating decreases the loss factor (3). The temperature at which the minimum occurs might correspond to the liquidus temperature of the enamel. The rate and degree of crystallization of a vitreous material increase as the liquidus temperature is reached and the increased crystallization rate would adversely affect the loss factor. Beyond the liquidus temperature, the crystallites redissolve and the enamel becomes again a homogeneous liquid giving rise to an increased damping. It is hoped that further studies would clarify this high temperature behavior of the vitreous enamel.

The damping effectiveness and the temperature profile of a constrained layer damping system are dependent on the damping material thickness and the constraining layer stiffness. These typical effects are shown for enamel constrained layer systems in Figure 49 for the iron-constrained and steel-constrained layer damping treatments. At lower temperatures (400-700°C), both the iron- and steel-constrained specimens exhibit similar damping trends which agree with the proposed theory. Nonetheless, at temperatures beyond 700°C, a difference in the damping behavior is noted. Whether to attribute this behavior to the differences in the elastic properties of the two constraining layers or to other conditions including crystallization of the vitreous enamel discussed earlier remains a matter for further investigation.

TABLE 23

 $\frac{\eta}{\phi}$ AT VARIOUS TEMPERATURES

Temperature °C	$\frac{\eta}{\phi}$ (Poise ⁻¹)	$\log \frac{\eta}{\phi}$
400	4.61×10^{-14}	-13.34
450	8.83×10^{-12}	-11.05
500	3.19×10^{-10}	-9.50
550	13.06×10^{-10}	-8.88
600	3.33×10^{-9}	-8.48
650	11.91×10^{-9}	-7.92
700	4.12×10^{-8}	-7.39
750	10.69×10^{-8}	-6.97
800	18.23×10^{-8}	-6.74

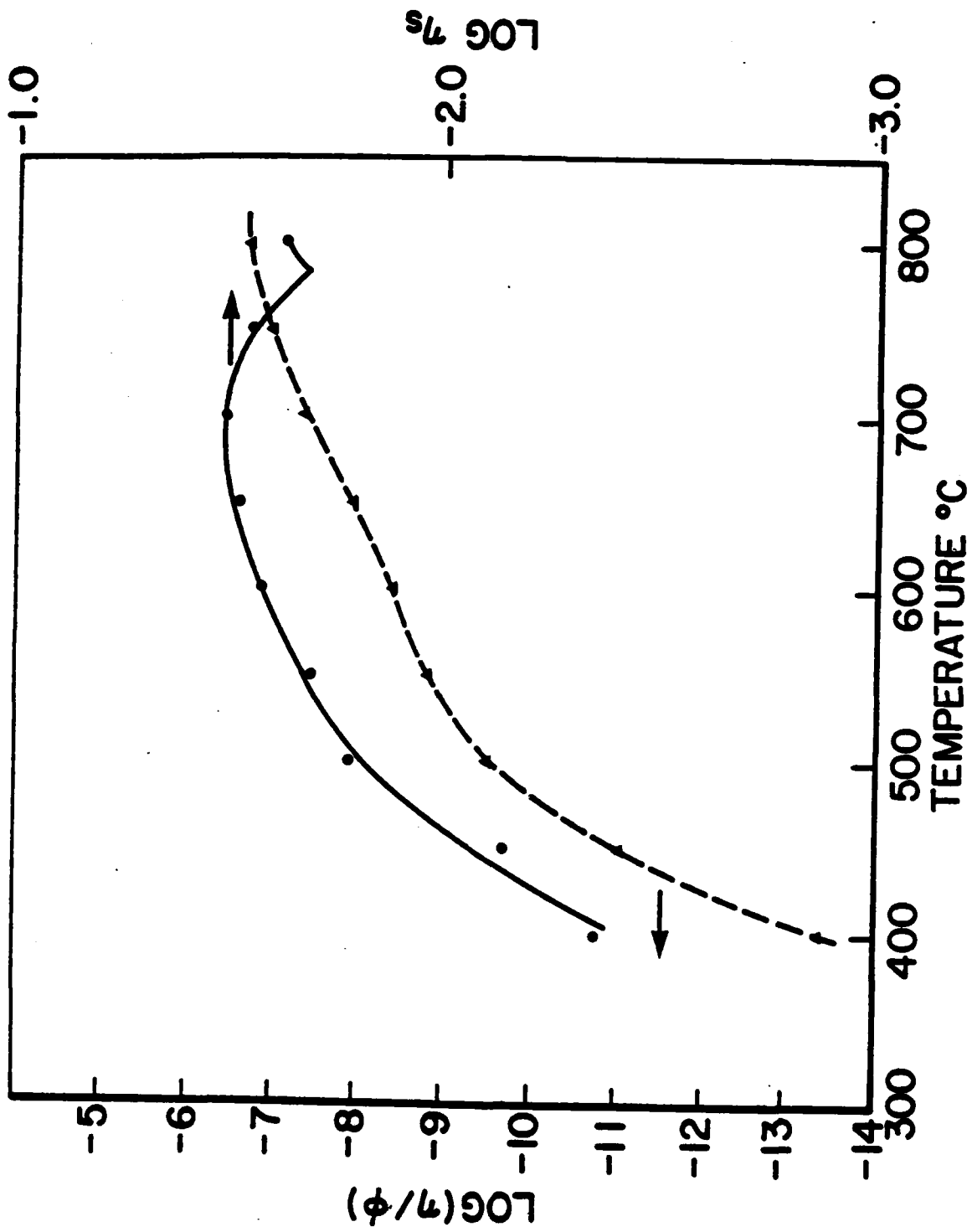


Figure 48. Shape of the Function $\text{Log } \frac{\eta}{\phi}$ versus Temperature.

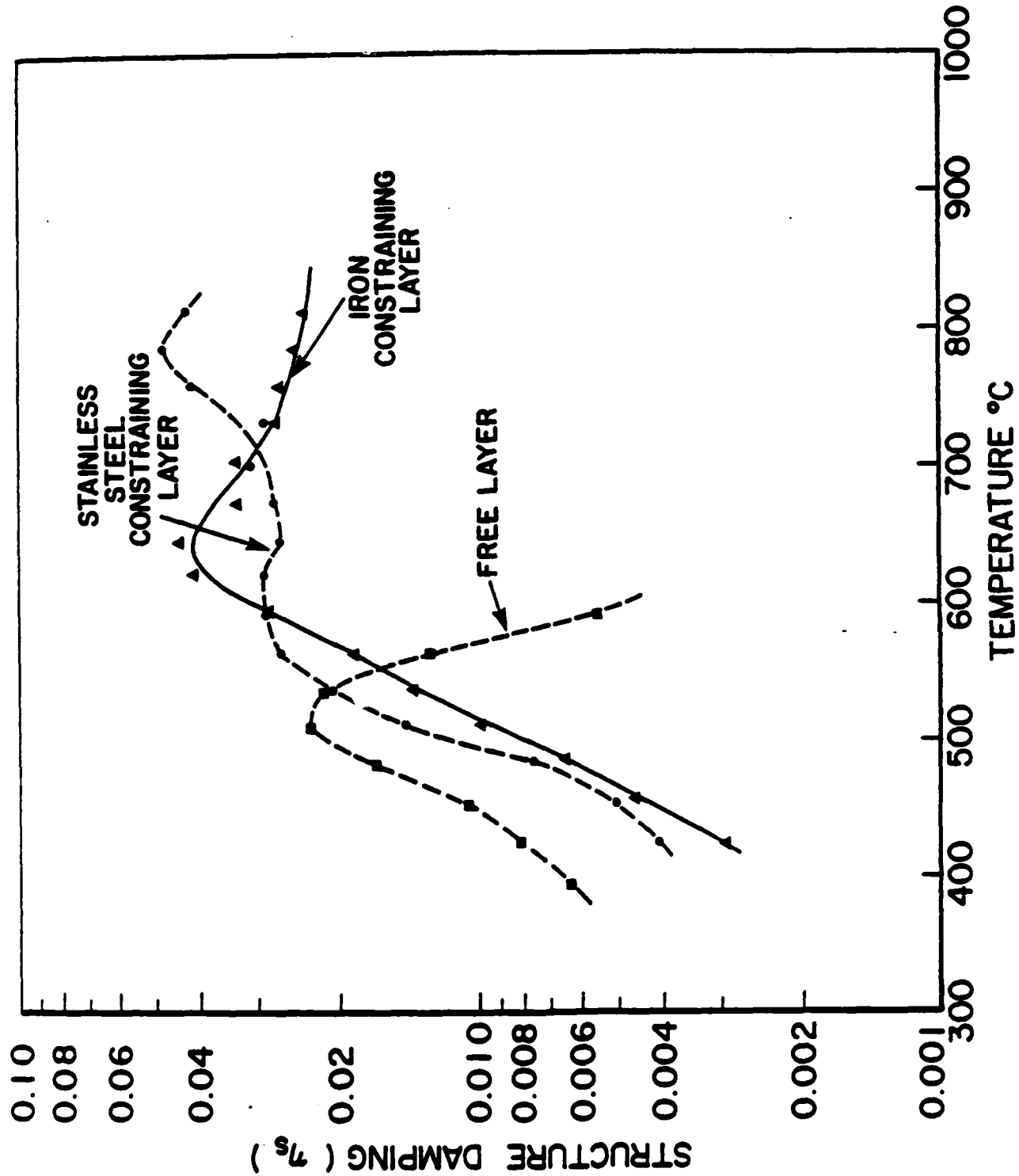


Figure 49. Structural Damping Versus Temperature for Free Layer, Iron-Constrained, and Steel-Constrained Damping [Mode 4].

CONCLUSIONS

From the results presented in the previous section, the following conclusions can be drawn.

(1) New compositions such as mixed alkali, lead silicate and low temperature glasses exhibited the characteristic damping properties in the viscoelastic range. The damping temperatures and the peak intensities were composition dependent. The fluoride composition initially showed a typical vitreous enamel damping peak; however, after a heat treatment significant broadening of the damping was noted. It was suggested that the broadening of the damping peak appears to be related to a precipitation phenomenon of a second phase during the heat treatment.

(2) It has been shown that there is a linear relationship between the glass transition temperature and the damping temperature. This suggests that the damping temperature is directly related to the viscosity. The viscoelastic damping occurs at a temperature near the softening point and corresponds to a viscosity range of $10^6 - 10^7$ poise.

(3) The viscosity range $10^6 - 10^7$ was found to be favorable for processes like nucleation and crystallization. Effects of nucleation and crystallization on the damping properties were studied for two soda-lime-silica type of composition. Progressive increase in the crystallinity decreased the loss factor of the two compositions and it was determined that the nucleation and crystallization have an adverse effect on the loss factor.

(4) It has been demonstrated that the concept of constrained layer damping is feasible and promising. The constraining layer smeared the free layer damping peak in such a fashion that the structural damping increased from a low value to a peak with increasing temperature and remained at the peak value even at temperatures over 800°C .

REFERENCES

1. "Development of High Temperature Vibration Damping Coatings," AiResearch Technical Report, U.S. Army Contract DA-44-009-AMC 838 (T), AiResearch Manufacturing Company of Arizona, Phoenix, February, 1966.
2. "High Temperature Damping System Development for the J-85-21 Afterburner Liner," University of Dayton Research Institute, UDR-TR-80-79, August, 1980.
3. "Evaluation of High Temperature Damping Applications to Increase Fatigue Life in Rotating Jet Engine Components," University of Dayton Research Institute, UDR-TR-80-82.
4. A. D. Nashif, "Enamel Coatings for High Temperature Damping Materials," Am. Ceram. Soc. Bull., 52 (12) 846-49, 1974.
5. P. I. Sridharan, "Damping in Porcelain Enamel Coatings," AFML-TR-74-191, 53 (12), 1976.
6. B. Kumar, C. A. Cannon, and G. A. Graves, Jr., "Effect of Composition on the Vibration Damping Properties of Glass (Vitreous Enamel) Coatings," Glass Technology, April, 1981.
7. W. A. Zdaniewski, G. E. Rindone, D. E. Day, "Review - The internal friction of glasses," J. Mat. Sci., 14, 763-75 (1979).
8. H. Oberst, Acoustica (Akustische Berhefte), 4, 181 (1952).
9. R. E. D. Bishop and D. C. Johnson, The Mechanics of Vibration, Cambridge Press, (1960).
10. "A Study to Determine the Effect of Glass Compositional Variations on Vibration Damping Properties," AFWAL-TR-80-4061.
11. B. Kumar, G. A. Graves, Jr. "Vitreous Enamel as a Vibration Damping Material," Amer. Ceram. Soc. Bull. 61 (4), 480-83, 1982.
12. B. Kumar, G. A. Graves, Jr., D. M. Hopkins, and M. L. Drake, "Nucleation, Crystallization, and Viscoelastic Damping in Vitreous Enamel," Advances in Ceramics, Vol. 4, Edited by J. H. Simmons, Dr. Uhlman, and G. H. Beall., Amer. Cer. Soc., 1982.
13. D. I. G. Jones, and C. M. Cannon, "Control of Gas Turbine Stator Blade Vibrations by Means of Enamel Coatings," J. of Aircraft, 12 (4), 226-230, 1975.